SPONTANEOUS EXPANSION AND MOBILIZATION OF GAS ABOVE DNAPL

SPONTANEOUS EXPANSION AND MOBILIZATION OF A DISCONTINUOUS GAS PHASE DUE TO MASS TRANSFER FROM DENSE NON-AQUEOUS PHASE LIQUID

By:
KEVIN G. MUMFORD
B.A.Sc., M.A.Sc.

A Thesis
Submitted to the School of Graduate Studies
in Partial Fulfillment of the Requirements
for the Degree of
Doctor of Philosophy

McMaster University

DOCTOR OF PHILOSOPHY (2008) McMaster University
(Civil Engineering) Hamilton, Ontario

Title: Spontaneous expansion and mobilization of a discontinuous gas phase due to mass transfer from dense non-aqueous phase liquid

AUTHOR: Kevin G. Mumford
B.A.Sc. (University of Waterloo)
M.A.Sc. (University of Waterloo)

SUPERVISORS: Dr. James E. Smith
Dr. Sarah E. Dickson

NUMBER OF PAGES: xvii, 150

Abstract

Groundwater contamination by dense non-aqueous phase liquids (DNAPLs), such as chlorinated solvents, continues to be a significant environmental problem. When released to the subsurface, either due to improper disposal or accidental release, DNAPLs can form complex source zones whose geometry is largely controlled by the geological heterogeneity of the subsurface. These source zones are composed of disconnected, immobile blobs or ganglia trapped by capillary forces (referred to as DNAPL residual) between high-saturation regions located at permeability interfaces (referred to as DNAPL pools). The slow dissolution of DNAPL pools can result in the contamination of groundwater for time periods on the order of decades to centuries.

The common conceptual model used in the investigation of DNAPL-contaminated sites is based primarily on the mass transfer from DNAPL to the surrounding aqueous phase in the saturated zone. However, the presence of a discontinuous gas phase above a DNAPL pool can significantly affect the mass transfer from the pool through repeated, spontaneous expansion and mobilization of the gas phase. This mechanism has not been included in the common conceptual models.

The goal of this research was to develop a quantitative understanding of discontinuous gas phase expansion and mobilization above a DNAPL pool. This goal was addressed using a combination of small-scale and intermediate-scale laboratory experiments. Small-scale, no-flow vial experiments were used to measure the expansion of single gas bubbles above DNAPL pools, and provide the basis for the development of an analytical model to assess the effect of expansion by multi-component partitioning on the mass

transfer from DNAPL pools. Small-scale flow cell experiments were used to measure spontaneous expansion rates in porous media, and provide visual data concerning the distribution of the gas phase. Small-scale air injection experiments were used to characterize the gas flow. Finally, an intermediate-scale flow cell experiment was used to provide larger-scale data concerning the transient distribution of the gas phase, and measure the effect of spontaneous expansion and mobilization on the aqueous-phase DNAPL constituent concentrations.

The combined results of these experiments established a detailed conceptual model for the spontaneous expansion and mobilization of a discontinuous gas phase above a DNAPL pool. In this conceptual model, spontaneous expansion of a discontinuous gas phase above a DNAPL pool occurs due to multi-component partitioning, and depends on the concentrations of both the volatile DNAPL and the other dissolved gases. This expansion is more likely to occur, and will be faster, in shallower systems (i.e. lower hydrostatic pressures) containing coarser media (i.e. lower capillary pressures), more volatile DNAPL, and higher concentrations of other dissolved gases (i.e. higher partial pressures). Mobilization of the expanding gas will occur as discontinuous gas flow in most sands, where the repeated trapping and coalescence of gas clusters can allow rapid, large-scale vertical transport of the gas phase. This discontinuous gas flow can produce macroscopic gas fingers composed of multiple, discrete gas clusters. These macroscopic fingers can reach substantial heights above the pool surface, but the growth occurs predominantly at the pool's leading edge due to the stripping of other dissolved gases. This expansion and mobilization can significantly affect the mass transfer from the DNAPL pool if the gas phase is in direct contact with the pool surface; or if the gas phase is close to the pool surface, covers a large fraction of the pool, and the groundwater flow is sufficiently slow. The partitioning of DNAPL constituent from the mobilized gas phase to the aqueous phase well above the pool surface can also change the spatial distribution of aqueous-phase DNAPL constituent concentrations, increasing them above those that are expected based on theoretical calculations for strictly DNAPL-water

systems, even at elevations where the concentrations are expected to be zero. The increased concentrations well above the pool surface can appear as short-duration events in the presence of a sustained gas phase, due to the partitioning of DNAPL constituents from the gas to the aqueous phase during multi-component mass transfer. The results of this research provide the necessary basis to begin incorporating this fundamental mechanism into the conceptual and mathematical models used for DNAPL-related research, the investigation of DNAPL-contaminated sites, and the design and application of DNAPL remediation technologies.

Acknowledgements

I would like to thank the many people that have helped me during my time at McMaster University. My supervisors, Dr. Jim Smith and Dr. Sarah Dickson, have supported my research efforts from the beginning, and have provided key advice concerning experiments, papers, and balancing the often complex mix of life and research. My committee members, Dr. Neil Thomson and Dr. Dieter Stolle, have also been very helpful, and I value the insight and support they offered along the way. I would also like to thank Dr. Carlos Filipe and Dr. John MacGregor for their encouragement and advice.

Jennie Kirby is an excellent technician, and I benefited significantly from her work and advice concerning the analysis of volatile organics. Michael Palme showed great creativity in the construction of the small-scale glass flow cells, and his help is appreciated. I am also grateful for the technical support provided by Peter Koudys and Anna Robertson.

I am very thankful for the financial support provided by the Natural Sciences and Engineering Research Council (NSERC) of Canada, the Ontario Government's Ontario Graduate Scholarships in Science and Technology (OGSST) initiative, and the McMaster University Department of Civil Engineering.

I would like to thank my family for their support, and my wife, Alison, for her love.

Preface

This thesis has been prepared according to the McMaster University regulations for theses consisting of previously published/prepared material. Chapters 2, 3, and 4 consist of material previously published as journal articles, and chapter 5 consists of material previously prepared for publication as a journal article. As such, the material in chapters 2, 3, 4, and 5 was co-authored. The original contributions made by the thesis author to the material in each of these chapters are outlined below:

Chapter 2

Title: Mass flux from a non-aqueous phase liquid pool considering spontaneous expansion of a discontinuous gas phase

Authors: Kevin G. Mumford, James E. Smith, and Sarah E. Dickson

Published in: *Journal of Contaminant Hydrology*

The vial experiments were conceived, designed, and conducted by K.G. Mumford. The interfacial tension measurements were conducted by K.G. Mumford. The development of the analytical model (Eq. 2.9) and fitting of the experimental data was conducted by K.G. Mumford. The relative flux model (Eq. 2.12) was developed by K.G. Mumford in consultation with J.E. Smith. Interpretation of the results was conducted by K.G. Mumford in consultation with J.E. Smith and S.E. Dickson. The text was written by K.G. Mumford and edited by J.E. Smith and S.E. Dickson.

Chapter 3

Title: New observations of gas-phase expansion above a dense non-aqueous phase liquid pool

Authors: Kevin G. Mumford, James E. Smith, and Sarah E. Dickson

Published in: *Vadose Zone Journal*

The flow cell experiment was designed by K.G. Mumford in consultation with J.E. Smith and S.E. Dickson, and was conducted by K.G. Mumford. Critical cluster length analyses were conducted by K.G. Mumford. Image capture, processing, and analysis were conducted by K.G. Mumford. Interpretation of pore-scale image data was conducted by K.G. Mumford. Interpretation of macro-scale image data was conducted by K.G. Mumford in consultation with J.E. Smith. The text was written by K.G. Mumford and edited by J.E. Smith and S.E. Dickson.

Chapter 4

Title: Slow gas expansion in saturated natural porous media by gas injection and partitioning with non-aqueous phase liquids

Authors: Kevin G. Mumford, Sarah E. Dickson, and James E. Smith

Published in: *Advances in Water Resources*

The small-scale flow cell was designed by K.G. Mumford. The experiments were designed by K.G. Mumford in consultation with J.E. Smith and S.E. Dickson, and conducted by K.G. Mumford. Analysis and interpretation of gas-volume, image, and pressure data was conducted by K.G. Mumford in consultation with J.E. Smith and S.E. Dickson. Cluster length measurements and theoretical comparisons were conducted by K.G. Mumford. The text was written by K.G. Mumford and edited by J.E. Smith and S.E. Dickson.

Chapter 5

Title: The effect of spontaneous gas expansion and mobilization on the aqueous-phase concentrations above a dense non-aqueous phase liquid pool

Authors: Kevin G. Mumford, James E. Smith, Sarah E. Dickson

Prepared for: *Journal of Contaminant Hydrology*

The flow cell experiment was designed by K.G. Mumford in consultation with J.E. Smith and S.E. Dickson, and was conducted by K.G. Mumford. Analysis and interpretation of effluent concentration data was conducted by K.G. Mumford in consultation with J.E. Smith and S.E. Dickson. The numerical model was conceived, and written by K.G. Mumford. The text was written by K.G. Mumford and edited by J.E. Smith and S.E. Dickson.

Table of Contents

List of Tables

List of Figures

Chapter 1

Introduction

1.1 Background

1.1.1 Problem Scope

Groundwater is an important natural resource. In the United States, 242 million people were served by public-water suppliers in 2000, with groundwater providing 37% of the total volume (Hutson et al., 2004). An additional 42.6 million people received water from user-controlled groundwater wells in 2000 (Hutson et al., 2004). In Canada, nine million people relied on groundwater for their drinking water in 1996 (Statistics Canada, 2003). In Ontario, an estimated three million people rely on groundwater as a source of drinking water, including 90% of people living in rural areas (MOE, 2004). The contamination of groundwater by organic compounds is common. Based on extensive sampling and analysis of groundwater in the United States, the United States Geological Survey (USGS) reported that one or more of 55 volatile organic compounds (VOCs) were present at concentrations greater than 0.2 μg/L in 19% of groundwater wells, and at concentrations greater than 0.02 μg/L in 51% of groundwater wells. The concentrations were found to be greater than the Maximum Contaminant Level (MCL) in 1-2% of the samples (Zogorski et al., 2006). In addition, an estimated 76% of the sites listed on the National Priorities List (NPL), which identifies significant abandoned hazardous waste sites, have groundwater contaminated by organic compounds (USEPA, 1993).

Many of the sites contaminated with organic compounds are associated with dense non-aqueous phase liquids (DNAPLs), which include chlorinated solvents, creosote, polychlorinated biphenyls (PCBs), and coal tar (USEPA, 2004). Many DNAPLs are associated with long-term groundwater contamination and significant remediation challenges (USEPA, 2004; Stroo et al., 2003; Mackay and Cherry, 1989). An estimated 60% of NPL sites are contaminated by DNAPLs (USEPA, 1993), and an estimated 15,000-25,000 DNAPL-contaminated sites exist in the United States (USEPA, 2003). The cost associated with these DNAPL-contaminated sites is significant. Assuming that the on-going management of these contaminated sites would be based on the application of pump-and-treat technology, the estimated cost is $2.7-$4.5 billion dollars per year, with a net present value based on 30 years of operation of $50-$100 billion dollars (USEPA, 2003).

1.1.2 DNAPLs in the Subsurface

DNAPLs are a significant environmental problem and remediation challenge due to a combination of physical and chemical properties, and their interaction with small- and large-scale heterogeneities in the subsurface. The term non-aqueous phase liquid (NAPL) refers to a group of compounds that can exist as a separate liquid phase in water, and those that have a density greater than water are referred to as DNAPLs. A DNAPL released above the water table will move downward through the vadose zone, and continue to move downward below the water table due to its density. The movement of DNAPL through the subsurface is controlled by capillary forces created by the interfacial tension between the separate fluid phases. The capillary forces acting on the DNAPL result in complex flow pathways, as the flowing DNAPL responds to small-scale heterogeneities in the subsurface. Where larger-scale heterogeneities are present, such as horizontal or sloping layers of lower-permeability material, DNAPL flow is controlled by the geometry of these structures, and can be transported substantial lateral distances from the release point, in directions independent of the direction of groundwater flow. This combination of capillary forces and geological heterogeneity create a complex distribution of DNAPL following a release, which is commonly referred to as a source

zone. These source zones are composed of disconnected, immobile blobs or ganglia trapped by capillary forces (referred to as DNAPL residual) between high-saturation regions located at permeability interfaces (referred to as DNAPL pools). Below the water table, the dissolution of DNAPL from source zones creates a dissolved phase plume, with aqueous concentrations greater than regulatory limits. These source zones can persist for extended periods of time (i.e. decades to centuries) due to mass transfer limitations created by geologic heterogeneities, the low solubility of most DNAPLs, and the low biotic and abiotic degradation rates in most groundwater systems. Detailed descriptions of processes affecting the contamination of groundwater by DNAPLs is provided by Schwille (1998) and Pankow and Cherry (1996).

The persistence of DNAPL source zones is typically associated with the presence of DNAPL pools (Anderson et al., 1992), which contain larger volumes of DNAPL than residual sources, and have lower mass transfer rates per unit volume (Sale and McWhorter, 2001). While some studies have investigated the dissolution of NAPL pools under non-equilibrium conditions (Chrysikopoulos, 1995; Kim and Chrysikopoulos, 1999; Seagren et al., 1999a; Lee and Chrysikopoulos, 2002; Seagren and Moore, 2003), local equilibrium between the aqueous-phase and NAPL at the surface of the pool is often assumed (e.g. Johnson and Pankow, 1992; Seagren et al., 1994; Holman and Javandel, 1996). Under local equilibrium conditions, which are expected for the dissolution of single component pools under most natural groundwater flow conditions (Seagren et al., 1999b), the mass transfer from a DNAPL pool is controlled by the rate at which DNAPL constituents are removed from the pool surface (Johnson and Pankow, 1992; Seagren et al., 1999b; Sale and McWhorter, 2001). Below the water table, DNAPL constituents are removed from the pool surface by advection and dispersion in the aqueous phase.

An understanding of the processes that control the mass transfer from DNAPL source zones is important for obtaining estimates of the time required for complete dissolution (i.e. source zone lifetime), and for characterizing DNAPL-contaminated sites. Sites with

suspected DNAPL contamination are typically characterized using a collection of different investigation techniques (USEPA, 2004). One available technique is the use of detailed aqueous sampling, in combination with a conceptual model of historical chemical use, site geology, and transport mechanisms, to locate source zones and infer distribution of DNAPL within the source zones (USEPA, 2004; Broholm et al., 1999; Pankow and Cherry, 1996). The conceptual models applied to sand and gravel sites are typically based on limited transverse horizontal and vertical dispersion in the saturated zone and, therefore, limited lateral and vertical spreading of the plume between the source zone and near-by sampling locations (Pankow and Cherry, 1996).

1.1.3 Discontinuous Gas Phases in DNAPL Source Zones

Roy and Smith (2007) presented the results of a unique study, which investigated systems containing both a DNAPL pool and a discontinuous gas phase in otherwise water-saturated porous media. This was different from most other studies of mass transfer from NAPL sources, which were conducted in strictly NAPL-water systems (Khachikian and Harmon, 2000; Oostrom et al., 2006) or in systems containing a continuous gas phase (e.g. Tillman and Smith, 2004; Conant et al., 1996; Sleep and Sykes, 1989). In their experiments using small flow cells packed with glass beads, Roy and Smith (2007) observed remarkable behaviour caused by the presence of the discontinuous gas phase. Initially trapped gas clusters in contact with the DNAPL pool underwent repeated expansion, fragmentation, and vertical mobilization, which resulted in increased gas saturations, local DNAPL displacement, an increased mass flux of aqueous-phase DNAPL constituent, and transient changes to the distribution of aqueous-phase DNAPL constituent. This spontaneous expansion of the gas phase was attributed to the partitioning of DNAPL constituent and other dissolved gases to the discontinuous gas phase. The results of this study suggest that there is a set of conditions, related to DNAPL, groundwater, and porous media properties, where the spontaneous expansion of a discontinuous gas phase could act as a significant mechanism to remove DNAPL constituents from the surface of DNAPL pools. Despite this potential significance, this

mechanism is not included in the common conceptual models applied to DNAPL-contaminated sites.

There are no studies in the literature that refer directly to the expansion of a multi-component gas phase and the subsequent mobilization in porous media, which would support the mechanistic explanation offered by Roy and Smith (2007), but related work has been presented in the petroleum, hydrogeology, and physics literature. Studies reported in the petroleum literature have been presented in the context of solution gas drive, and have focused on the expansion of single-component gas phases in systems dominated exclusively by capillary forces (e.g. Li and Yortsos, 1995; Satik et al., 1995; Firoozabadi and Kashchiev, 1996; Tsimpanogiannis and Yortsos, 2002; Arora and Kovscek, 2003), although the effects of gravity have been recently considered (Dominguez et al., 2000; Tsimpanogiannis and Yortsos, 2004). Studies reported in the hydrogeology literature have focused on the dissolution of multi-component gas phases in the context of interpreting trace gas concentrations in groundwater (Holocher et al., 2003), quantifying trapped gas using partitioning tracers (Cirpka and Kitanidis, 2001), and estimating mass transfer from trapped gas phases for remediation-based gas injection (Geistlinger et al., 2005). Only the study presented by Amos and Mayer (2006) considered the mobilization of a multi-component gas phase, which was presented in the context of biologically produced methane and was modeled using empirical expressions for gas mobility. Other studies in the hydrogeology literature have focused on discontinuous gas flow during air sparging applications (Brooks et al., 1999; Geistlinger et al., 2005; Selker et al., 2007), where mass transfer between the gas and aqueous phases is not considered, and the expansion is driven by a controlled injection of gas at a faster rate than that expected due to mass transfer processes. Studies reported in the physics literature have investigated discontinuous gas flow at low flow rates in experimental and numerical models (Wilkinson, 1984; Frette et al., 1992; Birovljev et al., 1995; Wagner et al., 1997a; b), where mass transfer is not considered. The potentially important implications of the spontaneous expansion and mobilization of discontinuous gas phases

in DNAPL source zones identified by Roy and Smith (2007), combined with the lack of literature that directly addresses the fundamental mechanism, represents a significant gap in our knowledge concerning the controlling processes in DNAPL source zones.

1.2 Research Objectives

The goal of this research was to develop a quantitative understanding of discontinuous gas phase expansion and mobilization above a DNAPL pool. To achieve this goal, research tasks were developed to address the following objectives:

1. Test the hypothesis that the expansion of a discontinuous gas phase in the presence of DNAPL is due to multi-component partitioning. This objective was addressed using small-scale laboratory experiments containing a single gas bubble above a DNAPL pool, and a newly developed analytical model for multi-component gas-phase expansion (Chapter 2).

2. Determine the conditions under which this mechanism could significantly affect the mass transfer rate from DNAPL pools. This objective was addressed using a newly developed screening-level analytical model for relative mass flux (Chapter 2).

3. Quantify the rate at which gas could be generated by spontaneous expansion due to DNAPL partitioning. This objective was addressed using small-scale experiments in static, porous media-free systems (Chapter 2), and in porous media-packed flow cells (Chapter 4).

4. Investigate the extent, discontinuous nature, and transient evolution of the gas phase produced by spontaneous expansion above a DNAPL pool in natural porous media. This objective was addressed using image data collected from small-scale (Chapter 4) and intermediate-scale (Chapter 3) flow-cell experiments with DNAPL pools, and using a combination of image and pressure data in small-scale air injection experiments (Chapter 4).

5. Quantify the effect of spontaneous expansion and mobilization on the aqueous-phase concentrations of DNAPL constituent downgradient of a DNAPL pool, including transient changes in the aqueous-phase concentration distribution, and the magnitude of the aqueous-phase concentrations compared to accepted models of DNAPL pool dissolution. This objective was addressed using effluent concentration data from an intermediate-scale flow-cell experiment (Chapter 5), and simulation results from a numerical model that combined multi-component mass transfer to discontinuous gas phases with a macroscopic invasion percolation approach for the expansion and mobilization of gas (Chapter 5).

1.3 Thesis Overview

This thesis has been prepared according to the McMaster University regulations for theses consisting of previously published/prepared material. Thus, the following chapters 2-5 consist of papers published in or prepared for academic journals. Each paper contains its own introduction and relevant background sections. As such, background material concerning multi-component partitioning is repeated in chapters 2-5, and background material concerning discontinuous gas flow is repeated in chapters 3-5. The chapters are presented as they appear in the journal papers, but the text format and heading, figure, table, and equation numbering have been changed to be consistent with this thesis.

Chapter 2 describes the experiments used to investigate spontaneous expansion in the absence of porous media, and under what conditions spontaneous expansion could result in significant mass transfer at DNAPL-contaminated sites. Chapter 3 describes the experiments used to investigate spontaneous expansion and mobilization in natural porous media, with an emphasis on the transient distribution of the gas phase. Chapter 4 describes the experiments used to quantify the spontaneous gas expansion rate in natural porous media, and investigate the nature of the resulting discontinuous gas flow. Chapter 5 describes the experiments and simulations used to quantify the effect of spontaneous expansion and mobilization of a discontinuous gas phase on aqueous-phase DNAPL

constituent concentrations downgradient of a DNAPL pool. Chapter 6 presents the overall conclusions and recommendations of this work.

References

Amos, R.T., Mayer, K.U., 2006. Investigating ebullition in a sand column using dissolved gas analysis and reactive transport modeling. Environ. Sci. Technol. 40 (17), 5361-5367.

Anderson, M.R., Johnson, R.L., Pankow, J.F., 1992. Dissolution of dense chlorinated solvents into groundwater. 3. modeling contaminant plumes from fingers and pools of solvent. Environ. Sci. Technol. 26 (5), 901-908.

Arora, P., Kovscek, A.R., 2003. A mechanistic modeling and experimental study of solution gas drive. Transport Porous Med. 51 (3), 237-265.

Birovljev, A., Wagner, G., Meakin, P., Feder, J., Jossang, T., 1995. Migration and fragmentation of invasion percolation clusters in 2-dimensional porous media. Phys. Rev. E. 51 (6), 5911-5915.

Broholm, K., Feenstra, S., Cherry, J.A., 1999. Solvent release into a sandy aquifer. 1. overview of source distribution and dissolution behavior. Environ. Sci. Technol. 33 (5), 681-690.

Brooks, M.C., Wise, W.R., Annable, M.D., 1999. Fundamental changes in in situ air sparging flow patterns. Ground Water Monit. R. 19(2), 105-113.

Chrysikopoulos, C.V., 1995. Three-dimensional analytical models of contaminant transport from nonaqueous phase liquid pool dissolution in saturated subsurface formations. Water Resour. Res. 31 (4), 1137-1145.

Cirpka, O.A., Kitanidis, P.K., 2001. Transport of volatile compounds in porous media in the presence of a trapped gas phase. J. Contam. Hydrol. 49, 263-285.

Conant, B.H., Gillham, R.W., Mendoza, C.A., 1996. Vapor transport of trichloroethylene in the unsaturated zone: field and numerical modeling investigations. Water Resour. Res. 32 (1), 9-22.

Dominguez, A., Bories, S., Prat, M., 2000. Gas cluster growth by solute diffusion in porous media. Experiments and automation simulation on pore network. Int. J. Multiphas. Flow 26, 1951-1979.

Firoozabadi, A., D. Kashchiev, D., 1996. Pressure and volume evolution during gas phase formation in solution gas drive process. SPE J. 1 (3), 219-227.

Frette, V., Feder, J., Jossang, T., Meakin, P., 1992. Buoyancy-driven fluid migration in porous-media. Phys. Rev. Lett. 68 (21), 3164-3167.

Geistlinger, H., Beckmann, A., Lazik D., 2005. Mass transfer between a multicomponent trapped gas phase and a mobile water phase: experiment and theory. Water Resour. Res. 41, doi:10.1029/2004WR003885.

Holman, H.-Y.N., Javandel, I., 1996. Evaluation of transient dissolution of slightly water-soluble compounds from a light nonaqueous phase liquid pool. Water Resour. Res. 32 (4), 915-923.

Holocher, J., Peeters, F., Aeschbach-Hertig, W., Kinzelbach, W., Kipfer, R., 2003. Kinetic model of gas bubble dissolution in groundwater and its implications for the dissolved gas composition. Environ. Sci. Tecnol. 37 (7), 1337-1343.

Hutson, S.S., Barber, N.L., Kenny, J.F., Linsey, K.S. Lumia, D.S., Maupin, M.A., 2004. Estimated use of water in the United States in 2000. U.S. Geological Survey Circular 1268.

Johnson, R.L., Pankow, J.F., 1992. Dissolution of dense chlorinated solvents into groundwater. 2. source functions for pools of solvent. Environ. Sci. Technol. 26 (5), 896-901.

Khachikian, C., Harmon, T.C., 2000. Nonaqueous phase liquid dissolution in porous media: current state of knowledge and research needs. Transport Porous Med. 38, 3-28.

Kim, T.-J., Chrysikopoulos, C.V., 1999. Mass transfer correlations for nonaqueous phase liquid pool dissolution in saturated porous media. Water Resour. Res. 35 (2), 449-459.

Lee, K.Y., Chrysikopoulos, C.V., 2002. Dissolution of a well-defined trichloroethylene pool in saturated porous media: experimental results and model simulations. Water Res. 36 (15), 3911-3918.

Li, X., Yortsos, Y.C., 1995. Theory of multiple bubble growth in porous media by solute diffusion. Chem. Eng. Sci. 50 (8), 1247-1271.

Mackay, D.M., Cherry, J.A., 1989. Groundwater contamination: pump-and-treat remediation. Environ. Sci. Technol. 23 (6), 630-636.

MOE, 2004. Groundwater studies in Ontario: mapping a hidden treasure. Queen's Printer for Ontario.

Oostrom, M., Dane, J.H., Wietsma, T.W., 2006. A review of multidimensional, multifluid intermediate-scale experiments: nonaqueous phase liquid dissolution and enhanced remediation. Vadose Zone J. 5 (2), 570-598.

Pankow, J.F., Cherry, J.A., 1996. Dense Chlorinated Solvents and other DNAPLs in Groundwater. Waterloo Press, Portland, Oregon.

Roy, J.W., Smith, J.E., 2007. Multiphase flow and transport caused by spontaneous gas phase growth in the presence of dense non-aqueous phase liquid. J. Contam. Hydrol. 89, 251-269.

Sale, T.C., McWhorter, D.B., 2001. Steady state mass transfer from single-component dense nonaqueous phase liquids in uniform flow fields. Water Resour. Res. 37 (2), 393-404.

Satik, C., Li, X., Yortsos, Y.C., 1995. Scaling of single-bubble growth in porous media, Phys. Rev. E. 51 (4), 3286-3295.

Schwille, F., 1988. Dense chlorinated solvents in porous and fractured media. Lewis Publishers, Inc., Michigan.

Seagren, E.A., Moore, T.O., 2003. Nonaqueous phase liquid pool dissolution as a function of average pore water velocity. J. Environ. Eng. 129 (9), 786-799.

Seagren, E.A., Rittmann, B.E., Valocchi, A.J., 1994. Quantitative evalutation of the enhancement of NAPL-pool dissolution by flushing and biodegradation, Environ. Sci. Technol. 28 (5), 833-839.

Seagren, E.A., Rittman, B.E., Valocchi, A.J., 1999a. An experimental investigation of NAPL pool dissolution enhancement by flushing. J. Contam. Hydrol. 37, 111-137.

Seagren, E.A, Rittman, B.E., Valocchi, A.J., 1999b. A critical evaluation of the local-equilibrium assumption in modeling NAPL-pool dissolution. J. Contam. Hydrol. 39, 109-135.

Selker, J.S., Niemet, M., Mcduffie, N.G., Gorelick, S.M., Parlange, J.-Y., 2007. The local geometry of gas injection into saturated homogeneous porous media. Transport Porous Med. 68 (1), 107-127.

Sleep, B.E., Sykes, J.F., 1989. Modeling the transport of volatile organics in variably saturated media. Water Resour. Res. 25 (1), 81-92.

Statistics Canada, 2003. Human activity and the environment. Catalogue no. 16-201-XIE.

Stroo, H.F., Unger, M., Ward, C.H., Kavanaugh, M.C., Vogel, C., Leeson, A., Marqusee, J.A., Smith, B.P., 2003. Remediating chlorinated solvent source zones. Environ. Sci. Technol. 37 (11), 224A-230A.

Tillman, F.D. Jr., Smith, J.A., 2004. Design and laboratory testing of a chamber device to measure total flux of volatile organic compounds from the unsaturated zone under natural conditions. J. Contam. Hydrol. 75, 71-90.

Tsimpanogiannis, I.N., Yortsos, Y.C., 2002. Model for the gas evolution in a porous medium driven by solute diffusion. AIChE J. 48 (11), 2690-2710.

Tsimpanogiannis, I.N., Yortsos, Y.C., 2004. The critical gas saturation in a porous medium in the presence of gravity. J. Colloid Interface Sci. 270, 388-395.

USEPA, 1993. Evaluation of the likelihood of DNAPL presence at NPL sites. EPA/540R-93-073.

USEPA, 2003. The DNAPL remediation challenge: is there a case for source depletion? EPA/600/R-03/143.

USEPA, 2004. Site characterization technologies for DNAPL investigations. EPA/542-R-04-017

Wagner, G., Birovljev, A., Meakin, P., Feder, J., Jossang, T., 1997a. Fragmentation and migration of invasion percolation clusters: Experiments and simulations. Phys. Rev. E. 55 (6), 7015-7029.

Wagner, G., Meakin, P., Feder, J., Jossang, T., 1997b. Buoyancy-driven invasion percolation with migration and fragmentation. Physica A. 245, 217-230.

Wilkinson, D., 1984. Percolation model of immiscible displacement in the presence of buoyancy forces. Phys. Rev. A. 30 (1), 520-531.

Zogorski, J.S., Carter, J.M., Ivahnenko, Tamara, Lapham, W.W., Moran, M.J., Rowe, B.L., Squillace, P.J., Toccaline, P.L., 2006. The quality of our Nation's water's – volatile organic compounds in the Nation's ground water and drinking-water supply wells. U.S. Geological Survey Circular 1292.

Chapter 2

Mass flux from a non-aqueous phase liquid pool considering spontaneous expansion of a discontinuous gas phase

The contents of this chapter have been published as: Mumford, K.G., Smith, J.E., Dickson, S.E., 2008. Mass flux from a non-aqueous phase liquid pool considering spontaneous expansion of a discontinuous gas phase. *Journal of Contaminant Hydrology*, 98, 85-96.

Abstract

The partitioning of non-aqueous phase liquid (NAPL) compounds to a discontinuous gas phase results in the repeated spontaneous expansion, snap-off, and vertical mobilization of the gas phase. This mechanism has the potential to significantly affect the mass transfer processes that control the dissolution of NAPL pools by increasing the vertical transport of NAPL mass and increasing the total mass transfer rate from the surface of the pool. The extent to which this mechanism affects mass transfer from a NAPL pool depends on the rate of expansion and the mass of NAPL compound in the gas phase. This study used well-controlled bench-scale experiments under no-flow conditions to quantify for the first time the expansion of a discontinuous gas phase in the presence of NAPL. Air bubbles placed in glass vials containing NAPL increased significantly in volume, from a radius of 1.0 mm to 2.0 mm over 215 days in the presence of

tetrachloroethene (PCE), and from a radius of 1.2 mm to 2.3 mm over 22 days in the presence of trans-1,2-dichloroethene (tDCE). A one-dimensional mass transfer model, fit to the experimental data, showed that this expansion could result in a mass flux from the NAPL pool that was similar in magnitude to the mass flux expected for the dissolution of a NAPL pool in a two-fluid (NAPL and water) system. Conditions favouring the significant effect of a discontinuous gas phase on mass transfer were identified as groundwater velocities less than ~0.01 m/day, and a gas phase that covers greater than ~10% of the pool surface area and is located within ~0.01 m of the pool surface. Under these conditions the mass transfer via a discontinuous gas phase is expected to affect, for example, efforts to locate NAPL source zones using aqueous concentration data, and predict the lifetime and risk associated with NAPL source zones in a way that is not currently included in the common conceptual models used to assess NAPL-contaminated sites.

2.1 Introduction

The contamination of soil and groundwater by non-aqueous phase liquids (NAPLs) is a multi-billion dollar problem in North America (USEPA, 2003). Light non-aqueous phase liquids (LNAPLs), such as gasoline and diesel fuel, and dense non-aqueous phase liquids (DNAPLs), such as chlorinated solvents and creosote, are released to the subsurface through accidental spills and improper disposal practices. Once released, NAPL flow is controlled by gravitational, viscous, and capillary forces resulting in the formation of source zones above and below the water table that are characterized by complex combinations of residual ganglia and high-saturation pools located at capillary interfaces (Schwille, 1988). Since the aqueous solubility of many NAPLs is orders of magnitude above drinking water limits, these source zones represent a long-term threat to groundwater quality.

An understanding of the processes that control NAPL dissolution is essential for the location of NAPL source zones using aqueous concentration data, the design of many NAPL remediation technologies (Khachikian and Harmon, 2000), and the accurate

assessment of long-term risk due to source zone dissolution. Several detailed experiments conducted in two-fluid systems (NAPL and water) have lead to a better understanding of NAPL dissolution from both residual and pooled sources below the water table (Khachikian and Harmon, 2000; Oostrom et al., 2006). Although some studies considered mass transfer to and from a gas phase, most of these studies focused on transport via a continuous gas phase in the unsaturated zone, which resulted in transport of NAPL compounds upwards to the ground surface (e.g. Tillman and Smith, 2004) or downwards to the saturated zone (e.g. Sleep and Sykes, 1989; Conant et al., 1996).

The study of NAPL mass transfer in NAPL/water systems and in systems containing a continuous gas phase has lead to a significant improvement in our understanding of NAPL dissolution. However, by focusing on these two systems an important scenario for NAPL mass transfer has been overlooked: the mass transfer of NAPL in systems containing a discontinuous gas phase. Instead of resulting in the advective/dispersive transport of gaseous NAPL compound, as is the case for a continuous gas phase, mass transfer to a discontinuous gas phase may result in the expansion (Cirpka and Kitanidis, 2001) and subsequent mobilization (Tsimpanogiannis and Yortsos, 2004) of the gas phase. This will affect the hydraulic properties of the system (Amos and Mayer, 2006a), the concentration of other dissolved gases (Cirpka and Kitanidis, 2001), and the vertical mass transfer rate of volatile compounds (Amos and Mayer, 2006b).

The role of discontinuous gas phases in groundwater systems is receiving increased attention in the literature, particularly with respect to multi-component gases (e.g. Cirpka and Kitanidis, 2001; Holocher et al., 2003; Amos et al., 2005; Geistlinger et al., 2005; Amos and Mayer, 2006a, 2006b; Roy and Smith, 2007). The presence of a discontinuous gas phase is most often associated with groundwater in the vicinity of the water table where recharge or water table oscillations have lead to the entrapment of atmospheric gases (e.g. Ronen et al., 1989; Ryan et al., 2000; Williams and Oostrom, 2000).

However, a discontinuous gas phase could also be created by the biogenic production of gases from microbial populations in excess of solubility limits, particularly in systems where methanogenesis (e.g. Beckwith and Baird, 2001; Amos et al., 2005; Rosenberry et al., 2006) or dentitrification (e.g. Soares et al., 1987; Blicher-Mathiesen et al., 1998) occur. The formation of a discontinuous gas phase can also result from the application of remediation technologies such as direct gas injection (Fry et al., 1997), the degassing of supersaturated solutions (Fry et al., 1997), and the production of carbon dioxide during the reaction of permanganate ion with chlorinated hydrocarbons (e.g. Schroth et al., 2001). As discussed by Or and Tuller (2003), a discontinuous gas phase in porous media can persist indefinitely in the crevices of the solid grains as the curvature of the gas-liquid interface adjusts to balance the contraction and expansion forces based on the geometry, wettability, and surface roughness of the crevice in which the gas phase resides. Therefore, it is highly likely that discontinuous gas phases will be present in many situations where NAPL source zones exist.

Recent research shows that discontinuous gases play a role in the dissolution of NAPL source zones (Roy and Smith, 2007). Where a discontinuous gas phase is initially present to act as a "seed" above a NAPL pool, Roy and Smith (2007) showed for the first time that the partitioning of NAPL compound to the gas phase resulted in the repeated expansion, snap-off, and vertical mobilization of the gas phase. This cycle of spontaneous expansion and mobilization altered the distribution of gas, water and NAPL in the source zone, increased the mass transfer rate of NAPL compound from the source zone, and altered the aqueous NAPL compound concentration profile above the pool compared to what was expected based on an existing dissolution model for NAPL/water systems. These observations suggest that transient changes in source zone morphology and mass transfer processes can occur for NAPLs in the presence of discontinuous gas phases. These changes are not currently considered in common conceptual models of NAPL-contaminated sites and will complicate efforts to locate, characterize, and model the dissolution of NAPL source zones.

The magnitude of the effect that an expanding discontinuous gas phase has on the mass transfer from a NAPL source zone will depend on the rate of expansion of the gas phase and the concentration of NAPL compound in that gas phase. Rapidly expanding gas phases will mobilize more frequently and, if they contain a significant mass of NAPL compound, will result in a higher average mass flux of NAPL compound vertically away from the NAPL source. No information exists in the current literature concerning the expected expansion rate of a discontinuous gas phase in the presence of NAPL, or the potential effect of that expanding gas phase on the overall mass transfer from a NAPL source. Therefore, the objectives of this study were to 1) quantify the expansion of a discontinuous gas phase in the presence of NAPL, and 2) develop a screening-level modeling tool to provide insight into the general conditions under which this mechanism may be significant. The second objective was met by deriving an analytical model for the expansion of a discontinuous phase under effective steady-state conditions, which was used to compare the magnitude of the mass transfer from a NAPL pool via a discontinuous gas phase to that expected via advection and dispersion in a strictly NAPL/water scenario.

Bench-scale experiments were used to measure the expansion of a discontinuous gas phase above a NAPL pool in a diffusion-controlled (no-flow) system for both tetrachloroethene (PCE) and trans-1,2-dichloroethene (tDCE). These NAPLs represent common groundwater contaminants (Moran et al., 2007) and are expected to result in spontaneous gas phase growth in porous media at different rates due to their significantly different vapour pressures (Roy and Smith, 2007).

2.2 Conceptual Model

The analytical model derived in this study is based on the theory presented by Cirpka and Kitanidis (2001) for the partitioning of multiple dissolved gases to a discontinuous gas phase. This theory has been implemented in several numerical solutions (e.g. Cirpka and Kitanidis, 2001; Geistlinger et al., 2005; Amos and Mayer, 2006a). However, for the

assessment of NAPL-contaminated sites it is important to determine if mass transfer via the repeated expansion, snap-off, and vertical mobilization of a discontinuous gas phase is significant prior to conducting detailed numerical simulations. If not, then detailed numerical simulations are not warranted. The analytical solution derived in this study will help to determine the general conditions where this mechanism may be significant, and serve as a screening-level modeling tool.

The analytical solution is derived based on the following assumptions: 1) the transport of all components to the gas phase occurs at an effectively steady rate, which leads to an effectively constant composition of the gas phase at later-time, 2) the partial pressure of compounds in the gas phase is in local equilibrium with the aqueous concentration at the gas-liquid interface, 3) the transport of NAPL compounds from the surface of the NAPL pool to the gas-liquid interface is described by the one-dimensional diffusion equation, and 4) the fragmentation of a gas cluster following snap-off produces two clusters with equal compositions. The physical context of these assumptions is discussed in the presentation of the conceptual model below.

The conceptual model for the expansion, snap-off, and vertical mobilization of a discontinuous gas phase above a NAPL pool due to the partitioning of NAPL and other dissolved gases is illustrated in Figure 2.1. An approximately uniform distribution of discontinuous gas clusters is assumed to exist above the entire surface of a horizontally extensive NAPL pool (Figure 2.1a), and lie within the concentration boundary layer created by the dissolution of the NAPL. The term gas cluster here refers to a discontinuous gas phase that occupies one or more pore bodies. Initially, these gas clusters do not contain any gas-phase NAPL compound and are in equilibrium with the dissolved gases in the surrounding aqueous phase. Therefore, a concentration gradient exists between the dissolved NAPL in the surrounding groundwater and the gas-liquid interface, which results in mass transport from the pool surface to the gas-liquid interface.

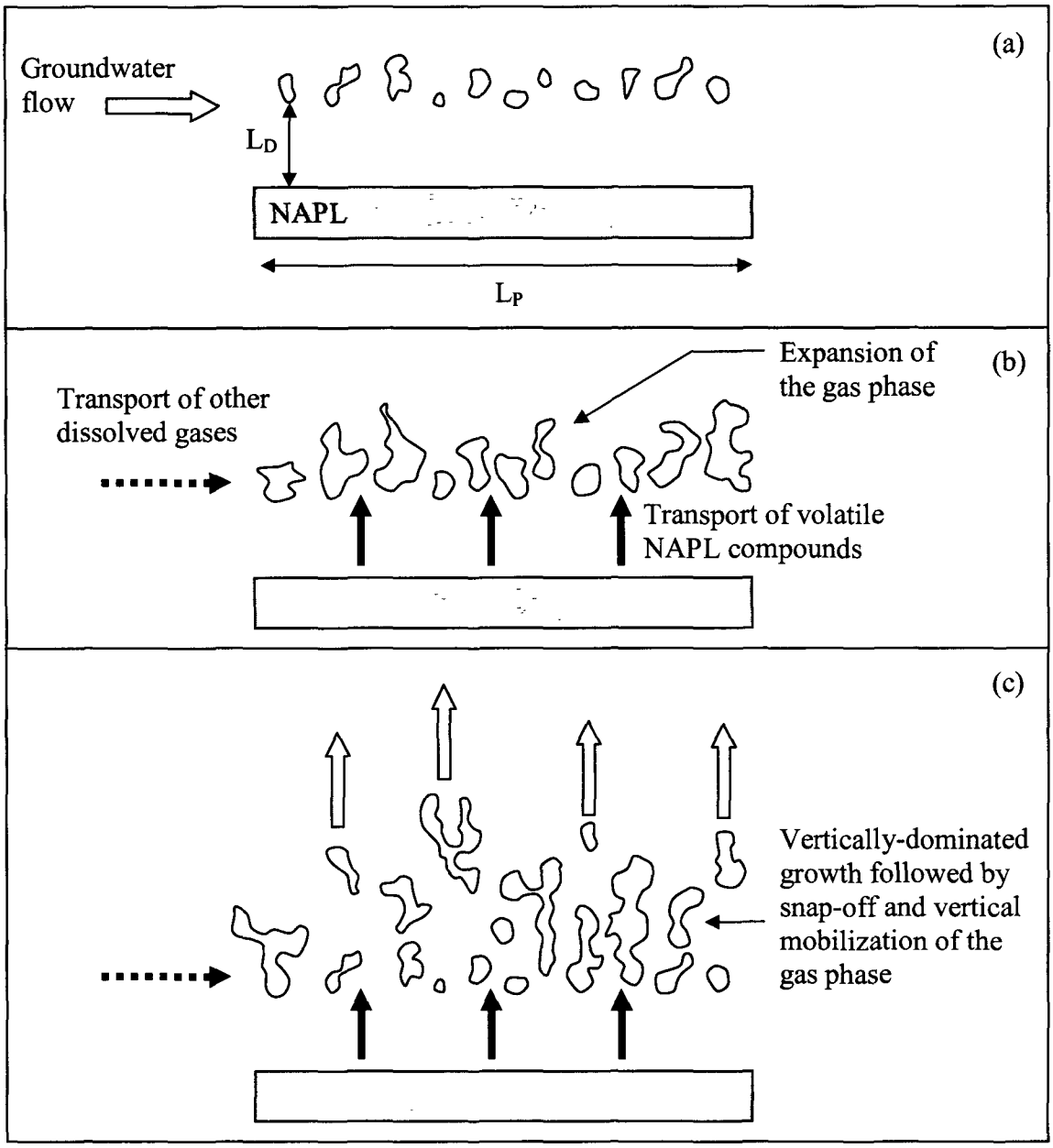

Figure 2.1. Conceptual schematic for the partitioning of NAPL compounds and other dissolved gases to a discontinuous gas phase above a NAPL pool showing (a) the initial condition of NAPL-free gas clusters uniformly distributed above the pool surface, (b) the steady transport of volatile NAPL and other dissolved gases resulting in the expansion of the gas phase, and (c) continued vertical expansion and snap-off of the gas phase, which results in a vertically mobile upper gas cluster and a lower gas cluster of equal composition that is able to undergo repeated expansion.

The partitioning of NAPL compound to the gas phase increases the volume of the gas phase while lowering the partial pressure of the other gases in the gas cluster according to the theory for the partitioning of multiple components to a discontinuous gas phase (Cirpka and Kitanidis, 2001). The lower partial pressure of the other gases creates concentration gradients from the bulk aqueous phase to the gas-liquid interface, resulting in the mass transport of those dissolved gases to the interface and continued expansion of the gas phase (Figure 2.1b). The composition of the gas phase achieves an effective steady-state relatively rapidly, where the partial pressure of each of the dissolved gases and the NAPL compound is effectively constant at a value lower than that which would be in equilibrium with the bulk aqueous phase. This effective steady-state results in the steady transport of all volatile species to the discontinuous gas phase.

At all times the pressure in the discontinuous gas phase is controlled by Dalton's law and the capillary pressure (i.e. the difference in pressure between the non-wetting and wetting fluids) as

$$P_g = P_w + P_c = \sum P_i^g \tag{2.1}$$

where P_g is the gas pressure, P_w is the bulk fluid pressure, P_c is the capillary pressure, and P_i^g is the partial pressure of compound i in the gas phase. The capillary pressure is given by the Young-Laplace equation

$$P_c = \sigma\left(\frac{1}{r_1} + \frac{1}{r_2}\right) = \frac{2\sigma}{r} \tag{2.2}$$

where σ is the gas-liquid interfacial tension, r_1 and r_2 are the principal radii of curvature of the gas-liquid interface, and r is the effective radius of curvature of the gas-liquid interface. The partial pressure of each compound in the gas phase is given by Henry's law

$$P_i^g = K_{Hi} C_i \tag{2.3}$$

where K_{Hi} is the Henry's law coefficient for compound i, and C_i is the aqueous phase concentration of compound i. This theory for the partitioning of multiple dissolved gases to discontinuous gas phases has been applied to the transport of partitioning tracers for the quantification of entrapped gas (Cirpka and Kitanidis, 2001), the dissolution of atmospheric gases from entrapped air (Holocher et al., 2003), the dissolution of bubbles that remain following gas injection (Geistlinger et al., 2005), and the transport of methane at a petroleum hydrocarbon contaminated site (Amos and Mayer, 2006a). It shows that where the sum of the partial pressures that would be in equilibrium with the concentrations of dissolved gases in the bulk aqueous phase is less than the gas pressure, a discontinuous gas phase will dissolve. However, where this sum is greater than the gas pressure, a discontinuous gas phase will expand. This expanding condition is expected for discontinuous gas phases present at NAPL-contaminated sites, where the volatile NAPL compounds contribute an additional partial pressure above the other dissolved gases present in the surrounding groundwater.

The rate of change in the pressure and volume of the gas phase due to the mass transfer of all volatile species is described by the ideal gas law under isothermal conditions

$$\frac{dn_t}{dt} = \frac{1}{RT} \frac{d\left(P_g V_g\right)}{dt} \tag{2.4}$$

where n_t is the total number of moles in the gas phase, t is time, R is the gas constant, T is the temperature, and V_g is the volume of the gas phase. For discontinuous gas phases in porous media the resulting changes in pressure and volume depend on the location of the gas-liquid interface within the pore geometry. If the radius of curvature of the gas phase increases with increasing volume (i.e. gas expansion within a partially gas-filled

pore body) then the change will be dominated by the change in volume at approximately constant pressure, assuming that $P_w >> P_c$. This corresponds to the pore-filling step described by Li and Yortsos (1995). If the radius of curvature of the gas phase decreases with increasing volume (i.e. gas phase pinned at pore throats) then the change will be dominated by an increase in pressure at approximately constant volume. This corresponds to the pressurization step described by Li and Yortsos (1995). A gas cluster will initially expand as a pore-filling step until it encounters a pore throat, at which time it will pressurize. If the partial pressure of the NAPL compound in equilibrium with the bulk aqueous phase is less than the displacement pressure of all the adjacent pore throats then expansion of the gas phase in that pore will stop. If the partial pressure of the NAPL compound is sufficiently large, then the displacement pressure will be exceeded and the gas phase will expand to fill or partially-fill an adjacent pore body.

Continued expansion of the gas cluster to multiple pore bodies will result in vertically-dominated growth in relatively coarse media (Dominguez et al., 2000) and/or the snap-off and vertical mobilization of gas clusters (Roy and Smith, 2007) as buoyancy forces exceed capillary forces (Tsimpanogiannis and Yortsos, 2004) (Figure 2.1c). A fragmented gas cluster will retain the same effective steady-state composition, with the upper cluster moving away from the pool surface and the lower cluster being able to undergo repeated expansion events. Under this conceptual model, the initial condition of a NAPL-free gas cluster is only true for expansion prior to the first snap-off event. For all repeated expansion events the gas cluster maintains the same effective steady-state composition.

The mechanism of repeated expansion, snap-off, and vertical mobilization will result in the partitioning of NAPL compound from the mobilized gas cluster to the groundwater well above a NAPL pool where aqueous concentrations of NAPL compound in the bulk aqueous phase are lower than those at the gas-liquid interface. Consequently, the mass transfer of NAPL compound to a discontinuous gas phase will result in greater vertical

transport of NAPL mass compared to the transport by aqueous-phase dispersion processes alone. This can result in greater vertical spreading of the aqueous plume above the pool and an increased rate of mass transfer from the surface of the pool (Roy and Smith, 2007).

2.3 Laboratory Experiments

The expansion of a discontinuous gas phase above a NAPL pool was measured using a small-scale experiment under no-flow conditions. The experimental set-up consisted of an inverted 1.5-mL vial inside a 20-mL vial, which was open to the atmosphere, as shown in Figure 2.2. The experiment was conducted without porous media to allow clear visualization of the gas phase and quantification of the gas-phase volume by image analysis. This set-up most closely matches the pore-filling step described above, where the radius of curvature of the gas phase increases with increasing volume.

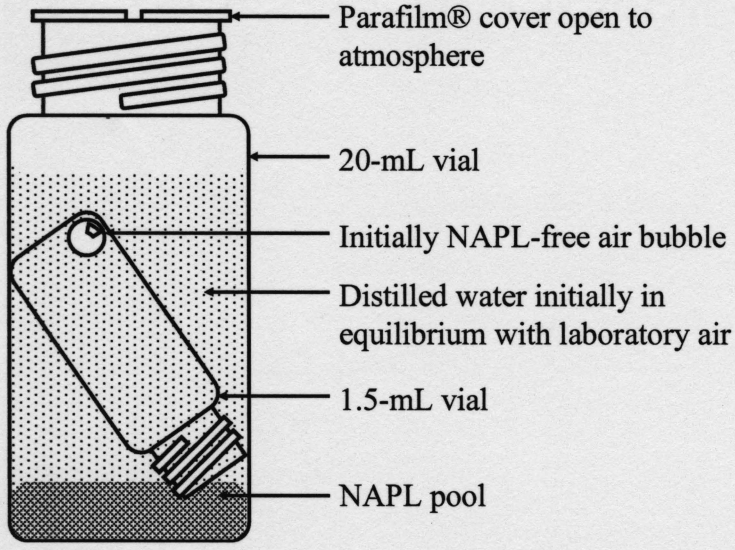

Figure 2.2. Set-up for PCE and tDCE experiments. Control experiments did not contain a NAPL pool.

A 5±1 μL air bubble was injected into each 1.5-mL vial, which was filled with distilled water. A NAPL pool was created by placing 1 mL of reagent grade PCE (Alfa Aesar, 99%) or tDCE (Alfa Aesar, 98%) dyed with 100 mg/L of Sudan 4 (Acros Organics) in the

20-mL vial. The thickness of the NAPL pool was such that the inner vial was open to both the aqueous and the NAPL phases (Figure 2.2). Control experiments were created by placing an additional 1 mL of distilled water in place of the NAPL. The water used was in equilibrium with laboratory air at room temperature (~25°C). The 20-mL vial was left open to the atmosphere through a small hole in a Parafilm® cover to allow the entry of atmospheric gases to the system while minimizing evaporative losses. Allowing atmospheric gases to enter the system was critical to the success of the experiment. Without the additional mass transfer of other dissolved gases to the bubble the expansion of the gas phase would cease as it became saturated with NAPL compound vapour. The NAPL experiments were conducted in triplicate and the control experiments were conducted in duplicate. Photographs of all experiments were taken using a hand-held digital camera (Canon A75 or Nikon P4) over a period of 215 days for the PCE and control experiments, and 22 days for the tDCE experiments. Air bubble radii were measured by image analysis using the software ImageJ (http://rsb.info.nih.gov/ij/).

Interfacial tensions used for the modeling of the gas-phase expansion in the NAPL experiments were measured using a drop volume tensiometer (Lauda TVT-1). The interfacial tension of interest was that which exists between aqueous and gas phases saturated with PCE or tDCE, which can be significantly lower than the air-water interfacial tension in an uncontaminated system (e.g. Hofstee et al., 1998; Oostrom et al., 2003). Saturated aqueous solutions of PCE and tDCE were created by placing 0.5 mL of NAPL in a 12 mL vial filled with distilled water, mixing with a vortex mixer, and allowing the solution to come to equilibrium over a period of 4 days. During measurement, drops of these aqueous solutions were formed in a sealed cuvette containing 0.5 mL of PCE or tDCE NAPL that had been allowed to come to equilibrium in the headspace of the cuvette for 1 to 4 hours. 68 measurements were conducted for the PCE-saturated system at drop formation times of 37 to 138 s, and 40 measurements were conducted for the tDCE-saturated system at drop formation times of 33 to 131 s, with 4 measurements at each drop formation time.

2.4 Model Development

2.4.1 Gas-phase Expansion

The rate of change in the total number of moles in the gas phase can be calculated as

$$\frac{dn_t}{dt} = \sum_i \frac{dn_i}{dt} \tag{2.5}$$

where n_i is the number of moles of compound i in the gas phase. This approach is consistent with existing multi-component models for variable-volume discontinuous gas phases (e.g. Cirpka and Kitanidis, 2001; Holocher et al., 2003; Geistlinger et al., 2005; Amos and Mayer, 2006a), which model the transport of each component. Alternatively, the rate of change in the total number of moles in the gas phase can be expressed as

$$\frac{dn_t}{dt} = \frac{d}{dt}\left(\frac{n_i}{y_i}\right) = \frac{1}{y_i}\frac{dn_i}{dt} + n_i \frac{d}{dt}\left(\frac{1}{y_i}\right) \tag{2.6}$$

where y_i is the mole fraction of compound i in the gas phase. Modeling the initial, rapid approach to steady-state using (2.6) is more complex than using numerical solutions that employ (2.5) due to the challenge of calculating the second term on the right-hand side. However, after the initial early-time growth of the gas phase, effective steady-state conditions are expected to dominate the behaviour of expanding gas phases above a NAPL pool at NAPL-contaminated sites. Under these conditions the transport of all volatile components to the gas phase is expected to be effectively steady, and the mole fraction of each component in the gas phase can be treated as effectively constant. Therefore, the right-hand side of (2.6) reduces to a single term involving the change in moles of a single compound and the mole fraction of that compound in the gas phase. Using this approach, the transport of any one component can be used to describe the total

volume change in the multi-component system. For the one-dimensional, dispersive, vertical transport of volatile components to the gas phase, this is given by

$$\frac{dn_t}{dt} = \frac{1}{y_i}\frac{dn_i}{dt} = \frac{1}{y_i}\frac{D_{i,z}A_D}{L_D}\left(C_{i,L} - C_{i,g}\right) \tag{2.7}$$

where L_D is the mass transfer path length, $C_i(z=L_D)=C_{i,L}$ is the aqueous concentration at the far boundary, $C_i(z=0)=C_{i,g}$ is the aqueous concentration at the gas-liquid interface, z is the vertical distance away from the gas-liquid interface, $D_{i,z}$ is the vertical dispersion coefficient (assumed equal to the molecular diffusion coefficient in these experiments), and A_D is the area available for mass transfer. For the purpose of this study, i was taken to be PCE or tDCE in the NAPL experiments, and dissolved air in the control experiments.

Equation (2.7) is advantageous since it can be used to derive an analytical solution for the expansion of a discontinuous gas phase above a NAPL pool. This will serve as a screening-level modeling tool for assessing the general conditions under which this mechanism may be significant at NAPL-contaminated sites, where the information required for more detailed numerical models (Cirpka and Kitanidis, 2001; Holocher et al., 2003; Geistlinger et al., 2005; Amos and Mayer, 2006a) may not be available and the effort required for detailed simulation may not be warranted.

The linear concentration gradient used in this expression is different from those used to derive expressions for the expansion of a discontinuous gas phase in free solution (e.g. Epstein and Plesset, 1950) or in the application of solution gas-drive (Li and Yortsos, 1995; Firoozabadi and Kashchiev, 1996; Tsimpanogiannis and Yortsos, 2002), which assume a radially symmetric concentration field and, therefore, employ a one-dimensional radial diffusion model. Such models would be more applicable to the

expansion of a discontinuous gas phase in a NAPL residual source zone or a dissolved NAPL compound plume.

Combining (2.1) – (2.4) and (2.7), assuming that the discontinuous gas phase is spherical ($r=r_g$), and that the bulk fluid pressure and interfacial tension are constant, gives the differential equation for the gas-phase radius as

$$\frac{y_i P_w r_g^{\,3} + \frac{4}{3} y_i \sigma r_g^{\,2}}{\left(P_{i,L} - y_i P_w\right) r_g - 2 y_i \sigma} \frac{dr_g}{dt} = \frac{D_{i,z} A_D RT}{4\pi L_D K_{Hi}} \tag{2.8}$$

where $P_{i,L}$ is the partial pressure in equilibrium with $C_{i,L}$, and r_g is the radius of the gas phase. Integrating between $r_g(t=0)=r_{g0}$ and $r_g(t)=r_g$ gives the analytical expression for the gas-phase radius as

$$\begin{aligned} &\frac{\beta_1 \beta_2^{\,3}}{3}\left(r_g^{\,3} - r_{g0}^{\,3}\right) + \frac{\beta_3 \beta_2^{\,2}}{2}\left(r_g^{\,2} - r_{g0}^{\,2}\right) - \beta_2 \beta_3 \beta_4 \left(r_g - r_{g0}\right) \\ &+ \beta_3 \beta_4^{\,2} \ln\left(\frac{\beta_2 r_g + \beta_4}{\beta_2 r_{g0} + \beta_4}\right) = \frac{\beta_2^{\,4} D_{i,z} A_D RT}{4\pi L_D K_{Hi}} t \end{aligned} \tag{2.9a}$$

where

$$\beta_1 = y_i P_w \tag{2.9b}$$

$$\beta_2 = P_{i,L} - y_i P_w \tag{2.9c}$$

$$\beta_3 = \frac{2}{3} y_i \sigma \left(2P_{i,L} + y_i P_w\right) \tag{2.9d}$$

$$\beta_4 = -2 y_i \sigma \tag{2.9e}$$

2.4.2 Estimated Mass Flux from a NAPL Pool

An expression for the mass flux of NAPL compound from the pool surface to the discontinuous gas phase is derived by taking *i* to be the NAPL compound of interest, dividing (2.7) by the area of the NAPL pool, substituting (2.3), and assuming that C_L=C_S at the surface of the NAPL pool to give

$$M_{gas} = \frac{D_z A_D C_S}{L_D A_P}\left(1 - \frac{P_g^{\,n}}{P^{vp}}\right) \tag{2.10}$$

where M_{gas} is the mass flux from the NAPL pool to the discontinuous gas phase, A_P is the surface area of the NAPL pool, C_S is the aqueous solubility of the NAPL compound, $P_g^{\,n}$ is the partial pressure of NAPL in the gas phase, and P^{vp} is the vapour pressure of the NAPL in equilibrium with C_S. M_{gas} describes the steady-state, area-averaged vertical mass transfer of NAPL compound from the surface of the pool to the first gas-liquid interface encountered above the pool surface. Once transported to the gas-liquid interface, this NAPL mass will partition to the gas phase and be transported away from the NAPL pool by a vertically mobile gas phase, where it can partition to the groundwater well above the pool surface. $P_g^{\,n}$ is assumed here to be constant, which results in the steady transport of NAPL mass to the gas phase. This is not true during the initial expansion of the gas phase prior to the first snap-off event when the gas phase is initially NAPL-free, but it is a reasonable approximation for the expansion that occurs between all other snap-off events, which result from the fragmentation of a gas cluster. Although the transport of mass to the gas phase is steady the mass transport away from the area immediately above the NAPL pool will be periodic as the gas phase undergoes repeated periods of expansion followed by snap-off and mobilization (Roy and Smith, 2007). The average mass transfer at steady-state, however, will be controlled by the transport of NAPL compound to the gas-liquid interface given by (2.10). This study makes no attempt to model the transport of NAPL mass away from the area immediately

above the surface of the NAPL pool, which will depend strongly on the buoyancy- and capillary-driven movement of the mobilized gas phase.

The magnitude of the mass flux described by (2.10) was compared to the theoretical mass flux from a NAPL pool expected to result from steady horizontal advection and vertical dispersion in a strictly NAPL/water scenario. This theoretical mass flux is given by (Johnson and Pankow, 1992)

$$M_{NAPL/water} = 2\theta C_S \sqrt{\frac{D_z v}{\pi L_P}} \tag{2.11}$$

where $M_{NAPL/water}$ is the mass flux from the NAPL pool expected in a NAPL/water scenario, θ is the porosity of the porous medium, L_P is the length of the pool in the direction of groundwater flow, and v is the pore-water velocity.

Equations (2.10) and (2.11) each assume that the vertical transport of NAPL mass occurs via transverse vertical dispersion. In (2.11) the vertical concentration gradient is controlled by advection and dispersion processes that create a concentration boundary layer, which changes in height along the pool surface in the direction of flow (e.g. Johnson and Pankow, 1992; Chrysikopoulos et al., 2003). In (2.10) the vertical concentration gradient is controlled by the buoyant transport of mobilized gas clusters and the competitive partitioning of multiple volatile species (Cirpka and Kitanidis, 2001) to the discontinuous gas phase, in addition to advection and dispersion processes. The buoyant transport of gas-phase mass limits the mass that is available for aqueous advective transport further along the pool and the partitioning of multiple species can result in lower aqueous concentrations than would be expected at similar distances in a strictly NAPL/water scenario due to local equilibrium with gas-phase partial pressures. The cumulative effect of these processes on the vertical concentration gradient is not currently known. Therefore, to allow an assessment of the magnitude of the mass

transfer due to an expanding discontinuous gas phase, the concentration gradient (bracketed term on the right-hand side of (2.10)) is defined using a representative value of P_g^n.

The two magnitudes of the mass transfers described by (2.10) and (2.11) were compared using the dimensionless expression

$$\frac{M_{gas}}{M_{NAPL/water}} = \frac{\sqrt{\pi}}{2\theta} A^* \left(1 - \frac{P_g^n}{P^{vp}}\right) \sqrt{\frac{1}{L^* Pe_z}} \tag{2.12}$$

where $A^*=A_D/A_P$ is the fraction of NAPL pool area available for mass transfer to the discontinuous gas phase, $L^*=L_D/L_P$ is the ratio of the dispersive mass transfer path length to the advective mass transfer path length, and $Pe_z=vL_D/D_z$ is the transverse vertical Peclet number.

2.5 Results and Discussion

2.5.1 Interfacial Tension Measurements

Great care was taken to measure the gas-liquid interfacial tension for aqueous and gas phases saturated with PCE or tDCE, and the results are shown in Table 2.1. These equilibrium gas-liquid interfacial tension values can have a significant effect on the behaviour of unsaturated systems (e.g. Hofstee et al., 1998; Oostrom et al., 2003), but to the authors' best knowledge directly measured values do not appear previously in the literature for many compounds, including PCE and tDCE. The gas-liquid interfacial tension values of 70.0±0.2 mN/m and 64.9±0.2 mN/m for PCE and tDCE, respectively, are higher than what might be expected based on literature values of other similar NAPLs such as carbon tetrachloride (Oostrom et al., 2003) or by approximations based on the application of Antonow's rule (Adamson, 1990). However, Hofstee et al. (1998) report the drainage of 391 mL of water from a fine sand following the emplacement of PCE,

which they attribute to a decrease in the air-water interfacial tension due to PCE contamination. Taking the height of the tension-saturated zone in their fine sand to be 40

Table 2.1. Parameter values for modeling gas phase expansion and dissolution

Parameter	All experiments		
Area for diffusion (mm^2)	80		
Diffusive path length (mm)	30		
Depth of water above gas phase (mm)	6		
Atmospheric pressure (Pa)	$1.0x10^5$		
Temperature (K)	298		
Gas constant (L·atm/mol·K)	0.08206		
	PCE	tDCE	Control
Aqueous diffusion coefficient (m^2/s)[1,2]	$1x10^{-9}$	$1x10^{-9}$	$2x10^{-9}$
Henry's Law coefficient ($atm·m^3/mol$)[3,4]	0.0174	0.00916	1.2826
Vapour pressure (Pa)[3]	$2.5x10^3$	$4.2x10^4$	$1.0x10^5$
Interfacial tension (mN/m)	70.0±0.2	64.9±0.2	72
Average initial gas-phase radius (mm)	1.0	1.2	1.1
Mole fraction in gas phase	$2.5x10^{-2}$	$4.1x10^{-1}$	1

[1]PCE and tDCE values calculated using the Wilke-Chang equation (Perry et al., 1997)
[2]air value from Epstein and Plesset (1950)
[3]PCE and tDCE values from Pankow and Cherry (1996)
[4]air value from Perry et al. (1997)

cm based on their data, and the decrease in height to be 1.1 cm based on the volume of water drained and the physical properties of the cell (tank dimensions 1.7 m x 1.0 m x 0.05 m; fine sand porosity of 0.406), the change in air-water interfacial tension can be approximated as decreasing from 72 mN/m to 70 mN/m. This is in excellent agreement with our directly measured result.

2.5.2 Expansion of the Discontinuous Gas Phase

Expansion of the discontinuous gas phase above a PCE and a tDCE pool is shown in Figure 2.3. Only one vial each of the NAPL and control experiments are shown for clarity, and show results typical of replicate experiments. Visual inspection of the images clearly shows the expansion of the gas phase in the vials containing PCE and tDCE, with expansion in the presence of tDCE occurring at a much faster rate. This expansion is consistent with the theory presented above for the partitioning of multiple volatile

compounds to a discontinuous gas phase. If only a single compound was being transported to the interface and partitioning to the gas phase, that compound would

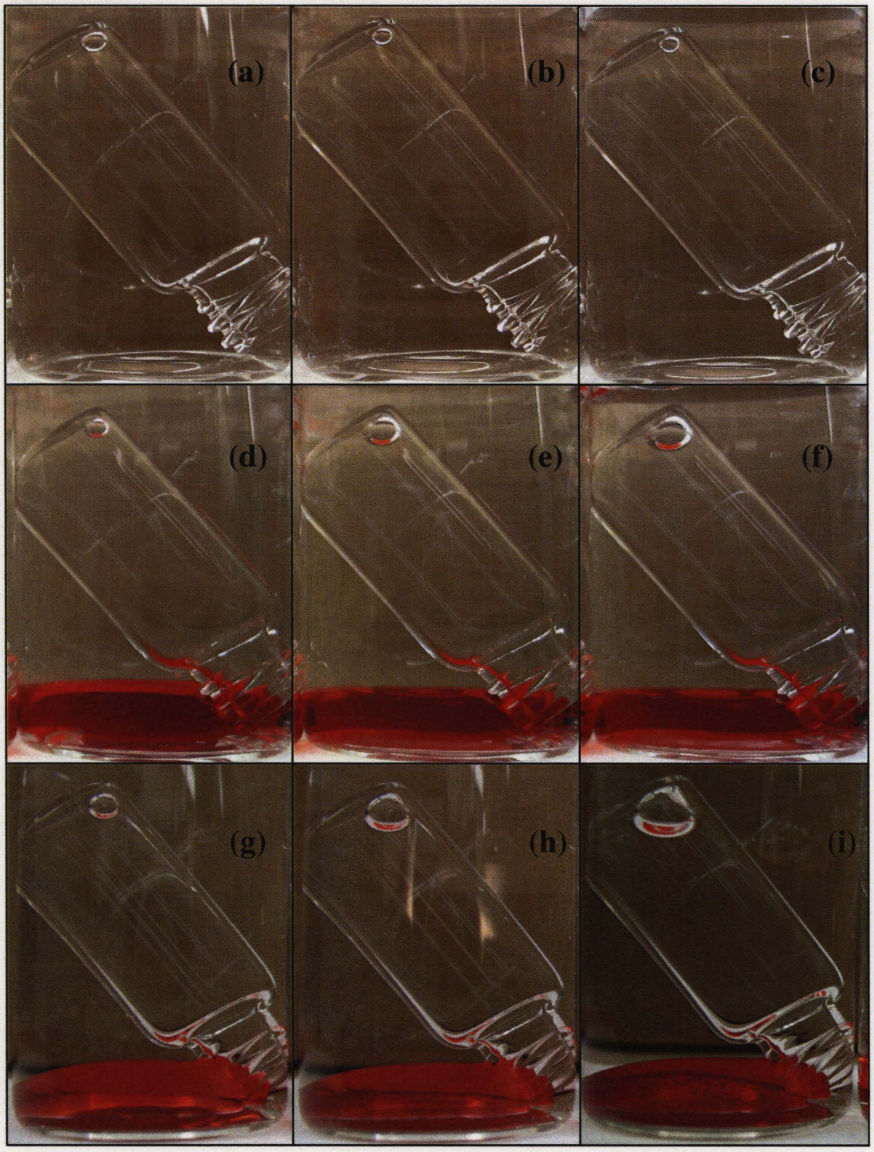

Figure 2.3. Images of control experiments at (a) 0 days, (b) 124 days, and (c) 215 days; PCE experiments at (d) 0 days, (e) 124 days, and (f) 215 days; and tDCE experiments at (g) 0 days, (h) 10 days, and (i) 22 days. Note that the red colour observed on the bottom shoulder of the inner vial and the lower surface of the gas bubble in the PCE and tDCE experiments is caused by reflection from the dyed NAPL pool and is not indicative of NAPL on these surfaces.

rapidly reach thermodynamic equilibrium and expansion of the gas phase would stop. These results also show that the mechanism of gas-phase expansion due to the mass transfer of NAPL compounds does not require NAPL-gas contact. Therefore, the mechanism is relevant in the vicinity of pools, residuals, and dissolved plumes, as suggested by Roy and Smith (2007).

The gas-phase radius is plotted versus time in Figure 2.4 as the average of replicate experiments. The average gas-phase radius increased from 1.0 mm to 2.0 mm in the PCE experiments over 215 days, and increased from 1.2 mm to 2.3 mm in the tDCE experiments over 22 days. The average gas-phase radius decreased from 1.1 mm to 0.8 mm in the control experiments over 215 days. The decrease in the gas-phase radius in the control experiments is expected since the laboratory air in the initial bubble is subjected to a higher pressure (i.e. the sum of hydrostatic and capillary pressures) and is thereby out of equilibrium with the surrounding water, which is in equilibrium with the atmosphere via the opening in the vial top. Therefore, a concentration gradient exists resulting in mass transfer to the bulk aqueous phase and the dissolution of the gas phase.

2.5.3 Modeling Gas-Phase Expansion

Equation (2.9) was used to model the data in Figure 2.4 using the parameter values listed in Table 2.1. Image analyses were used to estimate A_D and L_D, from the cross-sectional area of the inner vial and distance from the pool surface to the bubble. The atmospheric pressure was taken to be 10^5 Pa based on barometric pressure data available from Environment Canada, and the ambient temperature was taken to be 25 °C. Measurements of the water depth above the gas phase were used to estimate P_w, and $P_{i,L}$ was assumed to be equal to the NAPL vapour pressure. The control experiments were modeled using a composite dissolved air as the only volatile compound, and the PCE and tDCE experiments were modeled assuming the aqueous phase contained both dissolved air and the NAPL compound. The mole fraction of the controlling compound was taken as y_i=1 for the control experiments, and was used as the only fitting parameter for the PCE and tDCE experiments. The interfacial tension for the PCE-saturated and tDCE-saturated

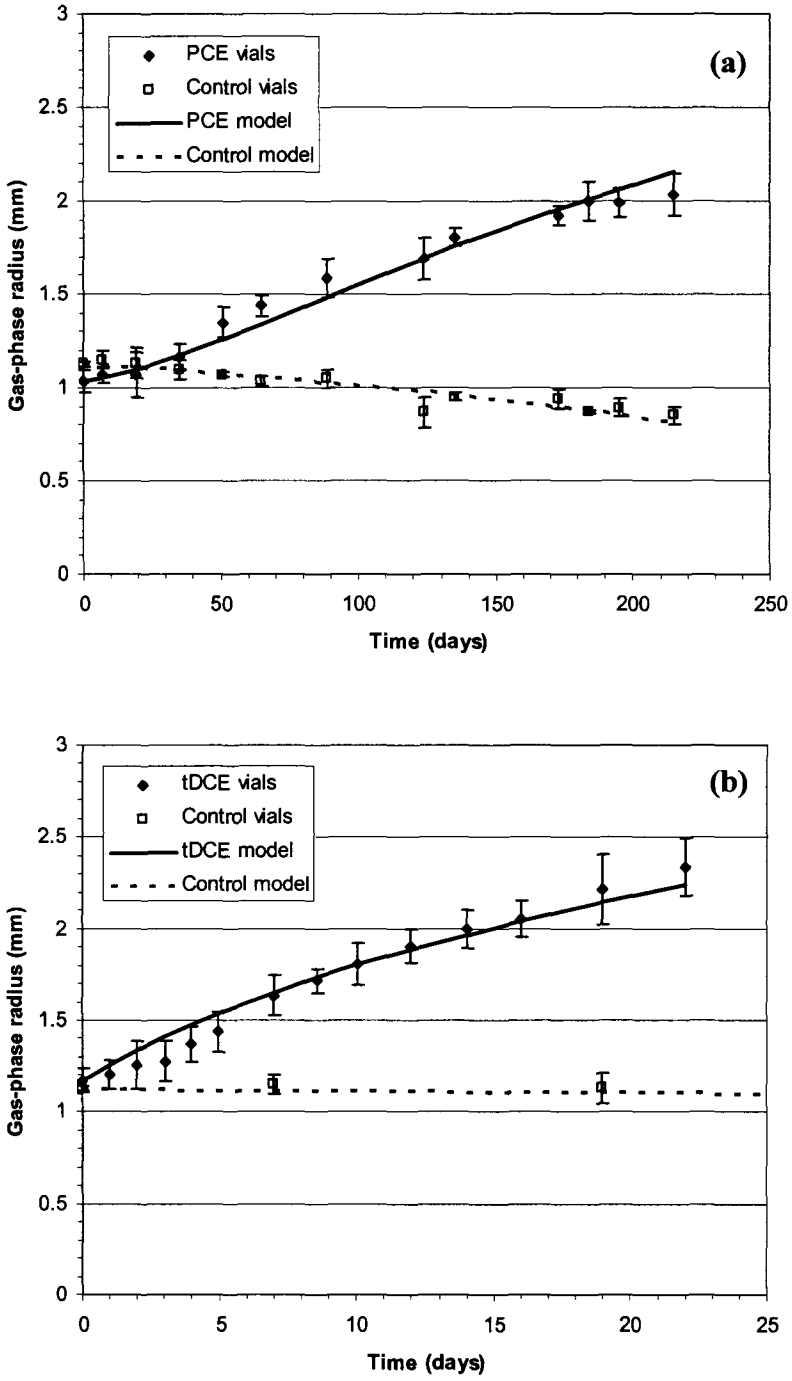

Figure 2.4. Gas-phase radius in the (a) PCE and control, and (b) tDCE and control experiments. The symbols represent average values measured by image analysis and the error bars represent one standard deviation based on replicate experiments. The lines represent the best-fit to the data using the one-dimensional linear diffusion mass transfer model (equation (2.9)).

systems were measured as described in section 2.3, and all other parameters were based on literature values (Table 2.1).

Equation (2.9) fit the data from the control experiments well without the use of any fitting parameters, and fit the data from the PCE and tDCE experiments well by using y_i as a fitting parameter. The good fit of the model to the control experiments indicates that a one-dimensional linear diffusion model is appropriate for the geometry of this system. Efforts to model these data using a radially symmetric mass transfer model (data not shown) resulted in the under prediction of the gas phase volume with time. The good fit of the model to the PCE and tDCE experiments supports the assumption of the steady transport of all other dissolved gases to the gas phase, which leads to an effectively constant mole fraction in the gas phase. The best fit to the PCE and tDCE experiment data, defined by the minimization of the sum of squared residuals, was obtained using y_i=2.5x10^{-2} and y_i=4.1x10^{-1} in (2.9), respectively. These best-fit mole fractions represent partial pressures of PCE and tDCE of 99.9% and 99.6% of the NAPL vapour pressures, respectively. Therefore, under the conditions of this study the concentrations of NAPL compound in the expanding discontinuous gas phase are very near saturation. However, they remain below saturation values due to the competitive partitioning of the other dissolved gases.

The difference in the shapes of the PCE and tDCE curves in Figure 2.3 is attributed to the lower interfacial tension in the tDCE experiments, which contributes to more rapid expansion of the gas phase at early time when the bubble volumes are small and capillary forces contribute more substantially to the total pressure of the gas phase. The over prediction of the gas-phase radius at early time (less than 5 days) for the tDCE experiments is attributed to the initial diffusion of the NAPL compound from the surface of the pool to the gas-liquid interface, since the initial condition of NAPL-free water is not considered in the development of (2.8). Specifically, at early time the gas phase contains very little NAPL compound and the interfacial tension of the gas-liquid interface

is expected to be closer to the surface tension of water (72 mN/m) than the value of 64.9 mN/m measured for the tDCE-saturated system. This leads to a higher gas-phase pressure and slower growth, as indicated by the flatter portion of the data at early time. The transient change in interfacial tension required to reproduce this behaviour is not included in (2.8), which assumes constant interfacial tension. Modeling of the initial approach to an effective steady-state would require the modeling of each volatile component. This could be accomplished using existing multi-component models (Cirpka and Kitanidis, 2001; Holocher et al., 2003; Geistlinger et al., 2005; Amos and Mayer, 2006a). However, modeling this early-time behaviour is not the focus of this study since the later-time behaviour that controls the processes at NAPL-contaminated sites is expected to occur under effectively steady-state conditions. The early-time, flat portion of the data is well modeled for the PCE experiments since the gas-liquid interfacial tension of 70.0 mN/m measured for the PCE-saturated system is not substantially different from the surface tension of water.

The ability of different NAPL compounds to depress the gas-liquid interfacial tension below the value for the surface tension of water can affect the process of repeated expansion, snap-off, and vertical mobilization of discontinuous gas phases. Roy and Smith (2007) reported that two mechanisms could be responsible for the expansion of a discontinuous gas phase: the partitioning of NAPL compounds and other dissolved gases to the gas phase, and changes in the interfacial properties including interfacial tension. Although the first mechanism was dominant in their experiments, Roy and Smith (2007) suggested that an increase in interfacial tension as the NAPL compound dissolved back into the groundwater well above the pool could restrict the vertical mobility of the gas phase. This is more applicable to NAPL compounds such as tDCE that cause a more substantial reduction in the gas-liquid interfacial tension. The partitioning of these compounds to a discontinuous gas phase would result in more rapid expansion and snap-off as the interfacial tension decreased with increasing NAPL compound concentrations in the liquid and gas phases. However, this would also facilitate trapping of the

mobilized gas phase closer to the surface of the NAPL pool as NAPL compound partitions to the aqueous phase and the interfacial tension rises.

The conditions of these experiments favour slow expansion of the gas phase controlled by a long mass transfer path length and transport of all gases by molecular diffusion alone. In a typical groundwater application the value of L_D could be less than the 30 mm used here. For example, Roy and Smith (2007) observed the preferential expansion of a discontinuous gas phase along the surface of a NAPL pool due to the differences in the displacement pressure for gas-NAPL and gas-water systems, resulting in direct contact between the gas and NAPL phases. The value of $D_{i,z}$ could also be greater than the value of molecular diffusion used here due to mechanical dispersion processes. The effect of mechanical dispersion on vertical mass transport is expected to be greater in systems containing discontinuous gas phases due to increased tortuosity. Due to the greater values of $D_{i,z}$ and lower values of L_D than those employed in these experiments, it is expected that the expansion rate of a discontinuous gas phase above a NAPL pool in a typical groundwater application would be greater than those observed in these vial-based experiments. That is, the vial-based data represents relatively conservative behaviour.

2.5.4 Comparison of Estimated Mass Fluxes

Figure 2.5 compares the magnitude of the mass transfer from a NAPL pool via an expanding gas phase to that expected via advection and dispersion in a strictly NAPL/water scenario using (2.12) versus L^*Pe_z for A^* values of 0.01, 0.1, and 0.5. Figure 2.5 was constructed using θ=0.35 as a representative value for sand and gravel aquifers, and P_g^n/P^{vp}=0.998 based on the results of the static vial experiments. Increased values of A^* represent conditions with an increased cross-sectional area of the discontinuous gas phase (in a plane parallel to the NAPL pool surface) relative to the area of the NAPL pool. Low L^*Pe_z values represent conditions where the distance from the pool surface to the gas phase is small relative to the length of the pool in the direction of groundwater flow, advective mass transport is slow, and transverse vertical dispersive mass transport is relatively fast. For example, given a transverse vertical dispersion

coefficient of $1x10^{-9}$ m^2/s, a discontinuous gas phase located 1 mm above a 10 m long pool subjected to a groundwater velocity of 0.001 m/day corresponds to $L^*Pe_z=1x10^{-6}$, and a discontinuous gas phase located 10 mm above a 10 m long pool subjected to a groundwater velocity of 0.01 m/day corresponds to $L^*Pe_z=1x10^{-3}$. Figure 2.5 shows that for large values of A^* and low values of L^*Pe_z the mass flux of NAPL compound to the discontinuous gas phase is large relative to the dissolution mass flux from a NAPL pool expected for a NAPL/water system. M_{gas} is estimated to be 10% of $M_{NAPL/water}$ for L^*Pe_z values of $2.6x10^{-5}$ and $6.4x10^{-4}$ and A^* values of 0.1 and 0.5, respectively, and equal to $M_{NAPL/water}$ for $L^*Pe_z=6.4x10^{-6}$ and $A^*=0.5$.

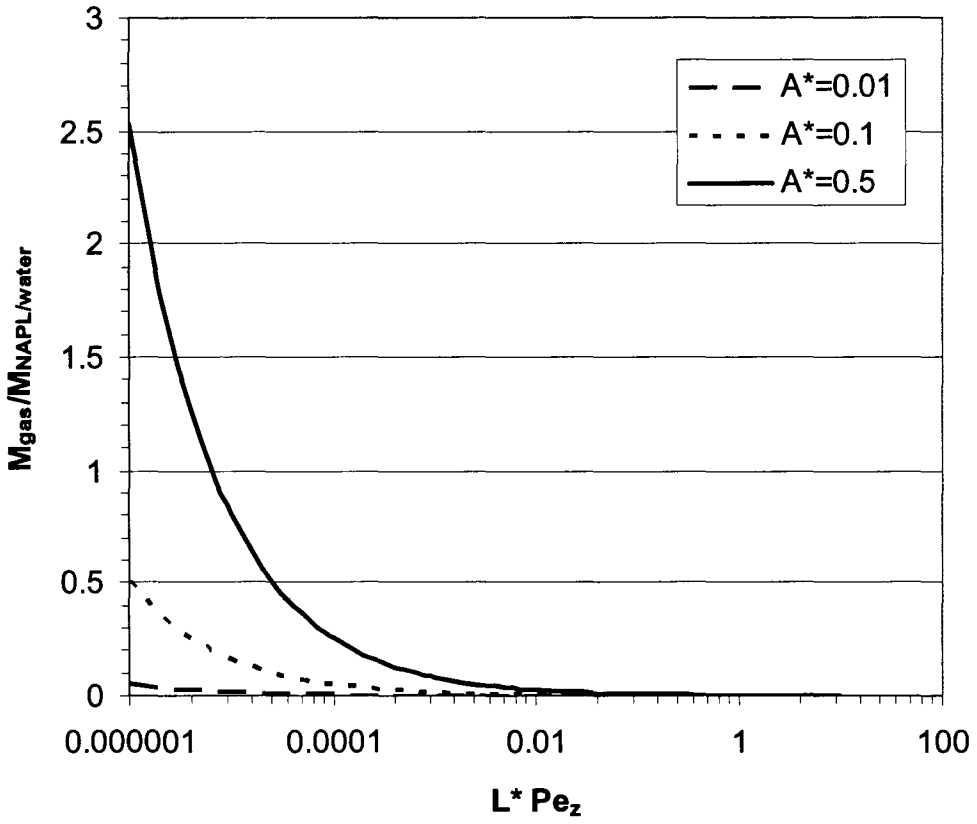

Figure 2.5. Comparison of estimated mass fluxes as a function of L^*Pe_z and A^*, assuming $\theta=0.35$ and $P_g^n/P^{vp}=0.998$.

Mass transfer from a NAPL pool to a discontinuous gas phase that is similar in magnitude to the mass transfer expected in a strictly NAPL/water scenario can

fundamentally change the mass transfer from the NAPL pool in two ways. First, NAPL mass that is removed from the surface of the pool and transported to the gas phase will be transported upwards by buoyant forces at a rate that greatly exceeds the rate of dispersion in the aqueous phase (Amos and Mayer, 2006b), which controls the vertical transport of NAPL compound mass in a NAPL/water system. This will result in greater vertical spreading of aqueous NAPL compound mass as NAPL compounds dissolve in the groundwater well above the NAPL pool (Roy and Smith, 2007). This will dramatically impact efforts to characterize source zone geometry based on aqueous concentration data since current conceptual models do not include any mechanism for this type of vertical mass transfer of NAPL compound. At NAPL-contaminated sites where this mechanism is active it is likely that NAPL compounds detected in groundwater well above a pool surface would be mistakenly attributed to another NAPL source up-gradient and above the NAPL pool.

Second, for the dissolution of a NAPL pool that occurs under local equilibrium conditions the total mass transfer is limited by the rate at which NAPL compound mass is transported away from the surface of the pool (Seagren et al., 1999). Under the NAPL/water conditions that are typically considered, mass is transported by advection and dispersion processes, with advection dominating at the down-gradient edge of long pools where the concentration gradients above the pool surface are small. The presence of a discontinuous gas phase that undergoes repeated expansion, snap-off, and vertical mobilization provides an additional mechanism for the removal of NAPL compound mass from the surface of the pool, and may significantly change the shape of the aqueous concentration boundary layer. This would increase the mass transfer rate from the pool surface and impact both the calculations of risk associated with that NAPL source as well as mass removal times.

Figure 2.5 assumes that the mass transfer rate of NAPL compound to the discontinuous gas phase is controlled by the mass transfer through the aqueous phase between the

surface of the NAPL pool and the gas-liquid interface. This is a reasonable assumption for conditions similar to the static experiments, where the transport of other dissolved gases to the gas-liquid interface and the mass transfer at the NAPL-water interface are not limiting. Where the advective transport of other dissolved gases to the gas-liquid interface is negligible, and the diffusive path length of other dissolved gases is significantly longer than that for the NAPL compound (e.g. a discontinuous gas phase present close to a NAPL pool located well beneath the water table under low-flow conditions) then it is expected that the steady-state value of P_g^n/P^{vp} would be greater than the value of 0.998 used to construct Figure 2.5 and the values of $M_{gas}/M_{NAPL/water}$ would be less than that shown in Figure 2.5. Under these conditions it is expected that an optimum groundwater velocity would exist, below which the expansion of the gas phase would be limited by the transport of the other dissolved gases.

Equation (2.12) predicts an unbounded increase in $M_{gas}/M_{NAPL/water}$ with decreasing values of L^*. It is expected, however, that as L_D approaches zero, and L^* approaches zero, the mass transfer will be limited by the mass transfer at the NAPL-water interface. Roy and Smith (2007) reported mass discharge values that correspond to $M_{gas}/M_{NAPL/water}$ =0.5 for the expansion, snap-off and vertical mobilization of a discontinuous gas phase in direct contact with a TCE pool. Assuming θ=0.35, P_g^n/P^{vp}=0.998, and A^*=1, (2.12) predicts $M_{gas}/M_{NAPL/water}$=0.5 for L^*Pe_z=1x10^{-4}. A^*=1 was used since Roy and Smith (2007) observed the preferential expansion of the gas phase along the surface of the NAPL pool, resulting in complete coverage of the pool surface. Given the groundwater velocity of 0.23 m/day and transverse vertical dispersion coefficient of 1.2x10^{-4} m^2/day used by Roy and Smith (2007), L^*Pe_z=1x10^{-4} corresponds to L_D=0.07 mm. This provides a reasonable lower limit on the value of L_D (dispersive mass transfer path length) based on the limited data available, below which the mass transfer to the discontinuous gas phase will be limited by processes other than the transport through the aqueous phase between the surface of the NAPL pool and the gas-liquid interface.

Figure 2.5 does not include the effects of capillarity (i.e. fine versus coarse porous media). Given the same mass-flux to the gas-liquid interface in coarse and fine materials, greater expansion will be required in the finer material for vertical mobilization of the discontinuous gas phase to occur (Tsimpanogiannis and Yortsos, 2004). However, this will simply result in the snap-off and mobilization of gas clusters at a lower frequency but containing a greater mass of NAPL compound. Therefore, the time-averaged mass flux away from the NAPL pool will be similar to that which occurs in the coarse material. However, for media that are significantly finer such that the capillary pressure required for entry into the pore throats is substantially higher than that in a gas-filled pore body then the gradient between the NAPL pool surface and the gas-liquid interface could be significantly reduced. This represents conditions under which most of the mass transfer occurs during the pressurization step described in section 2.2. Under these conditions mass transfer and the corresponding expansion of the gas phase would be reduced, and potentially stopped if the vapour pressure of the NAPL is less than the displacement pressure of the adjacent pore throats.

2.6 Conclusions

The results of this study show that a discontinuous gas phase expands in the presence of a NAPL pool, and that this expansion is consistent with the theory for the partitioning of multiple volatile compounds to a discontinuous gas phase. When the gas phase is not in direct contact with the NAPL pool, the expansion is controlled by the rate of mass transfer of NAPL compound through the aqueous phase to the gas-liquid interface, in addition to the mass transfer of other dissolved gases. Significant expansion was observed to occur over a period of weeks to months, with more rapid expansion observed for tDCE over PCE. Modeling results show that for the conditions investigated in this study the discontinuous gas phase is nearly saturated with NAPL compound during expansion. The modeling results also show that the mass flux expected from a NAPL pool to a discontinuous gas phase will be similar in magnitude to the dissolution mass flux expected from a NAPL pool in a NAPL/water system under conditions characterized

by groundwater velocities less than ~0.01 m/day, and a gas phase that covers greater than ~10% of the pool surface area and is located within ~0.01 m of the pool surface.

Where mass transfer to the discontinuous gas phase is significant, the dissolution behaviour of the NAPL pool will be different from that expected under typically considered NAPL/water conditions. The vertical spreading of dissolved NAPL mass will be significantly increased due to the transport via a mobile gas phase. In addition, the total mass transfer rate from the NAPL pool will be increased under local equilibrium controlled dissolution conditions due to the additional mechanism of repeated gas phase expansion, snap-off, and mobilization, which results in the increased transport of mass away from the pool surface. These fundamental changes are expected to directly affect, for example, efforts to locate NAPL source zones using aqueous concentration data, predict the risk associated with specific NAPL sources, and predict the total lifetime of NAPL source zones. The inclusion of these considerations into our conceptual models of NAPL source zones improves our fundamental understanding, provides opportunities to better interpret system behaviours, and promises to lead to new remediation technologies and improvements in existing technologies.

The results obtained using the analytical model derived in this study showed that the presence of a discontinuous gas phase will affect the mass transfer from NAPL pools under certain conditions. The analytical model and the comparison of estimated mass fluxes shown in Figure 2.5 will serve as a screening tool for assessing whether this mechanism may be significant at a particular NAPL-contaminated site. However, significant benefit will be realized through continued investigation of this mechanism and the use of more detailed mathematical models. Physically-based models for the expansion, snap-off, and mobilization of discontinuous gas clusters should be combined with kinetic models for multi-component mass transfer to discontinuous gas phases to describe transient changes in the aqueous concentration distributions and gas-phase saturations in both homogeneous and heterogeneous porous media under a variety of

source zone and background gas scenarios. In addition, reaction expressions for the generation of biogenic or remediation-based gases should be incorporated to accommodate a greater variety of natural and remediation situations. Such models will be potentially powerful tools for the investigation of NAPL-contaminated sites and other applications where the mass transfer to mobile discontinuous gas phases plays a key role.

Acknowledgements

This research was supported by the Natural Sciences and Engineering Research Council (NSERC) of Canada through its Discovery Grant Program and a Canada Graduate Scholarship to the first author. This manuscript benefited greatly from the reviews provided by one anonymous reviewer and Dr. Helmut Geistlinger. We gratefully acknowledge the technical assistance of Jennie Kirby.

References

Adamson, A.W., 1990. Physical Chemistry of Surfaces, 5th ed. John Wiley & Sons, Inc., New York, NY.

Amos, R.T., Mayer, K.U, Bekins, B.A., Delin, G.N., Williams, R.L., 2005. Use of dissolved and vapor-phase gases to investigate methanogenic degradation of petroleum hydrocarbon contamination in the subsurface. Water Resour. Res. 41, W02001, doi:10.1029/2004WR003433.

Amos, R.T., Mayer, K.U., 2006a. Investigating the role of gas bubble formation and entrapment in contaminated aquifers: Reactive transport modeling. J. Contam. Hydrol. 87, 123-154.

Amos, R.T., Mayer, K.U., 2006b. Investigating ebullition in a sand column using dissolved gas analysis and reactive transport modeling. Environ. Sci. Technol. 40 (17), 5361-5367.

Beckwith, C.W., Baird, A.J., 2001. Effect of biogenic gas bubbles on water flow through poorly decomposed blanket peat. Water Resour. Res. 37 (3), 551-558.

Blicher-Mathiesen, G., McCarty, G.W., Nielsen, L.P., 1998. Denitrification and degassing in groundwater estimated from dissolved dinitrogen and argon. J. Hydrol. 208, 16-24.

Cirpka, O.A., Kitanidis, P.K., 2001. Transport of volatile compounds in porous media in the presence of a trapped gas phase. J. Contam. Hydrol. 49, 263-285.

Chrysikopoulos, C.V., Hsuan, P.-Y., Fryillas, M.M., and Lee, K.Y., 2003. Mass transfer coefficient and concentration boundary layer thickness for a dissolving NAPL pool in porous media. J. Hazard. Mater. 97, 245-255.

Conant, B.H., Gillham, R.W., Mendoza, C.A., 1996. Vapor transport of trichloroethylene in the unsaturated zone: field and numerical modeling investigations. Water Resour. Res. 32 (1), 9-22.

Dominguez, A., Bories, S., Prat, M., 2000. Gas cluster growth by solute diffusion in porous media. Experiments and automation simulation on pore network. Int. J. Multiphas. Flow 26, 1951-1979.

Epstein, P.S., Plesset, M.S., 1950. On the stability of gas bubbles in liquid-gas solutions. J. Chem. Phys. 18 (1), 1505-1509.

Firoozabadi, A., D. Kashchiev, D., 1996. Pressure and volume evolution during gas phase formation in solution gas drive process. SPE J. 1 (3), 219-227.

Fry, V.A., Selker, J.S., Gorelick, S.M., 1997. Experimental investigations for trapping oxygen gas in saturated porous media for in situ bioremediation. Water Resour. Res. 33 (12), 2687-2696.

Geistlinger, H., Beckmann, A., Lazik D., 2005. Mass transfer between a multicomponent trapped gas phase and a mobile water phase: experiment and theory. Water Resour. Res. 41, doi:10.1029/2004WR003885.

Hofstee, C., Oostrom, M., Dane, Walker, R.C., 1998. Infiltration and redistribution of perchloroethylene in partially saturated, stratified porous media. J. Contam. Hydrol. 34, 293-313.

Holocher, J., Peeters, F., Aeschbach-Hertig, W., Kinzelbach, W., Kipfer, R., 2003. Kinetic model of gas bubble dissolution in groundwater and its implications for the dissolved gas composition. Environ. Sci. Tecnol. 37 (7), 1337-1343.

Johnson, R.L., Pankow, J.F., 1992. Dissolution of dense chlorinated solvents into groundwater. 2. source functions for pools of solvent. Environ. Sci. Technol. 26 (5), 896-901.

Khachikian, C., Harmon, T.C., 2000. Nonaqueous phase liquid dissolution in porous media: current state of knowledge and research needs. Transport Porous Med. 38, 3-28.

Li, X., Yortsos, Y.C., 1995. Theory of multiple bubble growth in porous media by solute diffusion. Chem. Eng. Sci. 50 (8), 1247-1271.

Moran, M.J., Zogorski, J.S., Squillace, P.J., 2007. Chlorinate solvents in groundwater of the United States. Environ. Sci. Technol. 41 (1), 74-81.

Oostrom, M., Hofstee, C., Lenhard, R.J., Wietsma, T.W., 2003. Flow behavior and residual saturation formation of liquid carbon tetrachloride in unsaturated heterogeneous porous media. J. Contam. Hydrol. 64, 93-112.

Oostrom, M., Dane, J.H., Wietsma, T.W., 2006. A review of multidimensional, multifluid intermediate-scale experiments: nonaqueous phase liquid dissolution and enhanced remediation. Vadose Zone J. 5 (2), 570-598.

Or, D., Tuller, M., 2003. Reply to comment by N. Kartal Toker, John T. Germaine, and Patricia J. Culligan on "Cavitation during desaturation of porous media under tension". Water Resour. Res. 39 (11), 1306, doi:10.1029/2003WR002492.

Pankow, J.F., Cherry, J.A., 1996. Dense Chlorinated Solvents and other DNAPLs in Groundwater. Waterloo Press, Portland, Oregon.

Perry, R.H., Green, D.W., Maloney, J.O., 1997. Perry's chemical engineers' handbook, seventh edition. McGraw-Hill, New York, New York.

Ronen, D., Berkowitz, B., Magaritz, M., 1989. The development and influence of gas bubbles in phreatic aquifers under natural flow conditions. Transport Porous Med. 4, 295-306.

Rosenberry, D.O., Glaser, P.H., Siegel, D.I., 2006. The hydrology of northern peatlands as affected by biogenic gas: current developments and research needs. Hydrol. Process. 20, 3601-3610.

Roy, J.W., Smith, J.E., 2007. Multiphase flow and transport caused by spontaneous gas phase growth in the presence of dense non-aqueous phase liquid. J. Contam. Hydrol. 89, 251-269.

Ryan, M.C., MacQuarrie, K.T.B., Marman, J., McLellan, J., 2000. Field and modeling evidence for a "stagnant flow" zone in the upper meter of sandy phreatic aquifers. J. Hydrol. 233, 223-240.

Schroth, M.H., Oostrom, M., Wietsma, T.W., Istok, J.D., 2001. In-situ oxidation of trichloroethylene by permanganate: effects on porous medium hydraulic properties. J. Contam. Hydrol. 50, 79-98.

Schwille, F., 1988. Dense chlorinated solvents in porous and fractured media. Lewis Publishers, Inc., Michigan.

Seagren, E.A, Rittman, B.E., Valocchi, A.J., 1999. A critical evaluation of the local-equilibrium assumption in modeling NAPL-pool dissolution. J. Contam. Hydrol. 39, 109-135.

Sleep, B.E., Sykes, J.F., 1989. Modeling the transport of volatile organics in variably saturated media. Water Resour. Res. 25 (1), 81-92.

Soares, M.I.M., Belkin, S., Abeliovich, A., 1987. Biological groundwater denitrification: laboratory studies. Wat. Sci. Tech. 20 (3), 189-195.

Tillman, F.D. Jr., Smith, J.A., 2004. Design and laboratory testing of a chamber device to measure total flux of volatile organic compounds from the unsaturated zone under natural conditions. J. Contam. Hydrol. 75, 71-90.

Tsimpanogiannis, I.N., Yortsos, Y.C., 2002. Model for the gas evolution in a porous medium driven by solute diffusion. AIChE J. 48 (11), 2690-2710.

Tsimpanogiannis, I.N., Yortsos, Y.C., 2004. The critical gas saturation in a porous medium in the presence of gravity. J. Colloid Interface Sci. 270, 388-395.

USEPA, 2003. The DNAPL remediation challenge: is there a case for source depletion? EPA/600/R-03/143.

Williams, M.D., Oostrom, M., 2000. Oxygenation of anoxic water in a fluctuating water table system: an experimental and numerical study. J. Hydrol. 230, 70-85.

Chapter 3

New observations of gas-phase expansion above a dense non-aqueous phase liquid pool

The contents of this chapter have been accepted for publication as: Mumford, K.G., Smith, J.E., Dickson, S.E., 2008. New observations of gas-phase expansion above a dense non-aqueous phase liquid pool. *Vadose Zone Journal*, In Press.

Abstract

The partitioning of volatile dense non-aqueous phase liquid (DNAPL) compounds to a discontinuous gas phase results in the repeated expansion, fragmentation, and vertical mobilization of gas clusters. This process has the potential to significantly affect the dissolution of DNAPL source zones and the characterization of DNAPL-contaminated sites, but has not been included in common conceptual models. This study presents new observations of discontinuous gas-phase growth above a 1,1,1-trichloroethane pool in a two-dimensional flow cell packed with 1.1-mm diameter sand. In contrast to the behavior observed in coarse glass beads, these visualization results show that the gas phase evolves as a collection of macroscopic fingers, composed of multiple trapped and disconnected gas clusters, and that the growth rate of these fingers is faster at the leading edge of the DNAPL pool due to the stripping of dissolved gases. These results provide valuable information for the incorporation of discontinuous gas phases in our evolving conceptual models of DNAPL source zones.

3.1 Introduction

The contamination of groundwater systems by dense non-aqueous phase liquids (DNAPLs) continues to be a significant environmental problem (Johnson et al., 2004). An increased understanding of the processes that control the dissolution of DNAPL source zones will help to improve the characterization and remediation of DNAPL-contaminated sites (Khachikian and Harmon, 2000). Recent studies show that one process that has been previously over-looked and is not included in current, common conceptual models for DNAPL dissolution is the repeated expansion, fragmentation, and vertical mobilization of discontinuous gas phases due to the partitioning of volatile DNAPL compounds (Roy and Smith, 2007). Flow cell experiments conducted by Roy and Smith (2007) showed that this process can change pore-scale DNAPL distributions and alter local aqueous-phase permeability, which can affect mass transfer from the source zone. They also reported an increase in the effluent mass flux and a change in the distribution of dissolved DNAPL above a trichloroethene (TCE) pool due to the buoyant vertical transport of gas clusters away from the pool surface.

The re-dissolution of DNAPL compounds from a mobilized discontinuous gas phase back into the surrounding groundwater is expected to be a strong function of the discontinuous gas-phase geometry, which has been reported for the mass transfer of volatile compounds during air sparging (e.g. Brooks et al., 1999), the dissolution of trapped gases (e.g. Geistlinger et al., 2005) and the dissolution of DNAPL residual (e.g. Khachikian and Harmon, 2000). The objective of this manuscript is to present novel results of our recent experiments that clearly demonstrate the transient distribution of an expanding discontinuous gas phase above a DNAPL pool in natural porous media. The observed distribution is substantially different than those observed in previous studies on the expansion of a discontinuous gas phase in the presence of DNAPL conducted in either porous media-free, no-flow reactors (Mumford et al., 2008) or flow cells packed with 1 mm- or 3 mm-diameter glass beads (Roy and Smith, 2007). This timely

contribution directly influences the rapidly emerging changes in our fundamental conceptual models of DNAPL source zones containing a discontinuous gas phase.

3.2 Theory

3.2.1 Gas-phase Expansion Above a DNAPL Pool

The expansion of a discontinuous gas phase above a DNAPL pool is driven by the partitioning of multiple dissolved gases to the gas phase (Roy and Smith, 2007; Mumford et al., 2008). These dissolved gases can include atmospheric gases (e.g. O_2, N_2), biogenic gases (e.g. CH_4, CO_2), and volatile partitioning tracers (e.g. SF_6) in addition to the DNAPL compound(s). In a multi-component system containing aqueous and gas phases, the partitioning of the volatile compounds to a gas cluster is controlled by the local equilibrium at the gas liquid interface defined by Henry's law

$$P_i^g = K_{Hi} C_i \tag{3.1}$$

where P_i^g is the partial pressure of compound i in the gas phase, K_{Hi} is the Henry's law coefficient for compound i, and C_i is the local aqueous phase concentration of compound i; and by the total pressure of the gas phase, defined by the sum of the hydrostatic and capillary pressures, according to Dalton's law

$$P_g = P_w + P_c = \sum_i P_i^g \tag{3.2}$$

where P_g is the gas pressure, P_w is the bulk liquid pressure, and P_c is the capillary pressure (Cirpka and Kitanidis, 2001). The term gas cluster here is used to describe a gas volume that is connected through one or more pore bodies, but is not macroscopically connected throughout the medium, and is treated as the non-wetting phase. The resulting multi-component partitioning can result in either the dissolution (Cirpka and Kitanidis, 2001; Holocher et al., 2003; Geistlinger et al., 2005) or the expansion (Cirpka and

Kitanidis, 2001; Amos and Mayer, 2006a,b; Roy and Smith, 2007; Mumford et al., 2008) of the discontinuous gas phase. Expansion is expected for discontinuous gases above DNAPL pools, as the partitioning of volatile DNAPL mass lowers the partial pressures of the other gases in the gas cluster below the values in equilibrium with their bulk aqueous concentrations, resulting in the transport of all dissolved gases across the gas-liquid interface (Mumford et al., 2008). This transport of all gases can occur even in systems where the partial pressure of the DNAPL compound is near saturation, and makes up only a small fraction of the total gas pressure (Mumford et al., 2008). Faster transport, and faster expansion, is expected for systems with low values of P_w and P_c, and containing DNAPLs with high vapor pressures (i.e. volatile DNAPLs in shallow, coarse media). In systems where the DNAPL vapor pressure is less than the capillary pressure, no expansion is expected. Lower values of P_c can also result from changes in gas-liquid interfacial properties, including the lowering of air-water interfacial tension due to contamination of the interface by DNAPL constituents (Roy and Smith, 2007; Mumford et al., 2008). Continued expansion of a discontinuous gas phase near the surface of a DNAPL pool will result in fragmentation and vertical mobilization of the gas phase, as buoyancy forces overcome local capillary forces (Roy and Smith, 2007), and the vertical transport of gas-phase DNAPL compounds.

Because changes in gas-phase volume are dependent on the mass transfer of all volatile components to the gas-liquid interface, the expansion of one discontinuous gas phase can affect the expansion of other discontinuous gas phases located further downstream (Cirpka and Kitanidis, 2001). That is, the transfer of volatile compounds to a vertically mobilized gas phase effectively strips those volatile compounds from the flow path, leaving less mass for transfer to the next downstream discontinuous gas phase. Thus, it is expected that multiple discontinuous gas phases located along the length of a DNAPL pool along the direction of flow will evolve at different rates, from faster to slower expansion in the downstream direction.

3.2.2 Unstable Gas Flow in Porous Media

Unstable drainage in a porous medium is expected for the upwards displacement of the wetting fluid by a significantly less dense non-wetting fluid (Frette et al., 1992; Birovljev et al., 1995; Glass et al., 2000; Tsimpanogiannis and Yortsos, 2004; Stöhr and Khalili, 2006; Geistlinger et al., 2006), or the downward displacement of the wetting fluid by a significantly more dense non-wetting fluid (e.g. Glass et al., 2000; Ewing and Berkowitz, 2001; Zhang and Smith, 2002) provided that the viscosity ratio of the two fluids and the rate of non-wetting fluid flow are insufficient to provide viscous stability (Geistlinger et al., 2006; Stöhr and Khalili, 2006). Under these circumstances, the growth of the non-wetting phase is described by a characteristic cluster width (ξ) and length (l_c) (Wilkinson, 1984; Wilkinson, 1986)

$$\xi \sim |Bo|^{-\nu/(\nu+1)} \tag{3.4}$$

$$l_c \sim |Bo|^{-1} r_p \tag{3.5}$$

$$Bo = \frac{\Delta\rho g r_p^{\,2}}{\sigma} \tag{3.6}$$

where Bo is the Bond number (ratio of buoyancy to capillary forces), ν is the correlation length exponent of percolation, r_p is a characteristic pore radius, $\Delta\rho$ is the density difference between the wetting and non-wetting fluids (water and gas, respectively, in this experiment), g is the acceleration due to gravity, and σ is the interfacial tension. The exponent $-\nu/(\nu+1)$ in (3.4) is equal to -0.57 in 2D (Frette et al., 1992; Birovljev et al., 1995; Tsimpanogiannis and Yortsos, 2004) and -0.47 in 3D (Wilkinson, 1986; Tsimpanogiannis and Yortsos, 2004; Stöhr and Khalili, 2006). In their pore-network simulations, Tsimpanogiannis and Yortsos (2004) found that the characteristic length for unstable displacement in a gravity field is described better by $l_c \sim |Bo|^{-0.44}$. Based on these

relationships, the geometry of unstable gas phase growth in porous media is expected to range from generally symmetrical, but irregular, clusters at low *Bo* (e.g. Frette et al., 1994) to long vertical chains of small, disconnected clusters at high *Bo* (e.g. Frette et al., 1992; Birovljev et al., 1995). At the extreme, these disconnected clusters approach the scale of a single pore body (Roosevelt and Corapcioglu, 1998).

The geometry of a disconnected gas phase in a porous medium can be described by the length at which fragmentation and mobilization of the gas cluster occurs due to reinvasion of water and entry of gas into new pore spaces. For unstable growth in a gravity gradient, reinvasion is caused by a local decrease in capillary pressure as a gas cluster grows vertically and is subjected to a lower hydrostatic pressure. Estimates of this critical cluster length are based on a balance of the pressures at the top and bottom of the gas cluster and the pressure drop across the height of the cluster (Glass et al., 2000; Geistlinger et al., 2006)

$$h_{crit} = \frac{P_c^{top} - P_c^{bottom}}{\Delta \rho g} \tag{3.7}$$

where h_{crit} is the critical cluster length, and P_c^{top} and P_c^{bottom} are the capillary pressures at the top and bottom of the cluster, respectively, when fragmentation and mobilization occur. Estimates of the critical cluster length in uniform glass beads and sand are presented in Figure 3.1. The values for uniform glass beads are calculated based on the theoretical expression presented by Geistlinger et al. (2006) with parameters fit to their reported estimates for 3 mm- and 4 mm-diameter glass beads. The values for sand are based on Brooks-Corey air-water capillary pressure-saturation parameters for four grades of Accusand (12/20, 20/30, 30/40, and 40/50 with median grain diameters (d_{50}) of 1.105 mm, 0.713 mm, 0.532 mm, and 0.359 mm, respectively) (Schroth et al., 1996). Based on the method proposed by Glass et al. (2000), values for P_c^{top} were estimated for effective non-wetting saturations of 0.3, and P_c^{bottom} was taken to be $\frac{1}{2}P_c^{top}$. Figure 3.1 shows that

a decrease in grain size or a change from uniform glass beads to natural porous media results in a considerable increase in the critical cluster length. That is, in media characterized by smaller grain sizes and higher capillary pressures, fragmentation and mobilization require longer gas clusters. It also shows that for grain diameters of 4 mm to 5 mm, the critical cluster length approaches the scale of a single grain, which can be assumed to be on the same order as a single pore.

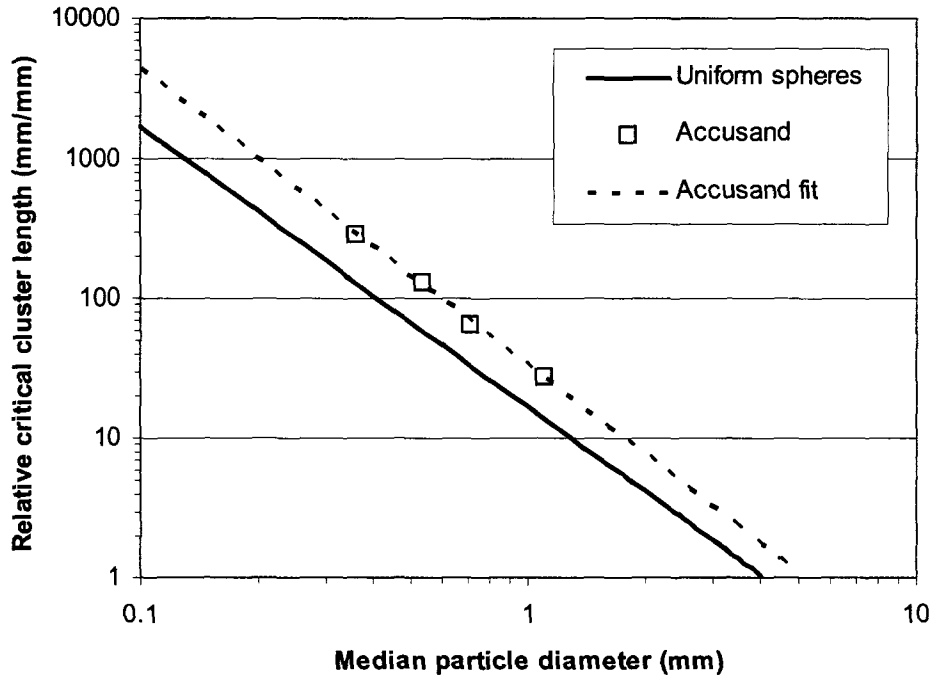

Figure 3.1. Relative critical cluster length (h_{crit}/d_{50}) for uniform glass beads and natural porous media based on four fractions of Accusand.

For mass transfer from discontinuous gas phases, the scale of the discontinuous gas clusters is an important consideration. Larger clusters will allow the rapid transport of DNAPL compounds by gas diffusion over larger distances, and vertically mobile clusters at the scale of a single pore will allow the rapid transport of DNAPL compounds by buoyancy-driven advection, assuming minimal trapping in homogenous systems. The vertical transport of DNAPL mass in systems characterized by intermediate-sized clusters

will be limited with respect to both of these mechanisms, as vertical diffusion will be dominated by transport through the aqueous phase between clusters, and buoyant advection will be limited by repeated trapping due to minor variations in the pore-scale geometry. Even under the limiting conditions induced by intermediate-sized clusters, however, the resulting rate of vertical transport can be greater than vertical diffusion and dispersion processes in water-saturated media (Amos and Mayer, 2006b; Roy and Smith, 2007).

3.3 Materials and Methods

3.3.1 Flow Cell Construction and Operation

Experiments were conducted in a two-dimensional flow cell (Figure 3.2) composed of two 1-cm thick glass plates sealed to a brass frame and an aluminum top plate. The inside dimensions of the flow cell were 68 x 59 x 1 cm^3. The influent side of the flow cell was packed with 6 mm-diameter glass beads (Propper Manufacturing Co., Inc. 030010), separated from the main pack by a perforated aluminum plate, to distribute the flow. Top and bottom confining layers were created by packing with 0.5 mm-diameter sand (40/50 Accusand, Unimin Corporation). The center of the cell was packed with 62 x 44 x 1 cm^3 of 1.1 mm-diameter sand (12/20 Accusand, Unimin Corportation). Schroth et al. (1996) report the properties of these sands. Microscopic and macroscopic air entrapment in the main pack were minimized by placing the sand in water under vacuum prior to packing, and continuously pouring the wet sand into the water-filled flow cell. The continuous pouring, together with the tapping of the glass plates with a rubber mallet following the pour, achieved a reasonably homogeneous pack.

The DNAPL used in the experiment was 1,1,1-trichloroethane (1,1,1-TCA), which has an aqueous solubility of 1310 mg/L and a vapor pressure of 1.66×10^4 Pa at 25°C (Pankow and Cherry, 1996). A 17-cm long DNAPL pool was created by injecting 16 mL of 1,1,1-TCA (VWR Canlab, 99.5%) dyed red with 100 mg/L Sudan 4 (Acros Organics) at a rate of 2 mL/hr using a syringe pump (Cole-Parmer EW-74901-10) and a 25-mL gastight

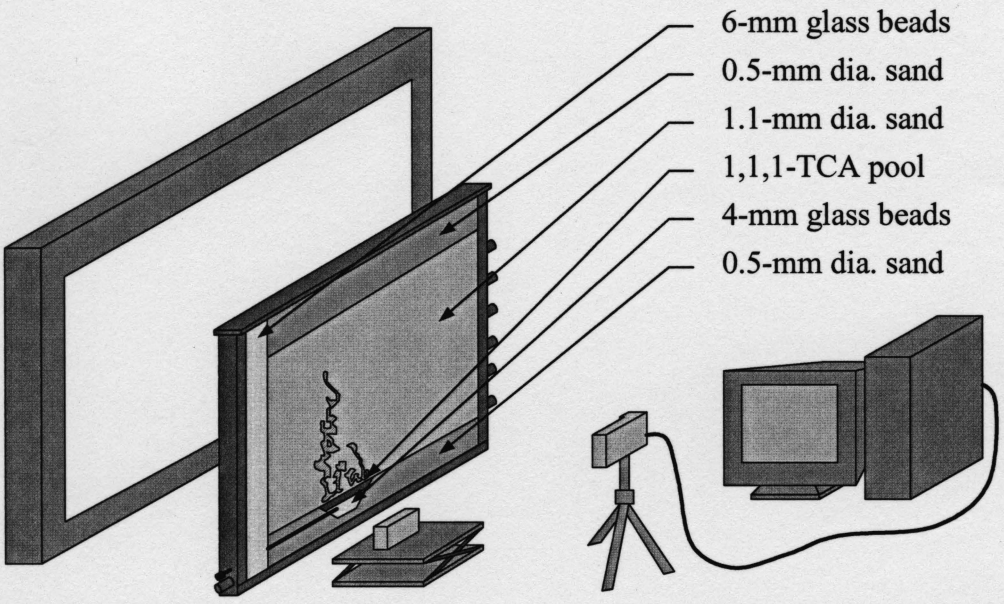

Figure 3.2. Experimental set-up showing the flow cell, light box and cameras for macro-scale and pore-scale imaging.

syringe (Hamilton 82520) through a 16-gauge stainless-steel needle (Hamilton 7748-02) inserted into the side of the flow cell. The needle was packed into a layer of 4 mm-diameter glass beads (Propper Manufacturing Co., Inc. 030008) placed in the bottom of a depression in the lower confining layer. An initial gas phase was emplaced by lowering the water table at a rate of 3 cm every 15 min using a constant head device until contact between the air and the surface of the DNAPL pool was observed. The water table was then immediately raised, at the same rate at which it was lowered, to trap air at a residual saturation expected to be similar to the reported residual air saturation for this sand (Schroth et al., 1996).

A solution of 200 mg/L of sodium azide (Fisher Scientific, >99%) in Nanopure water (Barnstead D11951) was pumped through the flow cell using a continuous-cycle syringe pump (Cole-Parmer EW-74901-50) and 60-mL syringes (BD 309653) at a rate of 0.93±0.02 mL/min for 70 days, corresponding to a pore-water velocity of 70 cm/day. The sodium azide acted as a biocide (Seagren et al., 1999; Chrysikopoulos et al., 2000; Roy et al., 2004) to prevent the generation of biologically-derived gases. Dissolved gases

were supplied to the flow cell throughout the experiment by saturating the influent water with laboratory air at 25°C. This was expected to provide a sufficient amount of dissolved gas to facilitate the multi-component expansion of the gas phase in the vicinity of the DNAPL pool, but not promote the generation of a gas phase by degassing of the solution elsewhere in the flow cell. Flow exited the effluent boundary through six ports connected to individual constant-head devices. The flow rate was measured by periodically placing the influent reservoir on an analytical balance (Mettler Toledo BD1201).

3.3.2 Image Collection and Processing

Macro-scale images of the evolving gas phase were collected using a CCD camera (Canon A640) connected to a personal computer equipped with software from the camera manufacturer. Images were collected automatically at a rate of one per hour and a resolution of approximately $(0.2\ mm)^2$/pixel. The flow cell was lit continuously by a light box equipped with four 36 Watt, 5000 Kelvin fluorescent tubes covered with a prismatic acrylic sheet, having a lit surface area of 102 cm x 71 cm (JUST Normlicht, Model No. 12849). The flow cell was positioned between the light box and the camera to allow visualization of the depth-averaged gas saturation by light transmission (Tidwell and Glass, 1994; Niemet and Selker, 2001; Oostrom et al., 2007). The flow cell was located 28 cm from the light box and 180 cm from the camera. The light box, flow cell and camera were covered by a rubber-backed curtain hung over a steel frame to minimize the effect of ambient lighting. Ambient air temperatures underneath the curtain were approximately 2°C higher than in the laboratory, which was not expected to significantly affect the results of the experiment. Pore-scale digital images were collected using a second CCD camera (Nikon Coolpix P4) mounted on an adjustable laboratory jack stand located 6 cm from the flow cell. Pore-scale images were collected at a rate of approximately one per day and a resolution of approximately $(0.023\ mm)^2$/pixel.

The transmitted light intensity values at each pixel were determined by converting the RGB image recorded by the camera to a grayscale image. The background image was

removed by calculating the difference in the optical density (McNeil et al., 2006) between the initial image and each subsequent image, corrected for temporal changes in lighting using the transmitted light intensity through a reference region

$$\Delta OD = OD_t - OD_0 = \log\left(\frac{I_0 I_t^{ref}}{I_t I_0^{ref}}\right) \tag{3.8}$$

where ΔOD is the difference in optical density, OD is the optical density, I is the transmitted light intensity and I^{ref} is the average transmitted light intensity over the reference region. The subscripts 0 and t refer to images collected initially and at time t, respectively. The reference region employed in this experiment was a section of the main pack that was not drained during the initial gas emplacement and, therefore, remained at a constant optical density throughout the experiment. The section was a 1-cm high x 10-cm long area located just above the lower confining layer and between 39 cm and 49 cm from the influent edge of the main pack. No attempt was made in this work to process the images for the quantification of point-wise saturation values (e.g. Tidwell and Glass, 1994; Glass et al., 2000; Niemet and Selker, 2001; O'Carroll and Sleep, 2007). All image processing was done using MatLab (Release 13, MathWorks, Inc.) and measurements of gas finger height in the images were conducted using ImageJ (http://rsb.info.nih.gov/ij/).

3.4 Results and Discussion

3.4.1 Pore-scale images

Pore-scale images collected at the pool surface between 5.9 cm and 7.5 cm from the upgradient edge of the pool at 0 days, 5 days and 10 days are shown in Figure 3.3. These images provide qualitative information regarding the transient behavior of gas clusters located at the surface of the front glass plate, and support the conceptual model of discontinuous gas-phase flow that occurs through the repeated expansion, fragmentation, and vertical mobilization of gas clusters near the surface of the DNAPL pool. Four gas

clusters (A, B, C, and D) have been outlined in Figure 3.3 to illustrate the variety of possible behaviors exhibited by individual gas clusters. Although the interfaces outlined for clusters C and D appear disconnected, the inspection of multiple images showed that the interfaces within each cluster were connected away from the front glass plate.

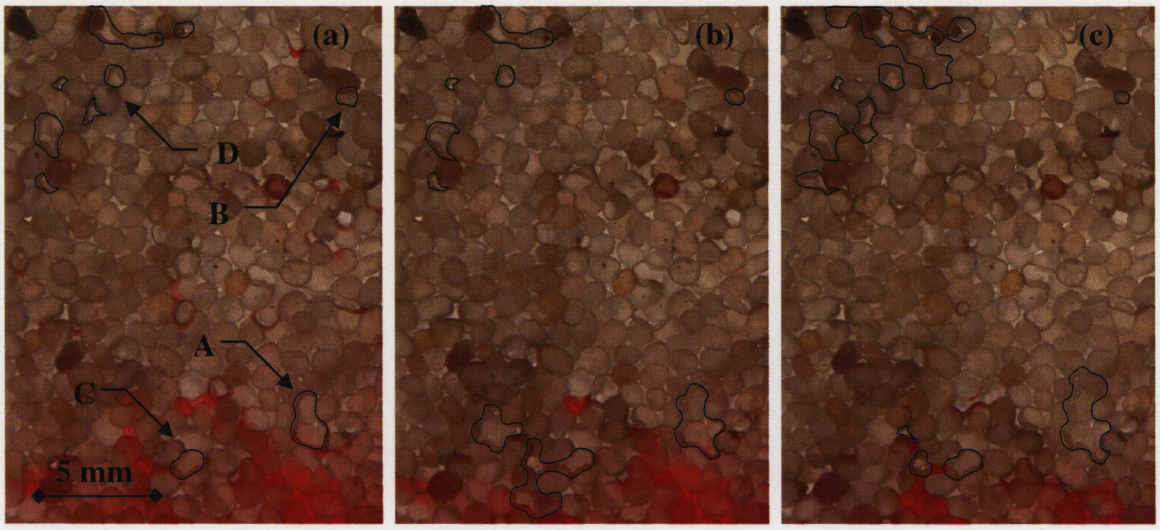

Figure 3.3. Pore-scale images of gas clusters near the surface of the DNAPL pool between 5.9 cm and 7.5 cm from the upgradient edge of the pool after (a) 0 days, (b) 5 days, and (c) 10 days. Selected gas clusters are outlined in black, and indicate (A) an expanding cluster, (B) a dissolving cluster, (C) a cluster that fragmented following expansion, and (D) a cluster that coalesced following dissolution.

These four gas clusters are present at two different elevations above the DNAPL pool surface. Clusters A and C are at the pool surface, and are in direct contact with DNAPL, and clusters B and D are 1.4 cm above the pool surface. The gas-phase concentrations in clusters A and C are expected to be near saturation values, with maximum 1,1,1-TCA partial pressures close to the vapor pressure of 1.66×10^4 Pa. The gas-phase concentrations in clusters B and D are expected to be in equilibrium with the local aqueous-phase concentrations. The magnitude of the local aqueous-phase concentrations can be approximated using a simple model for DNAPL pool dissolution (Johnson and Pankow, 1992)

$$\frac{C}{C_S} = erfc\left(\frac{z}{2\sqrt{D_z x/v}}\right) \tag{3.9}$$

where C_S is the aqueous solubility of the DNAPL, z is the elevation above the pool surface, D_z is the transverse dispersion coefficient, x is the length in the direction of flow, and v is the pore-water velocity. Taking z=1.4 cm, D_z=10^{-9} m^2/s, x=7 cm, and v=70 cm/d gives C/C_S=8x10^{-4}. Assuming that $C/C_S=P^g/P^{VP}$, where P^{VP} is the vapor pressure of the DNAPL, the maximum 1,1,1-TCA partial pressures in clusters B and D are expected to be approximately 1x10^1 Pa. The capillary pressure required for the expansion of a gas cluster to an adjacent pore body is expected to be near the air-entry value of 5.3x10^2 Pa for this sand (Schroth et al., 1996). Therefore, 1,1,1-TCA partial pressures are expected to be less than the capillary pressure required for expansion in clusters B and D, and greater than required in clusters A and C.

The behavior of clusters A and B is consistent with expectations based on consideration of the capillary entry pressure and 1,1,1-TCA partial pressure. The high 1,1,1-TCA partial pressure expected in cluster A results in expansion, while the low 1,1,1-TCA partial pressure expected in cluster B results in dissolution. This difference in behavior supports previous observations that local system properties strongly influence gas-phase expansion (Roy and Smith, 2007), due in part here to the steep concentration gradients at the leading edge of a dissolving DNAPL pool.

The behavior of clusters C and D is not readily explained simply by considering the expected 1,1,1-TCA partial pressures at the two locations. Over the first five days, cluster C expanded and cluster D dissolved, as expected. However, there was a decrease in the size of cluster C and an increase in the size of cluster D after 10 days. Inspection of pore-scale and macro-scale images collected between 5 and 10 days (not shown) strongly suggests that the change in volumes of clusters C and D were due to the vertical mobilization of gas from cluster C followed by coalescence with cluster D. The

difference in the behavior of clusters B and D, located at the same elevation above the DNAPL pool, shows that while the local aqueous concentrations at a gas cluster location suggest dissolution behavior, the effective steady-state behavior will also depend on the advective transport of a gas phase from lower gas clusters (i.e. cluster C to cluster D). This will result in long periods of slow dissolution punctuated by short periods of expansion by coalescence, which may cause a net expansion at that location over time.

The expansion and fragmentation of cluster C also illustrates the local displacement of DNAPL adjacent to the cluster. DNAPL-occupied pore spaces are filled with gas as the cluster expands, and are filled again with DNAPL following fragmentation. This supports previous observations that discontinuous gas-phase expansion, fragmentation and vertical mobilization can affect the local morphology of DNAPL source zones, and potentially affect local dissolution rates (Roy and Smith, 2007).

3.4.2 Macro-scale images

Selected macro-scale images are shown in Figure 3.4. An animation compiled from 280 still images at a frequency of 4 images/day is available in the supporting information (http://vzj.scijournals.org/). These images show the evolution of two macroscopic gas fingers. The upgradient finger developed within the first 6 days and exhibited considerable branching close to the upper confining layer after 40 days. The downgradient finger was clearly visible after 11 days.

Growth of the gas fingers occurred in a step-wise manner due to local variations in pore-scale displacement pressure. These local variations are present even in the relatively homogenous packing used in this experiment, and similar effects on unstable, non-wetting phase displacement have been observed (Birovljev et al., 1995; Glass et al., 2000; Zhang and Smith, 2002; Stöhr and Khalili, 2006; Geistlinger et al., 2006). This step-wise growth results from a combination of penetration events following the pressurization of a gas cluster (Li and Yortsos, 1995), and vertical mobilization events following the fragmentation of a gas cluster at the critical cluster length. These events were observed

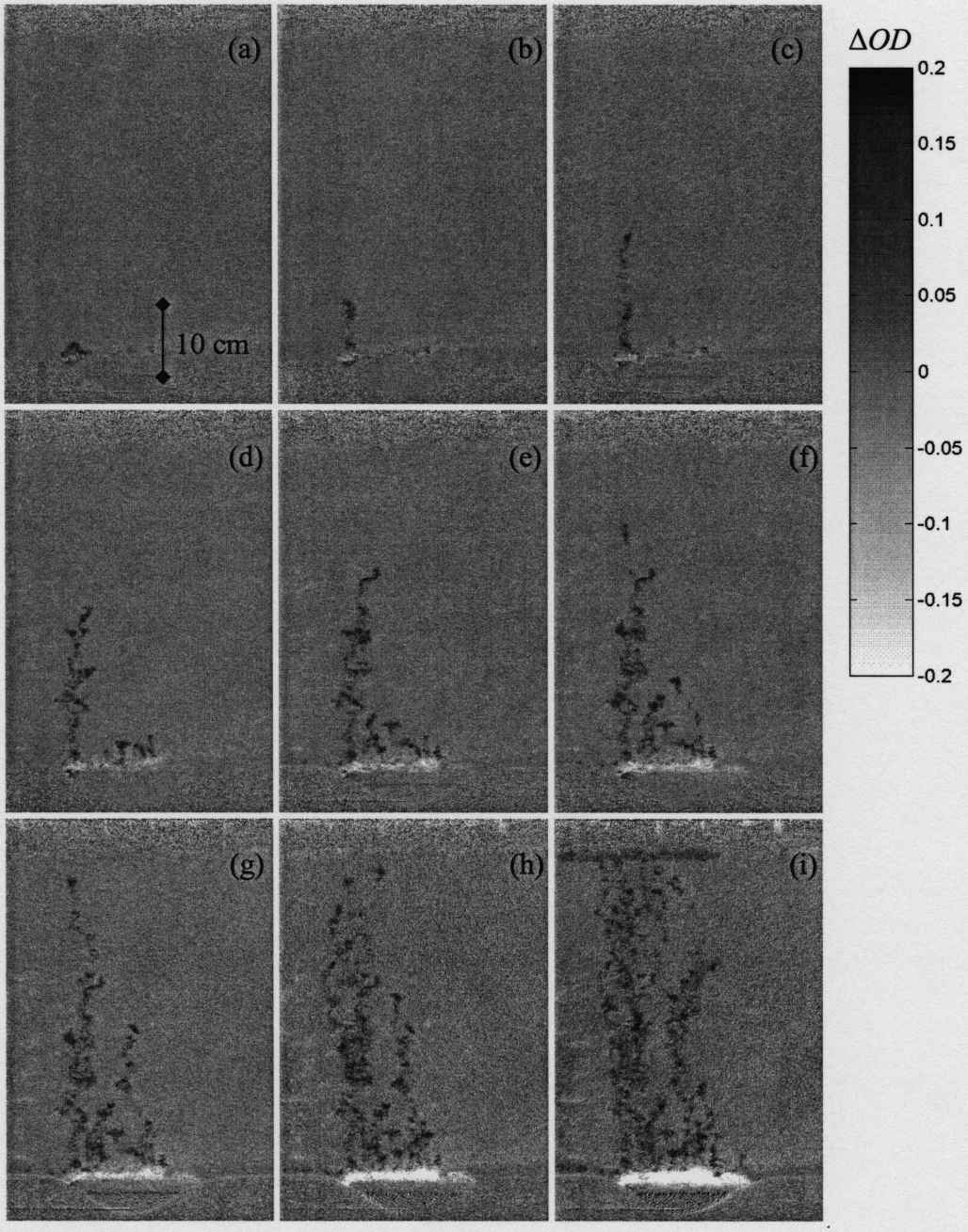

Figure 3.4. Gas distribution above the DNAPL pool at (a) 3 days, (b) 4 days, (c) 6 days, (d) 11 days, (e) 18 days, (f) 21 days, (g) 25 days, (h) 40 days, and (i) 70 days displayed as the difference in optical density between the initial (background) image and successive images (Equation 8). An increase in the gas saturation above the pool produced a darker image (increased optical density), and a decrease in the DNAPL saturation within the pool produced a brighter image (decreased optical density).

to occur at the upper-most tips of the fingers and in the main body of the fingers. Observed step-wise growth behind the upper-most finger tips indicates disconnections between the gas clusters that make up the macroscopic fingers. The step-wise growth of each finger is illustrated in Figure 3.5, which shows the maximum height of each finger during the 70-day duration of the experiment. It is important to note that periods of constant maximum height do not imply periods of no growth, as growth in lower branches of the fingers was often observed.

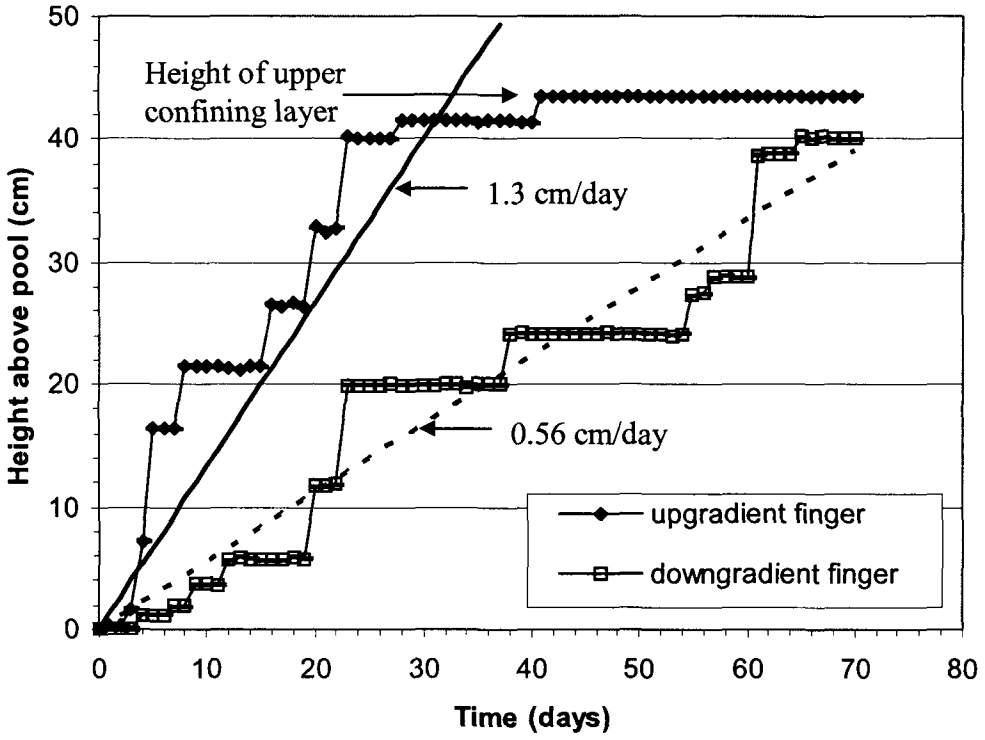

Figure 3.5. Gas-finger height above the surface of the DNAPL pool throughout the 70-day experiment, where the symbols represent measured finger-tip heights and best-fit lines represent the average growth rate of the upgradient (solid) and downgradient (dotted) fingers.

The upgradient and downgradient fingers reached heights of 44 cm and 40 cm above the pool surface, respectively, by the end of the 70-day experiment. A steady-state gas distribution was not achieved. The vertical growth of the upgradient finger was stopped when it reached the upper confining layer of the flow cell, and gas began to pool on the

underside of this capillary barrier (Figure 3.4i). The vertical growth of the downgradient finger had not reached a steady-state when the experiment was terminated due to gas mobilization into the influent glass-bead pack. Figures 4 and 5 show for the first time that the effects of an expanding gas phase above a DNAPL pool are not constrained to the local environment at the surface of the pool, but can impact the system on a REV-scale. This is different than observations by Roy and Smith (2007), who report a maximum gas height of 5 cm above a DNAPL pool in their flow cell experiments using 1 mm-diameter glass beads and TCE. The substantial difference in height is likely due to the vapor pressure of TCE of 1.0×10^4 Pa at 25°C (Pankow and Cherry, 1996), which is 60% of the vapor pressure of 1,1,1-TCA. However, the gas saturation of the influent water in the study by Roy and Smith (2007) was not reported, and may have contributed to different growth and dissolution conditions.

In addition to differences in maximum height, the extent of trapping shown in Figure 3.4 is substantially different from that reported for the glass bead experiments of Roy and Smith (2007). Although they reported that the trapping of mobilized gas clusters was common, they also reported that several mobilized clusters reached the top of their flow cell following mobilization. Figure 3.4 clearly shows that trapping of mobilized gas clusters in natural porous media is a primary mechanism, and that macroscopic vertical growth of the finger is made possible by repeated coalescence events. This is expected to be the primary growth pattern for the expansion of a discontinuous gas phase above a DNAPL pool at most field sites, where the lengths of the gas clusters are significantly greater than the scale of a single pore-body (Figure 3.1) and are easily trapped following mobilization due to the greater variation in pore sizes present in natural sands compared to uniform glass beads.

Figure 3.5 also shows that the average growth rate of the downgradient finger tip (0.56 cm/day) is slower than the average growth rate of the upgradient finger tip (1.3 cm/day). The two gas fingers are of similar width, and were both observed to span the thickness of

the flow cell. Therefore, the growth rate of the tip is taken to be a reasonable measure of the relative growth of each gas finger. The decreased growth rate of the downgradient gas finger is consistent with the process for the partitioning of multiple dissolved gases to a discontinuous gas phase, and observations of this effect have not been reported previously in the literature. While the effect of a reduced growth rate on the effective steady-state distribution of discontinuous gas above a DNAPL pool is yet to be determined, it is reasonable to expect that at some length along the DNAPL pool sufficient stripping of dissolved gases will occur to significantly limit discontinuous gas phase expansion.

3.5 Summary and Conclusions

Extensive discontinuous gas-phase expansion, fragmentation, and vertical mobilization was observed above a pool of 1,1,1-TCA in an intermediate-scale two-dimensional flow cell subjected to a flowing aqueous phase saturated with atmospheric gases. Pore-scale observations showed evidence of expansion, dissolution, fragmentation, and coalescence events that were highly dependent on local system properties. Macro-scale observations showed the vertical growth of discontinuous, macroscopic gas fingers dominated by the repeated trapping and mobilization of discontinuous gas clusters. They also showed the preferential growth of an upgradient gas finger compared to a downgradient gas finger due to the upgradient stripping of dissolved gases. These new observations of macroscopic gas-finger growth above a DNAPL pool illustrate that this mechanism will potentially impact systems at the REV-scale, that models describing this mechanism must consider the discontinuous nature of the gas fingers, and that the transient development of the gas fingers will be a function of the distance from the upgradient edge of the pool. This timely contribution directly influences the rapidly emerging changes in our fundamental conceptual models of DNAPL source zones containing a discontinuous gas phase.

Acknowledgments

This research was supported by the Natural Sciences and Engineering Research Council (NSERC) of Canada through its Discovery Grant Program and a Canada Graduate Scholarship to the first author.

References

Amos, R.T., and K.U. Mayer. 2006a. Investigating the role of gas bubble formation and entrapment in contaminated aquifers: Reactive transport modelling. J. Contam. Hydrol. 87:123-154.

Amos, R.T., and K.U. Mayer. 2006b. Investigating ebullition in a sand column using dissolved gas analysis and reactive transport modeling. Environ. Sci. Technol. 40:5361-5367.

Birovljev. A., G. Wagner, P. Meakin, J. Feder, and T. Jossang. 1995. Migration and fragmentation of invasion percolation clusters in 2-dimensional porous media. Phys. Rev. E. 51:5911-5915.

Brooks, M.C., W.R. Wise, and M.D. Annable. 1999. Fundamental changes in in situ air sparging flow patterns. Ground Water Monit. R. 19:105-113.

Chrysikopoulos, C.V., K.Y. Lee, and T.C. Harmon. 2000. Dissolution of a well-defined trichloroethylene pool in saturated porous media: Experimental design and aquifer characterization. Water Resour. Res. 36:1687-1696.

Cirpka, O.A., and P.K. Kitanidis. 2001. Transport of volatile compounds in porous media in the presence of a trapped gas phase. J. Contam. Hydrol. 49:263-285.

Ewing, R.P, and B. Berkowitz. 2001. Stochastic pore-scale growth models of DNAPL migration in porous media. Adv. Water Resour. 24:309-323.

Frette, V., J. Feder, T. Jossang, and P. Meakin. 1992. Buoyancy-driven fluid migration in porous-media. Phys. Rev. Lett. 68:3164-3167.

Frette, V., J. Feder, T. Jossang, P. Meakin, and K.J. Maloy. 1994. Fast, Immiscible fluid-fluid displacement in 3-dimensional porous-media at finite viscosity contrast. Phys. Rev. E. 50: 2881-2890.

Geistlinger, H., A. Beckmann, and D. Lazik. 2005. Mass transfer between a multicomponent trapped gas phase and a mobile water phase: Experiment and theory. Water. Resour. Res. 41:W11408, doi:10.1029/2004WR003885.

Geistlinger, H., G. Krauss, D. Lazik, and L. Luckner. 2006. Direct gas injection into saturated glass beads: Transition from incoherent to coherent gas flow pattern. Water Resour. Res. 42:W07403, doi:10.1029/2005WR004451.

Glass, R.J., S.H. Conrad, and W. Peplinski. 2000. Gravity-destabilized nonwetting phase invasion in macroheterogeneous porous media: Experimental observations of invasion dynamics and scale analysis. Water Resour. Res. 36: 3121-3137.

Holocher, J., F. Peeters, W. Aeschbach-Hertig, W. Kinzelbach, and R. Kipfer. 2003. Kinetic model of gas bubble dissolution in groundwater and its implications for the dissolved gas composition. Environ. Sci. Technol. 37:1337-1343.

Johnson, D.N., J.A. Pedit, and C.T. Miller. 2004. Efficient, near-complete removal of DNAPL from three- dimensional, heterogeneous porous media using a novel combination of treatment technologies. Environ. Sci. Technol. 38:5149-5156.

Johnson, R.L., and J.F. Pankow. 1992. Dissolution of dense chlorinated solvents into groundwater. 2. source functions for pools of solvent. Environ. Sci. Technol. 26:896-901.

Khachikian, C., and T.C. Harmon. 2000. Nonaqueous phase liquid dissolution in porous media: Current state of knowledge and research needs. Transport Porous Med. 38:3-28.

Li, X., and Y.C. Yortsos. 1995. Theory of multiple bubble-growth in porous-media by solute diffusion. Chem. Eng. Sci. 50:1247-1271.

McNeil, J.D., G.A. Oldenborger, and R.A. Schincariol. 2006. Quantitative imaging of contaminant distributions in heterogeneous porous media laboratory experiments. J. Contam. Hydrol. 84:36-54.

Mumford, K.G., J.E. Smith, and S.E. Dickson. 2008. Mass flux from a non-aqueous phase liquid pool considering spontaneous expansion of a discontinuous gas phase. J. Contam. Hydrol. 98:85-96.

Niemet, M.R., and J.S. Selker. 2001. A new method for quantification of liquid saturation in 2D translucent porous media systems using light transmission. Adv. Water Resour. 24:651-666.

O'Carroll, D.M., and B.E. Sleep. 2007. Hot water flushing for immiscible displacement of a viscous NAPL. J. Contam. Hydrol. 91:247-266.

Oostrom, M., J.H. Dane, and T.W. Wietsma. 2007. A review of multidimensional, multifluid, intermediate-scale experiments: Flow behavior, saturation imaging, and tracer detection and quantification. Vadose Zone J. 6:610-637.

Pankow, J.F., and J.A. Cherry. 1996. Dense Chlorinated Solvents and other DNAPLs in Groundwater. Waterloo Press, Portland, Oregon.

Roosevelt, S.E., and M.Y. Corapcioglu. 1998. Air bubble migration in a granular porous medium: Experimental studies. Water Resour. Res. 34:1131-1142.

Roy, J.W., J.E. Smith, and R.W. Gillham. 2004. Laboratory evidence of natural remobilization of multicomponent DNAPL pools due to dissolution. J. Contam. Hydrol. 74:145-161.

Roy, J.W., and J.E. Smith. 2007. Multiphase flow and transport caused by spontaneous gas phase growth in the presence of dense non-aqueous phase liquid. J. Contam. Hydrol. 89:251-269.

Schroth, M.H., S.J. Ahearn, J.S. Selker, and J.D. Istok. 1996. Characterization of miller-similar silica sands for laboratory hydrologic studies. Soil. Sci. Soc. Am. J. 60:1331-1339.

Seagren, E.A., B.E. Rittman, and A.J. Valocchi. 1999. An experimental investigation of NAPL pool dissolution enhancement by flushing. J. Contam. Hydrol. 37:111-137.

Stöhr, M., and A. Khalili. 2006. Dynamic regimes of buoyancy-affected two-phase flow in unconsolidated porous media. Phys. Rev. E. 73:036301.

Tidwell, V.C., and R.J. Glass. 1994. X-ray and visible-light transmission for laboratory measurement of 2-dimensional saturation fields in thin-slab systems. Water Resour. Res. 30:2873-2882.

Tsimpanogiannis, I.N., and Y.C. Yortsos. 2004. The critical gas saturation in a porous medium in the presence of gravity. J. Colloid Interf. Sci. 270:388-395.

Wilkinson, D. 1984. Percolation model of immiscible displacement in the presence of buoyancy forces. Phys Rev A. 30:520-531.

Wilkinson, D. 1986. Percolation effects in immiscible displacement. Phys. Rev. A. 34:1380-1391.

Zhang, Z.F., and J.E. Smith. 2002. Visualization of DNAPL fingering processes and mechanisms in water-saturated porous media. Transport Porous Med. 48:41-59.

Chapter 4

Slow gas expansion in saturated natural porous media by gas injection and partitioning with non-aqueous phase liquids

The contents of this chapter have been accepted for publication as: Mumford, K.G., Dickson, S.E., Smith, J.E., 2008. Slow gas expansion in saturated natural porous media by gas injection and partitioning with non-aqueous phase liquids. *Advances in Water Resources*, In Press.

Abstract

The partitioning of volatile non-aqueous phase liquid (NAPL) compounds to a discontinuous gas phase can result in the expansion of that gas phase, and the resulting gas flow can significantly affect the mass transfer from NAPL source zones. This recently reported gas flow generated by the spontaneous expansion of a discontinuous gas phase has not been extensively characterized in the literature. This study measured the expansion rate of a single gas cluster in a 1.1 mm sand above a pool of trans-1,2-dichloroethene (tDCE) in small-scale flow cell experiments. To characterize the gas flow, gas injection experiments in three sizes of sand were conducted at very slow injection rates typical of gas flow rates produced by gas expansion due to NAPL partitioning. Gas cluster spontaneous expansion rates above a tDCE pool were found to be 0.34±0.02 mL/day and 0.29±0.01 mL/day in duplicate experiments, which is

sufficiently slow to result in discontinuous gas flow in porous media with a grain size diameter greater than 0.02 mm. Measured capillary pressures during gas injection showed patterns consistent with discontinuous gas flow, and identified multiple fragmentation events and expansion by coalescence with trapped clusters. The combination of pressure data and light transmission images were used to identify fragmentation and obtain direct measurements of the critical cluster length (i.e. the length at which withdrawal of the gas phase from a pore space occurs) in quasi-two-dimensional porous media for the first time. The measured critical cluster lengths were 1.4-3.6 cm, 3.2-6.0 cm and 2.8-6.5 cm in 1.1 mm, 0.7 mm and 0.5 mm sands, respectively. These values agreed well with estimates of the critical cluster length made using previously reported equations, and parameters derived from the medium's capillary pressure-saturation relationship.

Keywords: NAPL dissolution; spontaneous gas expansion; unstable gas flow; buoyancy forces; capillary forces; gas injection

4.1 Introduction

Recent studies have shown that gas flow following the spontaneous expansion of a discontinuous gas phase can significantly affect the mass transfer from non-aqueous phase liquid (NAPL) pools [1]. These pools are typically responsible for the persistence of NAPL source zones [2] and the continued contamination of the surrounding groundwater at NAPL-contaminated sites over periods of decades to centuries. This recently reported mechanism of spontaneous gas expansion results in significant vertical gas flow away from the NAPL pool [3], potentially increasing the mass transfer rate and changing the spatial distribution of dissolved NAPL. This could affect efforts to locate NAPL source zones using aqueous concentration data, as well as the prediction of risks and lifetimes associated with NAPL source zones. Spontaneous gas expansion has been observed in the presence of a variety of NAPLs, including tetrachloroethene (PCE), trichloroethene (TCE), 1,1,1-trichloroethane (1,1,1-TCA), and trans-1,2-dichloroethene (tDCE), which have vapor pressures between 2.5×10^3 Pa and 4.2×10^4 Pa [1,3,4]. Because

spontaneous gas expansion is a function of the hydrostatic pressure, capillary pressure, and the concentrations of other dissolved gases in the groundwater, in addition to the vapor pressure of the NAPL, it is more likely to be active at NAPL-contaminated sites with higher volatility NAPL in shallow source zones and coarse media [3]. However, where additional dissolved gases can be generated in the vicinity of NAPL, such as by microbial activity, the additional partial pressure could result in expansion in deeper, finer systems.

This mechanism has not been characterized extensively in the literature. In particular, little is known concerning the nature of the resulting gas flow. Roy and Smith [1] observed repeated fragmentation and mobilization of an expanding discontinuous gas phase above pools of PCE, TCE and a mixture of benzene and PCE in 1-mm and 3-mm glass bead packs. In addition to repeated fragmentation and mobilization, Mumford et al. [3] observed extensive trapping and coalescence of a mobilized gas phase above a pool of 1,1,1-TCA in a 1.1-mm uniform sand. The gas-phase data presented in these previous studies are limited to qualitative observations of pore-scale processes, and measurements of the maximum vertical extent of the gas phase. No quantitative information is presented in these studies, or elsewhere in the literature, concerning the rate of generated gas flow or the transient distribution of the resulting disconnected gas clusters produced via this mechanism in porous media. Measurements of gas flow rate and distribution are important first steps toward better understanding the total mass transfer away from the pool and the dissolution of the volatized NAPL into the groundwater above the pool, respectively.

The current literature concerning gas flow in porous media does not adequately address this mechanism, which is expected to produce very low gas flow rates. This expectation is based on experiments conducted under diffusion-limited conditions, in the absence of porous media, where single gas bubbles were observed to expand at rates of $2x10^{-3}$ mL/day and $2x10^{-4}$ mL/day in the presence of tDCE and PCE, respectively [4]. Although

these rates were not measured in porous media, they suggest that gas flow generated by spontaneous expansion will be substantially slower than the injection rates used in other studies of gas flow in porous media, including 20-3000 mL/min [5], 10-5000 mL/min [6], 3-186 mL/min [7], and 240-5200 mL/min [8]. Gas was injected as a point source during these studies, using either porous stones (1-2 cm diameter) [5,8], or small-diameter injection points (2-5 mm diameter) [6,7]. Very few studies have reported results for the slow injection of gas in water-saturated porous media [6]. Glass et al. [9] injected CO_2 at 1.2 mL/min into uniform sand saturated with water. In an analogous study of unstable, non-wetting fluid injection, Frette et al. [10] injected a sucrose-water solution at 0.03 mL/min into a 18.3 x 18.3 x 28.3 cm^3 container packed with 2-mm long x 2-mm diameter plexiglass cylinders, saturated with dibutyl-phthalate. Their study used the sucrose-water solution as the injected, non-wetting fluid, and dibutyl-phthalate as the wetting fluid in place of gas and water, respectively. Our study investigated gas flow for injection rates of 0.001 and 0.01 mL/min, injected through a 2-mm diameter tube, which is capable of producing discontinuous flow [6] in media finer than 1 mm to 2 mm. A grain size of 1 mm to 2 mm is typically considered to be the transition point for continuous to discontinuous gas flow reported in the air sparging literature [5].

The purpose of this study is to characterize the gas flow in natural porous media resulting from the spontaneous expansion of a discontinuous gas phase at the surface of a NAPL pool. Two sets of bench-scale experiments were conducted in natural sand to 1) quantify the expansion rate of a discontinuous gas phase at the surface of a NAPL pool, and 2) measure the transient gas pressures and critical cluster lengths produced by the very slow injection of gas in three different sands. This study is the first to quantify the rate of spontaneous gas expansion above a NAPL pool in porous media, and represents the first data for the injection of gas at these very slow flow rates. In addition, this study provides the first direct measurement of discontinuous gas-cluster lengths in a porous medium with a thickness greater than one grain diameter, made possible by using a combination of imaging techniques and pressure measurements, in contrast to previous studies that

measured gas-cluster lengths [11,12] in monolayer packings of glass beads. The results of this study contribute to the refinement of the conceptual model for the spontaneous expansion of a gas phase in the presence of NAPL [1], and provide key quantitative data that will facilitate the incorporation of this mechanism into future numerical models.

4.2 Background

4.2.1 Expansion of multi-component discontinuous gas phases

The partitioning of multiple dissolved gases to a discontinuous gas phase is well described by Cirpka and Kitanidis [13] and has been used for numerous applications including the dissolution [14,15] and expansion [1,4,16] of discontinuous gas phases. Cirpka and Kitanidis [13] show that the dissolution or expansion of a multi-component gas phase results from the constraint

$$P_g = P_w + P_c = \sum_i P_i^g \tag{4.1}$$

where P_g is the gas pressure, P_w is the bulk liquid pressure, P_c is the capillary pressure, and P_i^g is the partial pressure of compound i in the gas phase. The capillary pressure is described by the Laplace equation of capillarity

$$P_c = \sigma\left(\frac{1}{r_1} + \frac{1}{r_2}\right) \tag{4.2}$$

where σ is the gas-liquid interfacial tension, and r_1 and r_2 are the principal radii of curvature of the gas-liquid interface. The partial pressure is described by Henry's law, assuming local thermodynamic equilibrium at the gas-liquid interface

$$P_i^g = K_{Hi} C_i \tag{4.3}$$

where K_{Hi} is the Henry's law coefficient for compound i, and C_i is the local aqueous phase concentration of compound i. The constraint given by (4.1) can result in local aqueous concentrations different from those in the bulk solution, which drives mass transfer between the bulk solution and the discontinuous gas phase. The resulting changes in the pressure and volume of the gas phase over time under isothermal conditions follows from the ideal gas law

$$\frac{dn_t}{dt} = \frac{1}{RT}\frac{d(P_g V_g)}{dt} \tag{4.4}$$

where n_t is the total number of moles in the gas phase, t is time, R is the gas constant, T is the temperature, and V_g is the volume of the gas phase. For mass transfer into a discontinuous gas phase (i.e. $dn_t/dt>0$) in porous media, the changes to pressure and volume occur in a series of pore-filling (approximately constant pressure) and pressurization (approximately constant volume) steps [17].

4.2.2 Gas flow in water-saturated porous media

Two different flow patterns have been observed for the upwards flow of gas in otherwise water-saturated porous media: continuous (also called channel or coherent) flow and discontinuous (also called bubbly, slug, or incoherent) flow [5-7]. Continuous flow is characterized by a collection of continuous channels which transport gas along a gas-phase pressure gradient. Discontinuous flow is characterized by the presence of multiple, discrete gas clusters, which may be either trapped or mobile, depending on the magnitude of local capillary and buoyancy forces. The difference between these two gas-phase distributions has a controlling effect on the mass transfer between the gas and aqueous phases [5]. For spontaneous gas expansion in particular, the occurrence of discontinuous gas flow allows the expansion of some gas clusters and the dissolution of others, as the mass transfer is controlled by the local aqueous concentrations at each individual gas-liquid interface [3].

The threshold between continuous and discontinuous flow has been based solely on the consideration of the Bond number [5,8]

$$Bo = \frac{\Delta\rho g r_p^{\,2}}{\sigma} \tag{4.5}$$

where Bo is the Bond number, $\Delta\rho$ is the density difference between the resident and invading fluids, g is the acceleration due to gravity, and r_p is a characteristic pore radius. In a review of the literature, Selker et al. [8] found that continuous flow dominated for $Bo<0.03$. Based on the ratio of pore necks to pore bodies used by Brooks et al. [5], this is consistent with the grain size threshold of approximately 1 mm to 2 mm for the injection of air in water-saturated porous media referred to in the air sparging literature.

Recent research, however, shows that the consideration of the Bond number alone is insufficient for the characterization of gas flow. Geistlinger et al. [6] and Stöhr and Khalili [7] report similar expressions for a critical flow rate, at which the friction forces resulting from the flow of gas in a channel stabilize the flow

$$Q_{crit} = \frac{\pi\Delta\rho g r_c^{\,4}}{8\mu_g} \tag{4.6}$$

where Q_{crit} is the critical gas flow rate above which gas flow is stable and continuous, r_c is the gas channel radius, and μ_g is the gas dynamic viscosity. A value of Q_{crit} capable of stabilizing the gas flow is only attainable in media where capillary forces dominate over gravity forces at the scale of a single pore [7]. Equation (4.6) shows that discontinuous flow is not limited to media of greater than 1 mm to 2 mm in diameter; it will occur in much finer media when the gas flow rate is sufficiently small.

4.2.3 Fragmentation and Mobilization

The flow of discontinuous gas clusters in porous media is controlled by both capillary and buoyancy forces, as described by studies that model gas flow using modified invasion percolation (MIP) in a gradient with fragmentation and mobilization [18-20]. For an immobile discontinuous gas phase (Figure 4.1a) to expand, whether due to the injection of additional gas or the partitioning of additional volatile compounds, the gas pressure in the cluster must overcome the sum of the hydrostatic and entry pressures in one of the adjacent pore throats

$$P_g \geq P_w + P_e \tag{4.7}$$

where P_e is the throat entry pressure. The entry pressure can be expressed as

$$P_e = \frac{2\sigma}{r_t} \tag{4.8}$$

where r_t is an effective pore throat radius, which implicitly includes contact angle considerations. Thus, the capillary pressure increases with the gas pressure until the throat entry pressure is reached. Once this local gas-phase entry pressure is achieved the gas phase expands into the adjacent pore body (Figure 4.1b) and the capillary pressure drops. This capillary pressure may be greater or less than the capillary pressure in the previous pore body, depending on the geometry of the new gas-liquid interface. This alternating sequence of pressurization and pore-entry [17] results in a dynamic fluctuating gas pressure. As expansion continues it is biased towards growth in the upwards vertical direction (Figure 4.1c) since the hydrostatic pressure decreases with height making the entry into pore throats above the cluster generally more favorable [21]. Therefore, although the gas pressure fluctuates, due to local pressurization and pore-entry events, the mean pressure decreases with increasing cluster height, due to the decrease in hydrostatic pressure as the cluster expands upward.

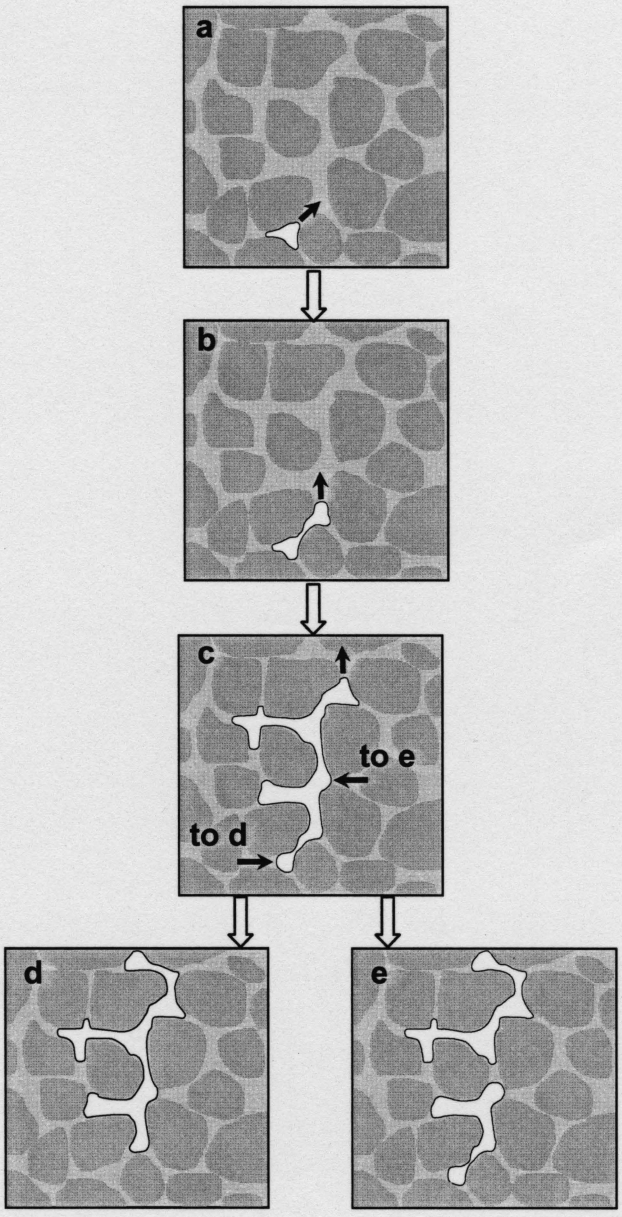

Figure 4.1. Stages of growth for a gas cluster in porous media showing (a) initial gas cluster, (b) expansion to adjacent pore space, (c) vertically dominated expansion, (d) mobilization, and (e) fragmentation, where the black arrows indicate the direction of interface movement between the different stages of growth.

As the length of the cluster extends vertically, the local curvature of the gas-liquid interface adjusts to maintain a uniform gas pressure throughout the cluster despite a

decrease in hydrostatic pressure with height. This results in greater radii of curvature (lower capillary pressure) towards the bottom of the cluster and lesser radii of curvature (high capillary pressure) towards the top. Once the length of the cluster reaches a critical value, the capillary pressure towards the bottom of the cluster drops to a value where the re-invasion of water into previously gas-occupied pore space is possible. This pressure is referred to as the withdrawal threshold [12,20] and is analogous to the terminal pressure (P_t) used to describe the formation of NAPL residual, which has been previously defined on the macroscopic scale using capillary pressure-saturation curves [22]. This re-invasion results in either the mobilization (Figure 4.1d) or the fragmentation (Figure 4.1e) of the cluster, depending on the location of the pore where re-invasion occurs. Following fragmentation, the lower gas cluster is at a lower capillary pressure than what is required for the entry into any of its adjacent pore throats. Therefore, pressurization of the entire cluster must occur again before repeated growth of that cluster is possible.

Expressions for estimating the critical cluster length have been reported based on a balance of pressure at the upper and lower tips of the cluster, and consideration of the hydrostatic pressure drop [6,9]

$$h_{crit} = \frac{P_c^{top} - P_c^{bottom}}{\Delta\rho g} \tag{4.9}$$

where h_{crit} is the critical cluster length, P_c^{top} is the capillary pressure at the top of the cluster and P_c^{bottom} is the capillary pressure at the bottom of the cluster, when fragmentation occurs. When it is reasonable to assume that $P_c^{top} >> P_c^{bottom}$, the critical length will be proportional to $Bo^{-1} \cdot r_p$ [21]. Geistlinger et al. [6] estimated the critical length to be on the order of the grain size for the injection of air into water-saturated uniform glass beads greater than 3 mm in diameter, and Glass et al. [9] estimated the critical length to be 4.2 cm for the injection of CO_2 into water-saturated uniform sand with a median grain size of 1.1 mm. Glass et al. [9] reported that their estimated value

was consistent with their experiments, as multiple fragmentation events were observed over a distance of approximately 20 cm, and Geistlinger et al. [6] reported that their estimated value was consistent with previously reported observations of discontinuous gas flow in media with grain sizes greater than 3 mm. This suggests that (4.9) can provide appropriate estimates of the critical cluster length. However, a direct comparison of experimental and predicted critical cluster lengths was not possible because the critical cluster lengths were not measured during the experiments.

4.3 Materials and methods

4.3.1 Flow cell

Both the NAPL pool and gas injection experiments were conducted using a small-scale (100 mm x 80 mm x 8 mm) glass flow cell (Figure 4.2). The flow cell was constructed of rectangular glass tubing, heated at the bottom to create a sealed base and then cut to length. 10-mm diameter glass tubing was installed on either side of the flow cell to serve as influent and effluent ports. The top of the flow cell was sealed by the compression of a rubber gasket along the top surface. Construction of the flow cell in this manner eliminated any seals near the bottom of the flow cell that could be incompatible with NAPL and allowed visualization of the entire domain.

4.3.2 Porous media

One of three size fractions of natural sand (Accusand, Unimin Corporation) were used in all experiments: 12/20, 20/30, and 30/40, referred to here as 1.1 mm, 0.7 mm, and 0.5 mm sand, with selected properties listed in Table 4.1. Bond numbers and critical flow rates were calculated using (4.5) and (4.6), respectively, for the displacement of water by air. These sands have been used extensively in bench-scale experiments of two-phase and three-phase flow processes due to the high degree of batch-to-batch reproducibility available from the manufacturer [23] and their ability to transmit sufficient light to allow visualization of flow processes in transparent, two-dimensional models [8,9,24-27].

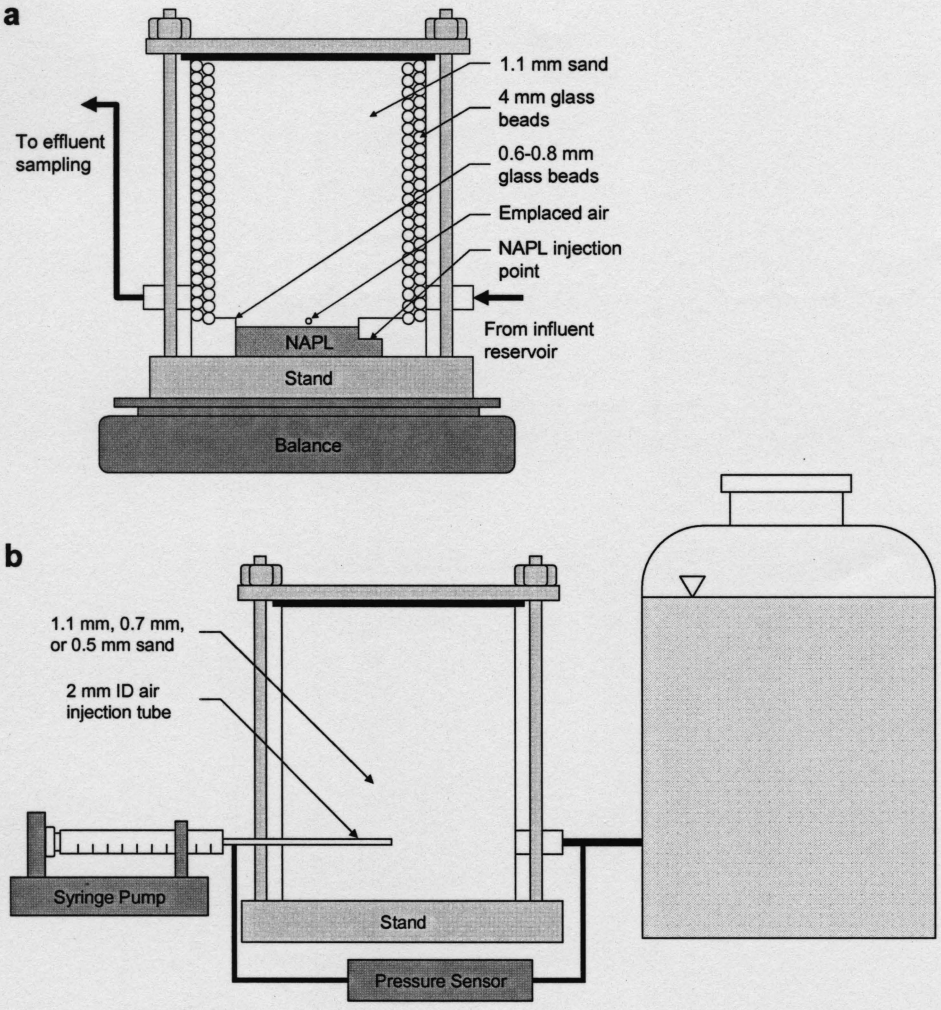

Figure 4.2. Experimental set-up for (a) gas expansion above a NAPL pool and (b) gas injection.

All sands were used as received from the manufacturer with no further processing except a thorough rinsing with distilled water to remove any fines that may have accumulated during shipping. Microscopic and macroscopic air entrapment in the sand were minimized by placing the sand in water under vacuum prior to packing, and continuously pouring the wet sand into the water-filled flow cell. The continuous pouring, together with the tapping of the flow cell walls with a small rubber mallet following the pour, achieved a reasonably homogeneous pack. The porosity of the sand pack in each

experiment (Table 4.2 and Table 4.3) was determined based on the known volume of the flow cell and the mass of sand used in the packing.

Table 4.1. Porous media properties

	1.1 mm sand	0.7 mm sand	0.5 mm sand
Size fraction	12/20	20/30	30/40
Median grain size (mm)[1]	1.105	0.713	0.532
Uniformity coefficient[1]	1.231	1.19	1.207
Air-entry pressure (cm of H_2O)[1,2]	5.42	8.66	13.03
Bond number[3]	4.2×10^{-2}	1.7×10^{-2}	9.6×10^{-3}
Critical flow rate (mL/min)[4]	1×10^{3}	1×10^{2}	6×10^{1}

[1]Schroth et al. (1996)
[2]Based on Brooks-Corey fitting parameters
[3]Calculated using (4.5) with σ=72 mN/m and $\Delta\rho$= 1000 kg/m^3
[4]Calculated using (4.6) with $\Delta\rho$=1000 kg/m^3, μ_g=0.02 mN·s/m^2, and taking r_c equal to half the median grain size

Table 4.2. Conditions and observations for gas expansion above a NAPL pool

Experiment No.	Packing	Porosity	Aqueous flow rate (mL/min)	Average gas expansion rate (mL/day)
1	1.1 mm sand	0.335	0.130	0.34±0.02
2	1.1 mm sand	0.334	0.125	0.29±0.01

4.3.3 Gas expansion above a NAPL pool

To measure the expansion of a discontinuous gas phase above the surface of a NAPL pool in experiments #1 and #2, the flow cell was packed as shown in Figure 4.2a. The center of the cell was packed with 1.1 mm sand, the bottom corners were packed with finer glass beads (0.6 to 0.8 mm diameter, Potters Industries) to contain the NAPL pool, and the influent and effluent walls were packed with 4 mm glass beads (Propper Manufacturing Co. Inc.) to distribute the flow along the height of the flow cell.

Midway through the packing procedure 0.6 mL of trans-1,2-dichloroethene (tDCE, Alfa Aesar, 98%) dyed with 100 mg/L of Sudan 4 (Acros Organics) was emplaced at the bottom of the cell to create a pool with a length of 4.3 cm. The tDCE was emplaced using a gastight syringe and a stainless steel needle, inserted into the packing from the top

and subsequently withdrawn. tDCE was selected for this experiment due to its relatively high vapor pressure of 4.2×10^4 Pa at 25°C [28], which was expected to result in relatively rapid expansion of the gas phase [4]. Following emplacement of the NAPL pool, a 4 μL bubble of laboratory air was emplaced 4 mm above the pool surface near the center of the front wall of the flow cell using the same technique as for the NAPL emplacement. Both the tDCE and the air were emplaced midway through the packing to allow easier insertion and withdrawal of the injection needle, and limit the creation of a preferential gas flow path due to rearrangement of the sand grains during needle withdrawal. By emplacing the tDCE and air midway through the packing, this potential preferential pathway was limited to a height of 2 cm above the pool surface.

Table 4.3. Conditions and observations for gas injection

Experiment No.	Air injection rate (μL/min)	Porosity	Critical cluster length (cm)	Capillary pressure during fluctuation phase (cm)		P_t/P_e
				Min. (P_t)	Max. (P_e)	
1.1 mm sand						
3	1	0.366	1.4	5.5	9.3	0.60
4	1	0.375	3.1	3.6	6.7	0.54
5	1	0.361	2.5	3.9	6.5	0.60
6	10	0.372	2.9	4.7	8.9	0.53
7	10	0.365	3.6	4.1	7.6	0.54
8	10	0.356	3.3	4.3	6.9	0.62
0.7 mm sand						
9	1	0.361	6.0	12.3	14.9	0.83
10	1	0.357	5.1	6.8	11.2	0.61
11	1	0.373	5.6	5.8	10.4	0.56
12	10	0.363	4.8	6.7	11.1	0.60
13	10	0.373	5.0	5.5	9.9	0.56
14	10	0.364	3.2	6.7	9.6	0.70
0.5 mm sand						
15	1	0.363	6.0	10.9	19.1	0.57
16	1	0.368	6.5	9.5	16.7	0.57
17	1	0.364	2.8	11.6	19.5	0.59

Distilled water saturated with laboratory air was pumped through the flow cell using a peristaltic pump (Cole-Parmer, model no. 7550-50). The effluent exited the flow cell

through a port located near the bottom of the cell, and was discharged through tubing at a fixed elevation located 1.5 cm below the top of the flow cell. The influent contained 200 mg/L of sodium azide to act as a biocide [29-31]. The flow rate was measured periodically by weighing the effluent (Table 4.2), which was collected in a flask covered to minimize evaporative losses.

To quantify the expansion of the gas phase the packed flow cell was placed on a laboratory balance (Mettler Toledo, model no. PG5002-SDR) throughout the experiment to measure the water mass lost from the flow cell due to displacement by the expanding gas. The water-mass loss was corrected for mass lost due to NAPL dissolution using a dissolution rate calculated from periodic sampling of the effluent and subsequent analysis of dissolved tDCE in experiment #2. The effluent from experiment #1 was not sampled, but the tDCE pools in each experiment were visually observed to dissolve at similar rates. Analysis of dissolved tDCE was conducted by gas chromatography-mass spectroscopy (Agilent 6890 GC, Agilent 5973 MS mass selective detector, Restek Rtx-502.2 60 m, 0.32 mm ID, 1.8 μm film thickness column) equipped with a headspace autosampler (Agilent 7694E). The temperature program for the GC oven was 40°C hold for 6 min, ramp at 10°C/min to 120°C, and ramp at 25°C/min to 220°C. The total effluent mass of 0.72±0.03 g, determined by integration of the breakthrough curve, was not significantly different from the injected mass of 0.76±0.03 g, which indicates a satisfactory mass balance. Based on the breakthrough data, tDCE was lost at a linear rate of $6.4 \times 10^{-2} \pm 2 \times 10^{-3}$ g/day, with no distinction between mass lost directly from the pool to the aqueous phase and mass lost from the pool to the aqueous phase through the gas phase. Assuming that all of the dissolved tDCE was replaced by water, the dissolution of the pool resulted in a change in mass of the flow cell of $1.25 \times 10^{-2} \pm 4 \times 10^{-4}$ g/day, which was used to correct the mass data. This rate represents 4% of the total mass change due to dissolution of the pool, and the displacement of water by the expanding gas phase.

4.3.4 Gas injection

To assess the flow of a slowly injected gas phase in experiments #3 - #17, the flow cell was packed as shown in Figure 4.2b. The flow cell was packed with 1.1 mm, 0.7 mm, or 0.5 mm sand. A 2-mm ID glass tube was inserted into a port and connected to a gastight syringe (Hamilton, 2.5 mL, model no. 1002) on a syringe pump (KD Scientific, model no. 230). The syringe pump was used to inject 1000 μL of laboratory air at rates of 1 μL/min or 10 μL/min (Table 4.3), which are well below the calculated Q_{crit} values. A relatively large-diameter injection tube was used to avoid the creation of an artificial fragmentation point, as would be created by using a tube with a diameter significantly less than that of the surrounding pore spaces, and promote fragmentation within the sand pack.

The second port was connected to a 9.7-cm diameter water reservoir. As a result of this wide diameter, the displacement of water by the injected air resulted in an increase in water level of only 0.1 mm by the end of the injection, effectively maintaining a constant water pressure on the flow cell throughout the experiment. The water reservoir was open to the atmosphere via a small hole in a Parafilm® cover. The water in the reservoir and the flow cell was saturated with laboratory air prior to beginning the experiment to minimize any changes in volume due to dissolution of the gas phase.

The pressure of the injected gas phase was measured using a differential pressure sensor (Honeywell, model no. DC005NDC4) attached to the tubing from the syringe and the water reservoir. The differential pressure was measured once per 0.5 μL of gas injected and was recorded using a datalogger (Campbell Scientific, model no. CR23X).

4.3.5 Visualization

Digital images of experiments #2 - #17 were collected using a CCD camera (Canon A640) connected to a personal computer equipped with software from the camera manufacturer. Images were collected at a resolution of $(0.05\ mm)^2$/pixel. The flow cell was located between the camera and a light source, which consisted of light from three

50W halogen bulbs (Liteline Corporation, model no. CF-130-B) reflected off a white background. This allowed visualization of the depth-averaged gas saturation by light transmission [25,32,33].

The digital images for experiments #3 - #17 were processed by aligning the images to correct for shifts between the camera and the flow cell, converting the collected RGB image to a grayscale intensity image, and then subtracting the background image by calculating the difference in optical density [3] using [34]

$$\Delta OD = OD_t - OD_0 = \log\left(\frac{I_0 I_t^{ref}}{I_t I_0^{ref}}\right) \tag{4.10}$$

where ΔOD is the difference in optical density, OD is the optical density, I is the transmitted light intensity and I^{ref} is the average transmitted light intensity over the reference region. The subscripts 0 and t refer to images collected initially and at time t, respectively. The intensity of the reference region was used to correct for temporal changes in lighting, and the reference region consisted of a 2.4 cm x 1 cm section of the sand that was unaffected by the injected gas phase. Following background subtraction, noise was reduced by processing using a median filter on a 3 x 3 pixel^2 (0.14 x 0.14 mm^2) area. Alignment of the images and measurement of critical cluster lengths were conducted using ImageJ (http://rsb.info.nih.gov/ij/), and all other processing was done using MatLab (Release 13, MathWorks, Inc.).

4.4 Results and Discussion

4.4.1 Gas expansion above a NAPL pool

During experiments #1 and #2, repeated expansion, fragmentation, and mobilization of the gas phase was observed. The discontinuous gas phase expanded across the surface of the NAPL pool, was vertically mobilized, and accumulated at the top boundary of the flow cell and in the coarse bead packs along the influent and effluent walls. Mobilized gas entered the coarse bead packs by migrating along the top boundary of the cell and by

penetrating the right-hand coarse bead pack near the NAPL injection point. Figure 4.3 shows the approximate distribution of the gas phase at three times for experiment #2, which were similar to those observed in experiment #1. The general behavior of the gas phase is consistent with previous experiments conducted in the 1.1 mm sand [3].

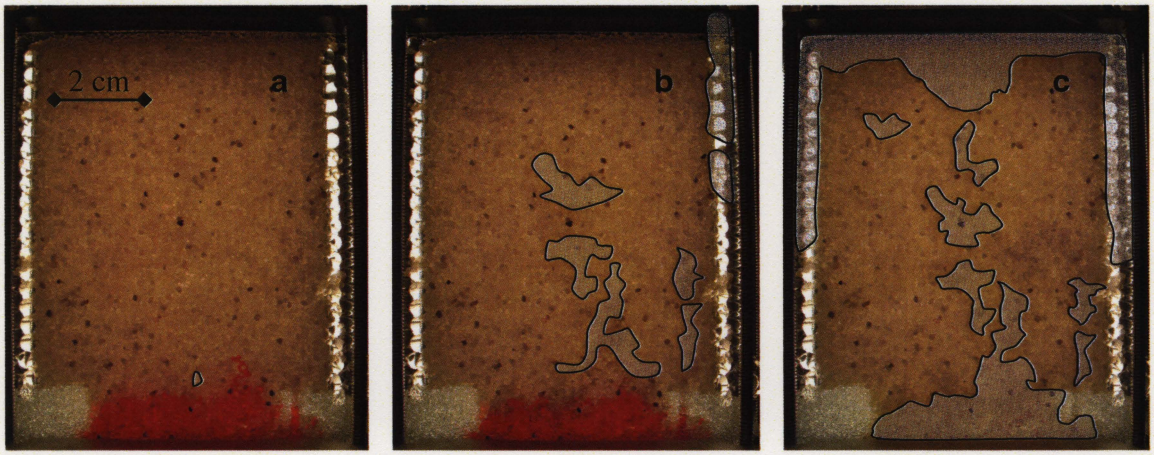

Figure 4.3. Approximate location of gas in the flow cell (indicated by the shaded areas) during experiment #2 (a) following initial emplacement of a 4 μL air bubble above the tDCE pool at 0 days, and after (b) 2 days and (c) 13.7 days.

The accumulation of gas in the flow cell over time is shown in Figure 4.4 for each of the duplicate experiments. The initial 4 μL air bubble expanded to 4.2 mL of gas after 13.1 days in experiment #1, and 4.5 mL of gas after 13.7 days in experiment #2. Treating the entire volume of the sand pack as a representative elementary volume, this represents a change in the macroscopic gas-phase saturation of 3 orders of magnitude, from $3x10^{-4}$ to $3x10^{-1}$. The average expansion rate over the duration of the experiment is given by the slope of the regression line, and was found to be 0.34±0.02 mL/day and 0.29±0.01 mL/day for experiments #1 and #2, respectively (Table 4.2). These results demonstrate good reproducibility of the expansion rate between the two experiments. The approximately linear increase of gas volume with time in Figure 4.4 implies the achievement of an effectively steady expansion rate, which requires the effectively steady mass transfer of tDCE and other dissolved gases to the gas phase. Evidence of

effectively steady mass transfer is consistent with previous studies on the expansion of discontinuous gas above NAPL pools [4].

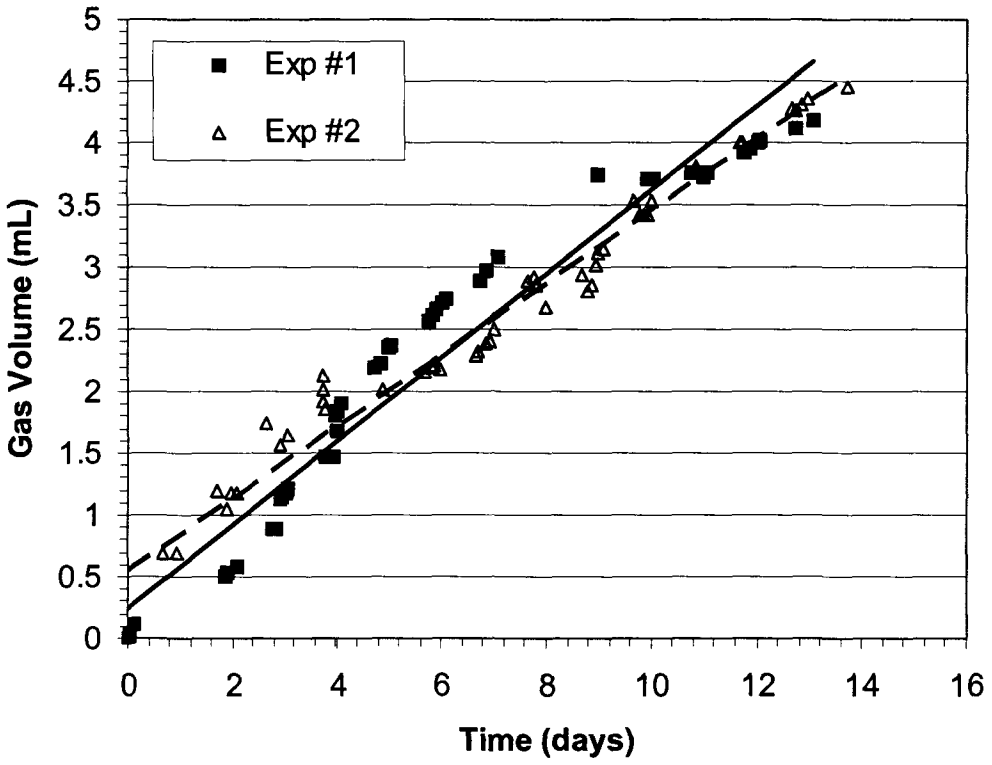

Figure 4.4. Volume of gas accumulated due to the expansion of an initially 4 μL air bubble above a tDCE pool during experiments #1 and #2, where the symbols represent the data and the lines represent the best-fit showing the average expansion rate over the total duration of each experiment. The standard deviation of each data point was estimated to be 0.014 mL, which is less than the size of the symbols used in this plot.

Based on (4.6) the critical gas flow rate for the 1.1 mm sand is expected to be $1x10^3$ mL/min, which is well above the observed gas expansion rate. Therefore, the flow here is expected to be discontinuous, which is consistent with the observations of repeated fragmentation and mobilization events. The expansion rates observed in experiments #1 and #2 are considered upper limits for the expected expansion rate of a single gas cluster located above the surface of a NAPL pool. The tDCE used in these experiments has a relatively high vapor pressure compared to other NAPLs where this mechanism may play

a significant role [1], which produces faster expansion rates [4]. Furthermore, early in the experiments the gas phase contacted the surface of the NAPL pool, which allowed rapid partitioning of the NAPL compound to the gas phase and a faster expansion rate [4]. Although the critical gas flow rate decreases with the grain size, the expansion rates observed here are below the critical gas flow rate for grain diameters greater than 0.02 mm, based on (4.6). Therefore, discontinuous gas flow is expected for the spontaneous expansion of a discontinuous gas phase driven by the partitioning of volatile NAPL compounds in fine to coarse sand.

4.4.2 Gas injection: Visualization

The transient distribution of the injected gas phase is illustrated in Figure 4.5 for experiments #8, #12, and #16, conducted in the 1.1 mm, 0.7 mm, and 0.5 mm sand, respectively. Figure 4.5 shows that the expansion of the injected gas is dominated by growth in the vertical direction, as expected for systems where gravitational forces play a significant role [21]. Growth was seen to occur as a series of short duration macroscopic events, referred to as "bursts" [18], separated by longer periods of no movement. These bursts were attributed to both the alternating pore-scale mechanisms of pressurization and pore-filling associated with the growth of a non-wetting fluid cluster [17] and the fragmentation and mobilization associated with the growth of a non-wetting fluid cluster subjected to a gravity field [18].

Evidence of burst growth is given in Figure 4.6, which shows two pairs of successive images from experiment #8 as the difference in optical density from the background image. The time between each image in a pair is 30 s. Figure 4.6 also shows the difference between each of the images in a pair. The two burst events shown in Figure 4.6 are the result of fragmentation and migration of the discontinuous gas cluster. Upon reaching the critical cluster length, the drop in the gas-phase pressure resulted in a corresponding drop in the local capillary pressure near the gas injection point. This resulted in the re-invasion of pores with water, fragmentation of the cluster, and the significant mobilization of gas from lower parts of the cluster to new pore spaces near the

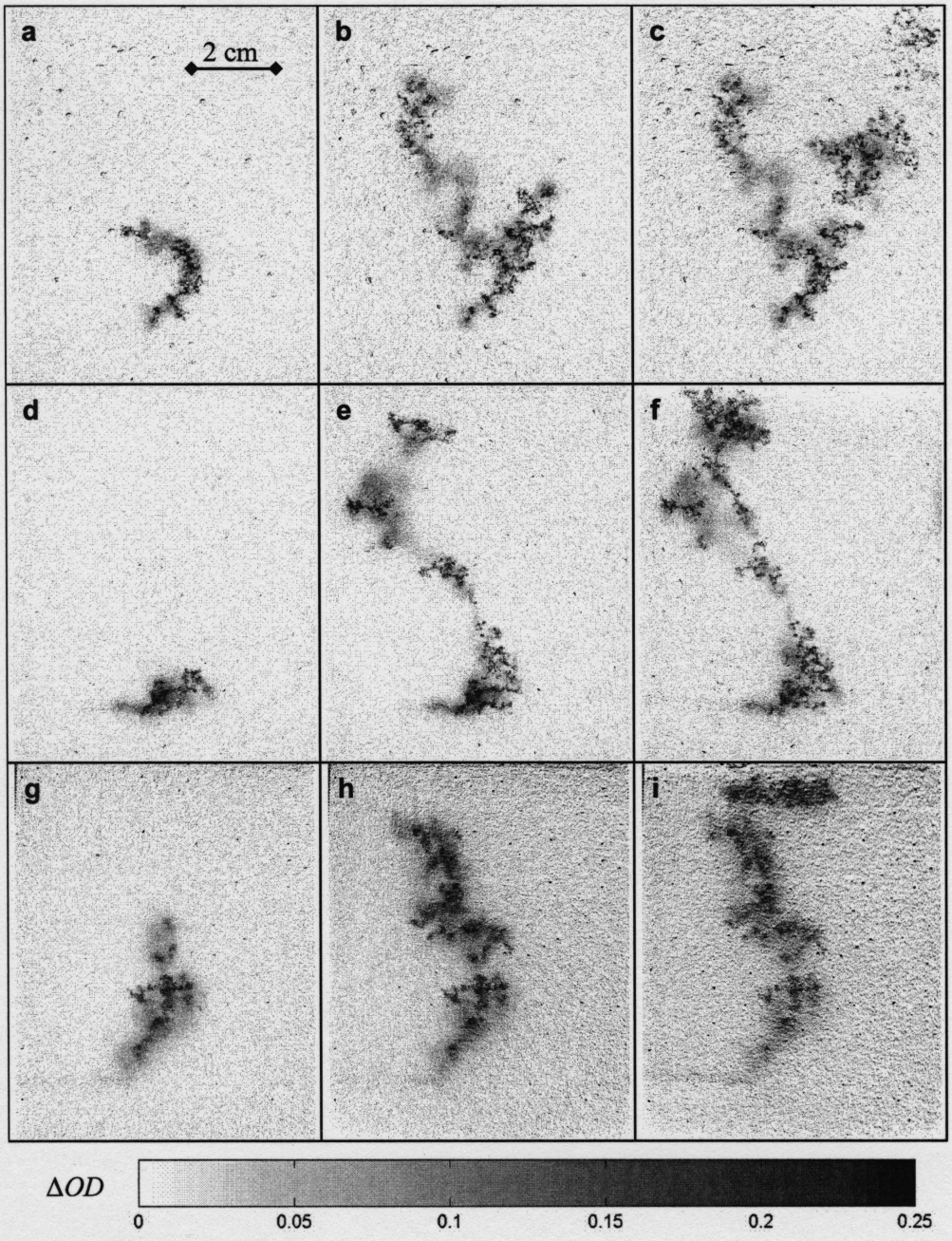

Figure 4.5. Distribution of gas in the 1.1 mm sand for experiment #8 after the injection of (a) 150 μL, (b) 400 μL, and (c) 800 μL of gas 15, 40, and 80 min after the start of injection, respectively; in the 0.7 mm sand for experiment #12 after the injection of (d) 150 μL, (e) 400 μL, and (f) 800 μL of gas 15, 40, and 80 min after the start of injection, respectively; and in the 0.5 mm sand for experiment #16 after the injection of (g) 150 μL, (h) 400 μL, and (i) 800 μL of gas 150, 400, and 800 min after the start of injection, respectively, displayed as the difference in optical density between the initial (background) image and successive images.

top of the cluster. The discontinuous nature of the gas clusters is highlighted by the results in Figure 4.6f, which show the mobilization of gas from the right-hand side of the gas distribution but not from the left-hand side.

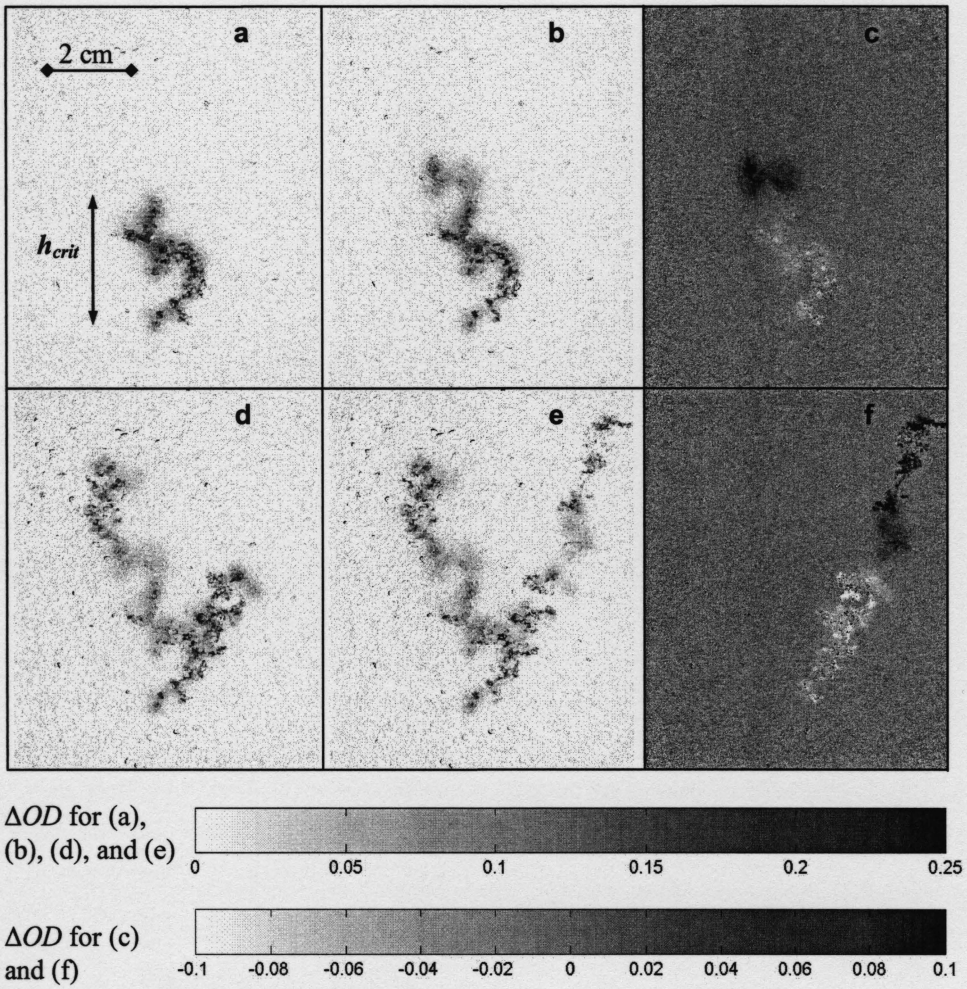

Figure 4.6. Gas distributions for experiment #8 after the injection of (a) 249 μL, (b) 254 μL, (d) 529 μL, and (e) 534 μL of gas displayed as the difference in optical density between the initial (background) image and successive images; and the difference in gas distributions between (c) 249 and 254 mL, and (e) 529 and 534 μL of gas injected, where a brighter image represents a decreased gas saturation (decreased optical density) and a darker image represents an increased gas saturation (increased optical density). The image in (a) was collected at the end of the drainage phase, and the transition to (b) is the result of the first fragmentation of the gas cluster. The critical cluster length is given by the length of the gas cluster in (a).

4.4.3 Gas Injection: Pressure measurements

Transient pressure measurements for experiments #8, #12, and #16 are shown in Figure 4.7, conducted in the 1.1 mm, 0.7 mm, and 0.5 mm sands, respectively. These results are representative of the general patterns observed in all other gas injection experiments. Figure 4.7 shows three phases in the evolution of the capillary pressure: 1) initial pressurization, 2) drainage, and 3) pressure fluctuation, which have also been reported for air injection into glass beads [6]. During the initial pressurization phase the capillary pressure rises as gas is injected into the pore space immediately adjacent to the injection tube. Since the gas phase is continuous throughout the injection syringe, injection tube, and pressure sensor tubing, this pressurization requires a greater gas volume than what is expected for the pressurization of a gas cluster in a single pore. The total gas injection and pressure measurement system had a volume of 9 mL, which affected the volume required to pressurize the gas phase during the initial pressurization and the pressure fluctuation phases. The initial pressurization phase ends when the first pore space adjacent to the injection tube is invaded and the gas cluster begins to expand within the porous medium. Entry pressures at the end of the initial pressurization stage were measured to be 7±1 cm, 11±2 cm, and 19±5 cm in the 1.1 mm, 0.7 mm, and 0.5 mm sand, respectively. As expected, this entry pressure increased with decreasing grain size, and did not vary substantially between experiments at the same grain size due to the uniformity of these sands. However, it is not equal to the value of the air-entry pressure reported for the sands (Table 4.1) since not all pore spaces are available for entry. Therefore, the displacement values observed here represent the lowest local capillary pressure of the available adjacent pore spaces.

During the drainage phase the capillary pressure generally decreased with additional gas injection due to vertical growth of the gas cluster, which resulted in decreased hydrostatic pressure at the upper gas-liquid interface and lower gas pressures. The short-term periods of increasing capillary pressure during this phase are caused by the invasion of pores with greater local capillary pressure during gas expansion. The drainage phase ends when the gas cluster reaches the critical cluster length for the first time, and fragmentation occurs.

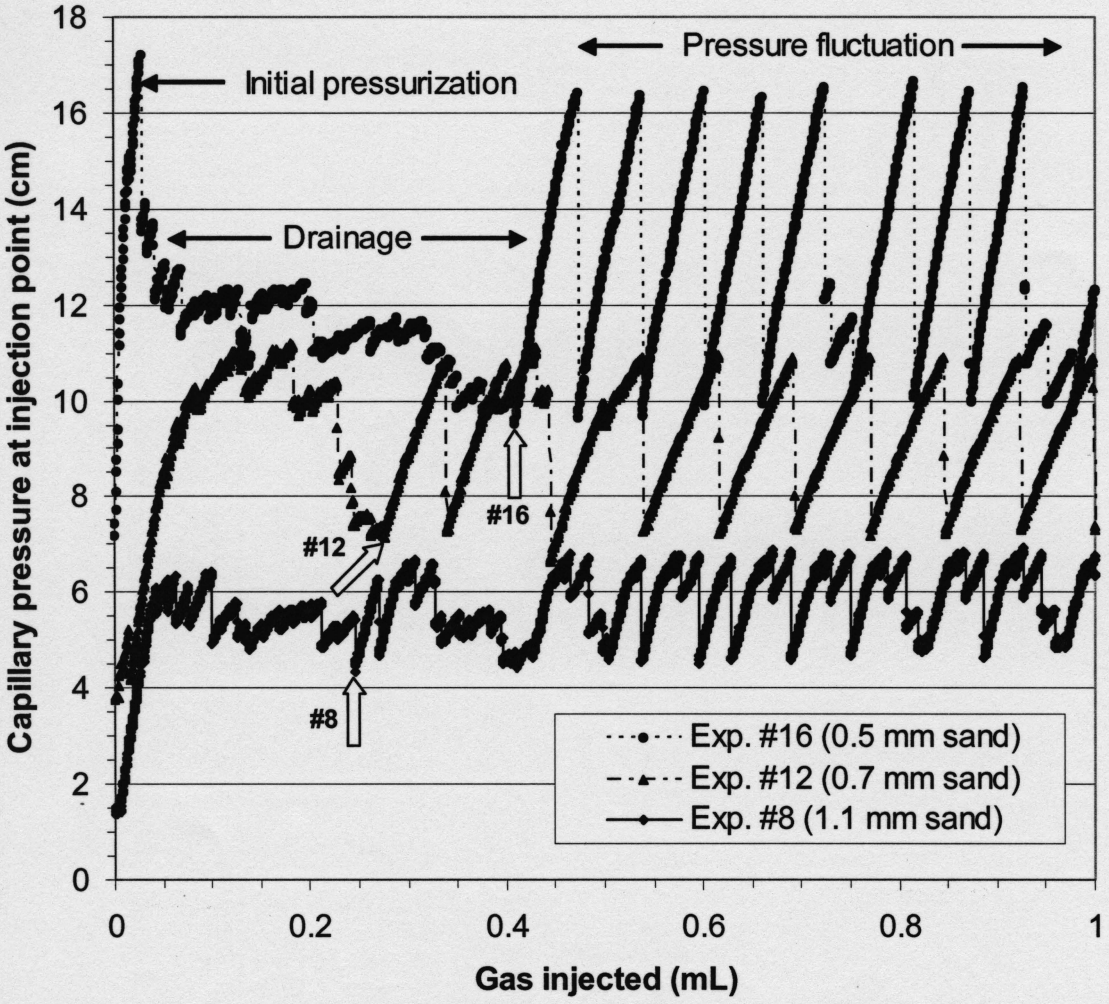

Figure 4.7. Capillary pressure measured at the gas injection point for experiments #8, #12, and #16. The 1 mL of gas was injected at 10 μL/min for 100 min in experiments #8 and #12, and at 1 μL/min for 1000 min in experiment #16. The end of the drainage phase, and the occurrence of the first fragmentation event, is indicated by the white arrows for each experiment.

During the pressure fluctuation phase the capillary pressure undergoes cycles of increasing and decreasing pressure due to the repeated fragmentation of the gas cluster attached to the injection tube, which indicates discontinuous gas flow [6]. These cycles are bounded by maximum and minimum pressures (Table 4.3), which represent the pore-scale entry (P_e) and terminal (P_t) pressures, respectively, at the fragmentation point. As

discussed for the initial pressurization phase, the entry pressures are not necessarily equal to the air-entry pressures reported for these sands due to the limited pore spaces sampled by the gas phase. However, as expected, they follow the same trend as the reported air-entry pressures and increase with decreasing grain size. The ratio P_t/P_e had an average value of 0.60 and was not significantly different between the different sands. This is consistent with values of P_t/P_e between 0.44 and 0.71 reported by Gerhard and Kueper [22] based on their analysis of data from capillary pressure-saturation curves in several multi-fluid porous media systems in the literature and their own NAPL infiltration experiments.

The transition from the minimum to maximum capillary pressures is due to pressurization of the gas cluster, and appears as a constant, positive-slope pressure increase at the beginning of each fluctuation cycle in Figure 4.7. The slope of this line is an artifact of the experimental set-up caused by the volume of the injection syringe and pressure sensor tubing, as discussed for the initial pressurization phase. In the absence of equipment and instrumentation, this volume required for pressurization would be significantly less. The effect of the injection syringe and pressure sensor tubing volume was verified in a separate experiment where the volume of the measurement system was changed, and a corresponding change in the pressurization slope was observed (data not shown).

The transition from maximum to minimum capillary pressure is due to expansion of the gas cluster, which occurs in a manner unlike during the initial drainage phase due to the presence of trapped gas clusters along the pathway of expansion. These trapped clusters form portions of a disconnected "pipeline" [18] that provides access to gas-occupied pore spaces at greater elevations. Where larger trapped clusters are located close together, minimal volume is required to reconnect a cluster of critical length, and the decrease in capillary pressure followed by fragmentation is very rapid. This is the case for most of the cycles in experiments #12 and #16. In the remaining cycles, and the cycles observed in experiment #8, the trapped clusters are smaller and more separated, resulting in several

coalescence events prior to the re-achievement of the critical cluster length. These coalescence events result in rapid changes in the capillary pressure with no fragmentation, and produce the secondary fluctuations prevalent in the data from experiment #8.

The pattern of fluctuating pressure in each experiment is very consistent between cycles. The consistent maximum and minimum pressures indicate that fragmentation is occurring in the same pore space and returning to a lower capillary pressure dictated by the critical cluster length following fragmentation. The consistent pattern of secondary fluctuation during the decrease from maximum to minimum pressure indicates that the same pathway is being followed during expansion. Changes in this pattern of secondary fluctuation represent a change in the expansion pathway. The differences observed in experiment #16 following the injection of 0.7 mL and 0.9 mL of gas were due to a difference in the distribution of trapped clusters caused by fragmentation and mobilization events at greater elevations. This resulted in secondary fluctuations in capillary pressure prior to achieving the critical cluster length in 2 of the 8 cycles. The change in the secondary fluctuation observed in experiment #8 after 0.33 mL of gas injected was due to branching of the injected gas cluster, which produced an additional drainage event between 0.33 and 0.46 mL injected. Branching here refers to the selection of different flow paths by mobilized gas clusters between subsequent mobilization events. Branching of the clusters was observed in 7 of the 12 experiments conducted in the 1.1 mm and 0.7 mm sands, despite the very slow flow rates and nearly inviscid non-wetting phase. This type of branching in natural porous media under the conditions used in this study is unexpected, since branching is typically attributed to viscous effects [7,10,35,36]. However, the onset of branching was observed to occur during mobilization events, which suggests that the velocity of a mobilized gas cluster may be a more appropriate indication of the potential for branching than the mean velocity of the injection front. This velocity is expected to be high. For example, a rise velocity of 17-20 cm/s has been reported for single bubbles in 4-mm diameter glass beads [37].

The possibility of pipeline growth as the dominant gas-phase mass transport mechanism is an important consideration for the mass transfer of volatile NAPLs from the surface of NAPL pools. An expanding gas cluster will reach greater heights at a much faster rate if trapped gas is available for pipeline growth. Due to the narrow concentration boundary layers above NAPL pools [38,39] most of the trapped gas above a NAPL pool will be under conditions that favor dissolution due to hydrostatic and capillary pressures. Only the gas clusters near the pool surface will be capable of expansion due to NAPL compound partitioning [3]. If a gas cluster near the pool surface is capable of expanding to the critical cluster length faster than the dissolution of the trapped gas clusters well above the pool, then the presence of the trapped gas clusters will be sustained due to repeated fragmentation and migration of lower clusters, and their coalescence with upper clusters. Evidence of this macro-scale gas transport by repeated coalescence events has been shown for the spontaneous expansion of a discontinuous gas phase above a NAPL pool [3]. If dissolution of the trapped gas clusters well above the pool happens faster than expansion of the lower cluster to the critical length, then the pipeline will not be sustained and the effect of the mass transport via spontaneous expansion of the discontinuous gas phase will be limited to a height above the pool less than or equal to the critical cluster length.

4.4.4 Gas Injection: Critical cluster length

Direct measurement of the critical cluster length requires a clear indication of when fragmentation of a gas cluster occurs. Visually identifying closely spaced, but separated clusters in a quasi-two-dimensional porous medium using light transmission is not possible due to the point-wise errors associated with the light transmission technique [25], and the additional blurring of the image associated with sharp transitions between phases and gas clusters that do not occupy the entire width of the pack [9]. This prevents the accurate differentiation between two clusters separated by a few pores and two sub-clusters connected by a single gas-filled pore. To overcome this limitation, the time of fragmentation was identified using the transient pressure measurements, rather than the

image data. At the end of a drainage phase (Figure 4.7) the minimum pressure is achieved and the gas cluster undergoes fragmentation for the first time. Until that fragmentation occurs, the gas exists as a single, connected phase that extends from the injection point to the top of the cluster. The height of this connected cluster is equal to the critical cluster length. Therefore, the image collected immediately prior to fragmentation at the end of the drainage phase can be used to measure the critical cluster length. An example is shown in Figure 4.6, where the fragmentation that occurred between 249 μL and 254 μL was the fragmentation at the end of the drainage phase (Figure 4.7), and the length of the cluster in Figure 4.6a is equal to the critical cluster length.

Measurements of the critical cluster length are listed in Table 4.3 for each of the gas injection experiments. Critical cluster lengths range from 1.4-3.6 cm, 3.2-6.0 cm and 2.8-6.5 cm in the 1.1 mm, 0.7 mm and 0.5 mm sands, respectively. For comparison, theoretical values of the critical cluster lengths were calculated using (4.9), where P_c^{top} and P_c^{bottom} were estimated according to the method proposed by Glass et al. [9]. P_c^{top} was taken to be the capillary pressure at an effective non-wetting saturation of S_{enw}=0.3, calculated here using the Brooks-Corey capillary pressure-saturation relationship and parameters reported for main drainage [23], and P_c^{bottom} was taken to be $\frac{1}{2}P_c^{top}$. Estimates of the critical cluster length from each of the three sands were fit to a power-law relationship, which is shown as the solid line in Figure 4.8. A value of S_{enw}=0.3 was selected by Glass et al. [9] based on the approximate percolation threshold in an uncorrelated cubic lattice. However, they found that their estimates were not sensitive to the choice of S_{enw}, which was also found here. To illustrate the sensitivity of the theoretical critical cluster length estimates to the choice of S_{enw}, power-law relationships were also fit to estimates based on S_{enw}=0.2 and S_{enw}=0.4 (Figure 4.8), and only minor differences exist. This is expected for these sands, which have little variation in pore sizes, and show little change in capillary pressure with saturation at intermediate

saturations. However, the sensitivity is expected to be greater in less uniform media, and additional investigation is warranted.

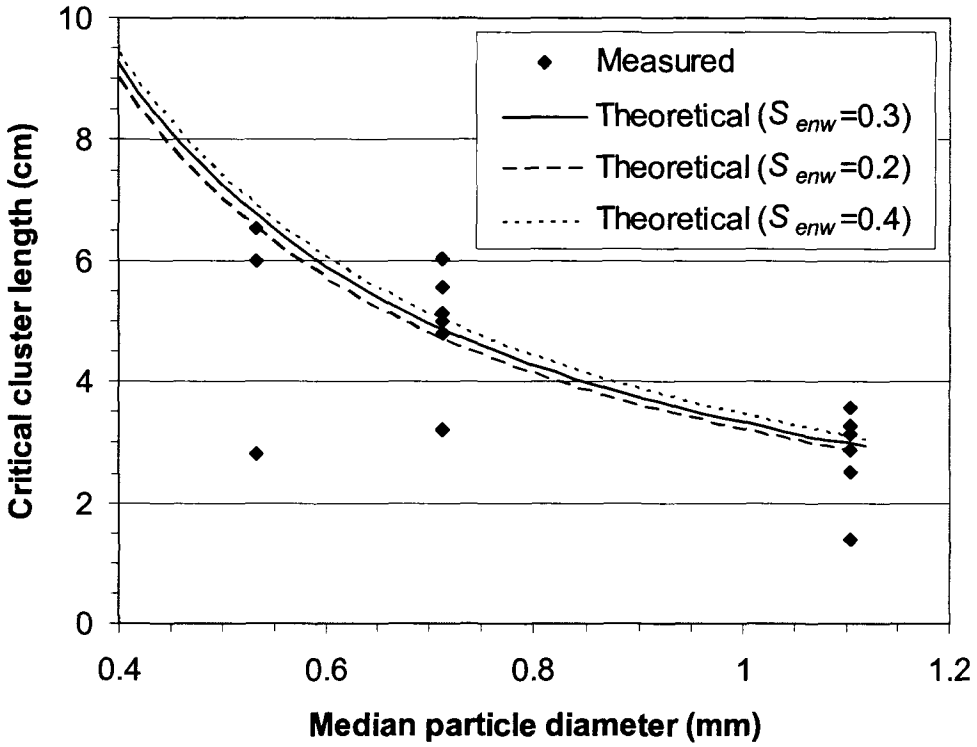

Figure 4.8. Measured critical cluster lengths (symbols) for the 1.1 mm, 0.7 mm, and 0.5 mm sand compared to theoretical estimates (lines) based on equation (4.9), calculated using capillary pressure values at effective non-wetting saturations of 0.2, 0.3, and 0.4.

Figure 4.8 shows that the data agree well with the theoretically predicted values. Variation in the critical cluster length between experiments is expected due to the pore-scale heterogeneity present in even these relatively uniform sands. The low values of 1.4 cm, 3.2 cm, and 2.8 cm observed in experiments #3, #14, and #17, respectively, represent situations where conditions favorable to fragmentation were present in the packing (i.e. larger pore spaces with lower P_c present above smaller pore spaces with greater P_c). The results in Figure 4.8 provide the first experimental evidence that the critical cluster length may be reasonably estimated using data obtained from capillary pressure-saturation

curves. However, additional studies designed to test the relationship in different media, and using different fluids, would be beneficial.

4.5 Conclusions

In this study the spontaneous expansion rate of discontinuous gas in 1.1 mm sand above a NAPL pool was quantified, and the gas flow was characterized by slowly injecting air into 1.1 mm, 0.7 mm, and 0.5 mm sands at rates similar to the flow produced by the partitioning of volatile NAPL compounds to a discontinuous gas phase. The expansion of a single, initially NAPL-free gas cluster above a 4.3 cm-long tDCE pool in 1.1 mm sand resulted in discontinuous gas flow, with repeated expansion, fragmentation, and mobilization of the gas phase. Average expansion rates of 0.34±0.02 mL/day and 0.29±0.01 mL/day were measured in duplicate experiments, which resulted in an expansion from 4 μL to 4.2-4.5 mL of gas in 13.1-13.7 days. This work shows that the spontaneous expansion of gas due to the partitioning of volatile NAPL can be expected to result in discontinuous gas flow in porous media with a grain size diameter greater than 0.02 mm.

Injections of air into 1.1 mm, 0.7 mm, and 0.5 mm sand at 1 μL/min and 10 μL/min resulted in discontinuous gas flow characterized by vertically-dominated gas distribution patterns and growth as short-duration bursts. Measured gas pressures showed the consistent, repeated return of capillary pressure to maximum and minimum values that represent pore-scale entry (P_e) and terminal (P_t) pressures, respectively, at the fragmentation point. The average value of P_t/P_e=0.60 was consistent with values reported in the literature.

Patterns in the transient pressure data were used to identify fragmentation events, which was not possible using images from light transmission data alone. This allowed the first direct measurement of critical gas cluster lengths in quasi-two-dimensional porous media. The critical cluster lengths were measured to be 1.4-3.6 cm, 3.2-6.0 cm and 2.8-6.5 cm in the 1.1 mm, 0.7 mm and 0.5 mm sands, respectively. These values agreed well with

estimates of the critical cluster length made using previously reported equations, and parameters derived from the medium's capillary pressure-saturation relationship.

Patterns in the transient pressure data were also used to provide insight into pipeline growth behavior and the onset of branching during expansion of the gas phase. Understanding pipeline growth, where rapid vertical expansion of the gas phase occurs through coalescence with trapped clusters above, is important for understanding the effect of expanding discontinuous gas clusters on NAPL pool dissolution. If pipeline growth can be sustained above a NAPL pool, due to slower dissolution of upper gas clusters compared to the growth of those near the pool surface, then the effect of spontaneous gas expansion on the spatial distribution of dissolved NAPL will be greater. Prediction of this effect will require numerical models capable of reproducing the fragmentation and migration processes that are controlled at the pore-scale, as well as simulating multi-component partitioning to a discontinuous gas phase. While modified invasion percolation (MIP) techniques have been successful in reproducing flow patterns produced by the unstable displacement of a wetting fluid by a non-wetting fluid with fragmentation [18-20], the expansion of the non-wetting fluid is not coupled to mass transfer. Published models for multi-component mass transfer to a discontinuous gas phase [13,15,40] make use of a continuum formulation that cannot simulate the onset of mobilization [13] without the use of empirically-derived expressions [16]. Future research will look at coupling mass transfer to models capable of simulating pore-controlled behavior, similar to the approach employed to study the drying of porous media (e.g. [41,42]).

Acknowledgements

This research was supported by the Natural Sciences and Engineering Research Council (NSERC) of Canada through its Discovery Grant Program and a Canada Graduate Scholarship to the first author. We gratefully acknowledge the technical assistance of Jennie Kirby, Michael Palme, and Peter Koudys.

References

[1] Roy JW, Smith JE. Multiphase flow and transport caused by spontaneous gas phase growth in the presence of dense non-aqueous phase liquid. J Contam Hydrol 2007;89: 251-269.

[2] Anderson MR, Johnson RL, Pankow JF. Dissolution of dense chlorinated solvents into groundwater. 3. modeling contaminant plumes from fingers and pools of solvent. Environ Sci Technol 1992;26(5): 901-908.

[3] Mumford KG, Smith JE, Dickson SE. New observations of gas-phase expansion above a dense non-aqueous phase liquid pool. Vadose Zone J 2008; In press.

[4] Mumford KG, Smith JE, Dickson SE. Mass flux from a non-aqueous phase liquid pool considering spontaneous expansion of a discontinuous gas phase. J Contam Hydrol 2008;98: 85-96.

[5] Brooks MC, Wise WR, Annable MD. Fundamental changes in in situ air sparging flow patterns. Ground Water Monit R 1999;19(2): 105-113.

[6] Geistlinger H, Krauss G, Lazik D, Luckner L. Direct gas injection into saturated glass beads: Transition from incoherent to coherent gas flow pattern. Water Resour Res 2006;42: doi:10.1029/2005WR004451.

[7] Stöhr M, Khalili A. Dynamic regimes of buoyancy-affected two-phase flow in unconsolidated porous media. Phys Rev E 2006;73: 036301.

[8] Selker JS, Niemet M, Mcduffie NG, Gorelick SM, Parlange J-Y. The local geometry of gas injection into saturated homogeneous porous media. Transport Porous Med 2007;68(1): 107-127.

[9] Glass RJ, Conrad SH, Peplinski W. Gravity-destabilized nonwetting phase invasion in macroheterogeneous porous media: Experimental observations of invasion dynamics and scale analysis. Water Resour Res 2000;36(11): 3121-3137.

[10] Frette V, Feder J, Jossang T, Meakin P. Buoyancy-driven fluid migration in porous-media. Phys Rev Lett 1992;68(21): 3164-3167.

[11] Birovljev A, Wagner G, Meakin P, Feder J, Jossang T. Migration and fragmentation of invasion percolation clusters in 2-dimensional porous media. Phys Rev E 1995;51(6): 5911-5915.

[12] Wagner G, Birovljev A, Meakin P, Feder J, Jossang T. Fragmentation and migration of invasion percolation clusters: Experiments and simulations. Phys Rev E 1997;55(6): 7015-7029.

[13] Cirpka OA, Kitanidis PK. Transport of volatile compounds in porous media in the presence of a trapped gas phase. J Contam Hydrol 2001;49: 263-285.

[14] Holocher J, Peeters F, Aeschbach-Hertig W, Kinzelbach W, Kipfer R. Kinetic model of gas bubble dissolution in groundwater and its implications for the dissolved gas composition. Environ Sci Tecnol 2003;37(7): 1337-1343.

[15] Geistlinger H., Beckmann A, Lazik D. Mass transfer between a multicomponent trapped gas phase and a mobile water phase: experiment and theory. Water Resour Res 2005;41: doi:10.1029/2004WR003885.

[16] Amos RT, Mayer KU. Investigating ebullition in a sand column using dissolved gas analysis and reactive transport modeling. Environ Sci Technol 2006;40(17): 5361-5367.

[17] Li X, Yortsos YC. Theory of multiple bubble growth in porous media by solute diffusion. Chem Eng Sci 1995;50(8): 1247-1271.

[18] Wagner G, Meakin P, Feder J, Jossang T. Buoyancy-driven invasion percolation with migration and fragmentation. Physica A 1997;245: 217-230.

[19] Glass RJ, Yarrington L. Mechanistic modeling of fingering, nonmonotonicity, fragmentation, and pulsation within gravity/buoyant destabilized two-phase/unsaturated flow. Water Resour Res 2003;39(3): doi:10.1029/2002WR001542.

[20] Tsimpanogiannis IN, Yortsos YC. The critical gas saturation in a porous medium in the presence of gravity. J Colloid Interface Sci 2004;270: 388-395.

[21] Wilkinson D. Percolation model of immiscible displacement in the presence of buoyancy forces. Phys Rev A 1984;30(1): 520-531.

[22] Gerhard JI, Kueper BH. Capillary pressure characteristics necessary for simulating DNAPL infiltration, redistribution, and immobilization in saturated porous media. Water Resour Res 2003;39(8): doi:10.1029/2002WR001270.

[23] Schroth MH, Ahearn SJ, Selker JS, Istok JD. Characterization of miller-similar silica sands for laboratory hydrologic studies. Soil Sci Soc Am J 1996;60(5): 1331-1339.

[24] Schroth MH, Istok JD, Selker JS. Three-phase immiscible fluid movement in the vicinity of textural interfaces. J Contam Hydrol 1998;32: 1-23.

[25] Niemet MR, Selker JS. A new method for quantification of liquid saturation in 2D translucent porous media systems using light transmission. Adv Water Resour 2001;24: 651-666.

[26] Conrad SH, Glass RJ, Peplinski WJ. Bench-scale visualization of DNAPL remediation processes in analog heterogeneous aquifers: surfactant floods and in situ oxidation using permanganate. J Contam Hydrol 2002;58: 13-49.

[27] Weisbrod N, Niemet MR, Rockhold ML, McGinnis T, Selker JS. Migration of saline solutions in variably saturated porous media. J Contam Hydrol 2004;72: 109-133.

[28] Pankow JF, Cherry JA. Dense Chlorinated Solvents and other DNAPLs in Groundwater. Portland, Oregon: Waterloo Press, 1996.

[29] Seagren EA, Rittman BE, Valocchi AJ. An experimental investigation of NAPL pool dissolution enhancement by flushing. J Contam Hydrol 1999;37: 111-137.

[30] Chrysikopoulos CV, Lee KY, Harmon TC. Dissolution of a well-defined trichloroethylene pool in saturated porous media: Experimental design and aquifer characterization. Water Resour Res 2000;36(7): 1687-1696.

[31] Roy JW, Smith JE, Gillham RW. Laboratory evidence of natural remobilization of multicomponent DNAPL pools due to dissolution. J Contam Hydrol 2004;74: 145-161.

[32] Tidwell VC, Glass RJ. X-ray and visible-light transmission for laboratory measurement of 2-dimensional saturation fields in thin-slab systems. Water Resour Res 1994;30(11): 2873-2882.

[33] Oostrom M, Dane JH, Wietsma TW. A review of multidimensional, multifluid, intermediate-scale experiments: Flow behavior, saturation imaging, and tracer detection and quantification. Vadose Zone J 2007;6(3): 610-637.

[34] McNeil JD, Oldenborger GA, Schincariol RA. Quantitative imaging of contaminant distributions in heterogeneous porous media laboratory experiments. J Contam Hydrol 2006;84: 36-54.

[35] Ewing RP, Berkowitz B. A generalized growth model for simulating initial migration of dense non-aqueous phase liquids. Water Resour Res 1998;34(4): 611-622.

[36] Glass RJ, Conrad SH, Yarrington L. Gravity-destabilized nonwetting phase invasion in macroheterogeneous porous media: Near-pore-scale macro modified invasion percolation simulation of experiments. Water Resour Res 2001;37(5): 1197-1207.

[37] Roosevelt SE, Corapcioglu MY. Air bubble migration in a granular porous medium: experimental studies. Water Resour Res 1998;34(5): 1131-1142.

[38] Johnson RL, Pankow JF. Dissolution of dense chlorinated solvents into groundwater. 2. source functions for pools of solvent. Environ Sci Technol 1992;26(5): 896-901.

[39] Chrysikopoulos CV, Hsuan P-Y, Fryillas MM, and Lee KY. Mass transfer coefficient and concentration boundary layer thickness for a dissolving NAPL pool in porous media. J Hazard Mater 2003;97: 245-255.

[40] Amos RT, Mayer KU. Investigating the role of gas bubble formation and entrapment in contaminated aquifers: Reactive transport modeling. J Contam Hydrol 2006;87: 123-154.

[41] Laurindo JB, Prat M. Numerical and experimental network study of evaporation in capillary porous media. Phase distributions. Chem Eng Sci 1996;51(23): 5171-5185.

[42] Yiotis AG, Stubos AK, Boudouvis AG, Yortsos YC. A 2-D pore-network model of the drying of single-component liquids in porous media. Adv Water Resour 2001;24: 439-460.

Chapter 5

The effect of spontaneous gas expansion and mobilization on the aqueous-phase concentrations above a dense non-aqueous phase liquid pool

The contents of this chapter have been prepared for publication as: Mumford, K.G., Smith, J.E., Dickson, S.E., 2008. The effect of spontaneous gas expansion and mobilization on the aqueous-phase concentrations above a dense non-aqueous phase liquid pool. Prepared for Submission to *Journal of Contaminant Hydrology*.

Abstract

The spontaneous expansion and mobilization of discontinuous gas above dense non-aqueous phase liquid (DNAPL) pools can affect the aqueous-phase concentrations of the DNAPL constituents above the pool. The results of an intermediate-scale, two-dimensional flow cell experiment showed that the discontinuous gas flow produced by spontaneous expansion, driven by the partitioning of 1,1,1-TCA from the surface of a DNAPL pool, resulted in detectable aqueous-phase concentrations of 1,1,1-TCA well above the pool surface. These concentrations were greater than expected, and were present at greater-than-expected elevations, based on a conventional model for DNAPL pool dissolution in the absence of a discontinuous gas phase. Additionally, this study showed that the discontinuous gas flow produced transient behavior in the aqueous-phase concentrations, where the elevated concentrations occurred as short-term, pulse-like

events. These results suggest that the spontaneous expansion and mobilization of discontinuous gas in DNAPL source zones could lead to the misdiagnosis of source zone architecture using aqueous concentration data, and that the transient nature of the elevated concentrations could further complicate the difficult task of source zone characterization.

5.1 Introduction

The spontaneous expansion of discontinuous gas phases has been recently identified as a potentially significant mechanism affecting the mass transfer from dense non-aqueous phase liquid (DNAPL) pools (Roy and Smith, 2007; Mumford et al., 2008a). This mechanism is driven by the partitioning of volatile DNAPL compounds to an initially trapped gas phase, which leads to the continued partitioning of other dissolved gases to the gas phase, expansion, and vertical mobilization of the gas phase. Under site-specific conditions that produce slow mass transfer from the DNAPL pool to the aqueous phase, but relatively rapid mass transfer to an expanding gas phase, this mechanism could shorten pool lifetimes (Mumford et al., 2008a). In addition, the partitioning of DNAPL constituents from a mobilized gas phase to the aqueous phase well above the pool could change the spatial distribution of aqueous-phase DNAPL constituents (Roy and Smith, 2007), potentially confounding efforts to locate and characterize the architecture of DNAPL source zones.

A few studies have examined the expansion and mobilization of gas during spontaneous expansion (Roy and Smith, 2007; Mumford et al., 2008a;b;c), but very little information is available concerning the aqueous-phase DNAPL constituent concentrations produced by the mobilized gas phase. The only reported data were presented by Roy and Smith (2007), who measured effluent aqueous-phase trichloroethene (TCE) concentrations at multiple heights above a TCE pool emplaced in a small-scale flow cell packed with 1-mm glass beads and containing a residual gas phase. They showed that in the presence of an expanding and repeatedly mobilized gas phase, the aqueous concentration profile was different than the profile expected to result from transverse vertical dispersion under the typically-considered NAPL-water pool dissolution conditions. They also showed that the

aqueous concentrations increased over time throughout the 92-day experiment. The effect of spontaneous expansion and mobilization on the spatial distribution of aqueous-phase DNAPL constituents is potentially more important than the effect on pool lifetime since it may play a significant role at a wider variety of DNAPL-contaminated sites. That is, the partitioning of DNAPL constituents from a mobilized gas phase may confound source zone investigation efforts even at sites where gas-phase transport is not responsible for a relatively high portion of the total mass transfer from the DNAPL pools. Therefore, further investigation is needed to better understand the effect of spontaneous gas expansion and mobilization on the spatial distribution of aqueous-phase DNAPL constituents, and further facilitate the appropriate incorporation of this mechanism into our evolving conceptual models of DNAPL-contaminated sites.

The purpose of this study was to investigate spontaneous gas expansion and mobilization above a DNAPL pool, and its effect on downgradient aqueous-phase concentrations. An intermediate-scale laboratory experiment was conducted in a two-dimensional flow cell packed with 1.1 mm-diameter uniform sand, and containing an emplaced pool of 1,1,1-trichloroethane (1,1,1-TCA). The effluent concentration results from this experiment were significantly different than those previously reported in experiments with glass beads (Roy and Smith, 2007). A numerical model was used to aid the interpretation of the experimental data and provide additional insight into the highly transient nature of the effluent concentrations.

5.2 Background

5.2.1 Gas-phase partitioning in multi-component systems

The spontaneous expansion of discontinuous gas phases near DNAPL pools, and their subsequent dissolution away from the pool, is controlled by the partitioning of multiple volatile components (Roy and Smith, 2007; Mumford et al., 2008a). Multi-component partitioning to discontinuous gas phases has recently been considered in several groundwater applications, including the transport of partitioning tracers (Cirpka and

Kitanidis, 2001); the transport of methane, nitrogen, and argon (Amos and Mayer, 2006a); the dissolution of entrapped atmospheric (Holocher et al., 2003), and injected (Geistlinger et al., 2005; Balcke et al., 2007) gases; the ebullition of methane and carbon dioxide in methanogenic sediments (Amos and Mayer, 2006b), and the performance of a permeable reactive barrier (Williams et al., 2007). In these previous studies, the competitive partitioning of multiple dissolved gases to the gas phase resulted in either the expansion or dissolution of the gas phase, depending on the concentrations of all dissolved gases in the surrounding groundwater, the gas-phase pressure, the partitioning coefficients, and the mass transfer rate constants. For systems containing discontinuous gas phases and DNAPL, the gas near DNAPL is expected to expand, and gas further away is expected to dissolve (Roy and Smith, 2007; Mumford et al., 2008a).

Cirpka and Kitanidis (2001) present a system of equations that describes the gas saturation of a representative elementary volume (REV) based on local equilibrium partitioning

$$P_g = \sum_i \frac{C^t{}_i H_i}{1 + \left(\frac{H_i}{RT} - 1\right) S_g} \tag{5.1}$$

where P_g is the total gas pressure, $C^t{}_i$ is the total concentration of compound i in the aqueous and gas phases, H_i is the Henry's law coefficient for compound i, R is the gas constant, T is the temperature, and S_g is the gas saturation. The aqueous-phase, gas-phase and total concentrations are defined by

$$C_i = \frac{P_i}{H_i} \tag{5.2}$$

$$C^g{}_i = \frac{P_i}{RT} \tag{5.3}$$

$$C^t_i = (1 - S_g)C_i + S_g C^g_i \tag{5.4}$$

where C_i and C^g_i are the aqueous- and gas-phase concentrations of compound i, and P_i is the partial pressure of compound i. Alternate, kinetic expressions have also been employed to describe dynamic changes in gas-phase volume due to multi-component partitioning (Holocher et al., 2003; Geistlinger et al., 2005), but it is expected that local equilibrium conditions will dominate for the flow conditions at most DNAPL-contaminated sites. The total gas pressure is defined by

$$P_g = P_w + P_c \tag{5.5}$$

where P_w is the water pressure and P_c is the capillary pressure. Eqs. (5.1)-(5.5) are commonly implemented using the assumption $P_g \approx P_w$ (Cirpka and Kitanidis, 2001; Amos and Mayer, 2006a) since changes in S_g are relatively insensitive to small changes in P_g. Alternatively, an expression for P_c can be included in the system of equations using a capillary pressure-saturation relationship such as the Brooks-Corey expression

$$\left(\frac{P_c}{P_d}\right)^{-\lambda} = \frac{(S_w - S_{wr})}{(1 - S_{wr})} = S_{we} \tag{5.6}$$

where P_d is the displacement pressure, λ is the pore-size distribution index, S_w=1-S_g is the water saturation, S_{wr} is the residual water saturation, and S_{we} is the effective water saturation. Using Eqs. (5.1)-(5.6), values of $S_g(t)$, $P_i(t)$, and $C_i(t)$ can be determined from values of $C^t_i(t)$ given information concerning component partitioning (H_i), system conditions (P_w and T), and the capillary pressure-saturation relationship (P_d, λ, and S_{wr}).

5.2.2 Discontinuous gas flow in porous media

The slow expansion of discontinuous gas phases near DNAPL pools is expected to produce discontinuous gas flow (Mumford et al., 2008c), which occurs as multiple, discrete gas clusters rather than as continuous channels of connected gas (Brooks et al., 1999; Geistlinger et al., 2006; Stöhr and Khalili, 2006). Discontinuous gas flow in porous media results from the local competition between buoyancy and capillary forces. As a small, trapped gas cluster expands within a collection of connected pores, the buoyancy force increases. Due to the density difference between the two fluids, continued expansion leads to vertically-biased growth. This produces a capillary pressure gradient across the length of the cluster equal to the hydrostatic gradient, with greater capillary pressure at the top than at the bottom. At a critical cluster length (Glass et al., 2000; Geistlinger et al., 2006) the capillary forces trapping the cluster are exceeded, water imbibes near the lower portion of the cluster where capillary forces are lowest, and buoyant mobilization of the cluster occurs (Wagner et al., 1997; Glass and Yarrington, 2003; Tsimpanogiannis and Yortsos, 2004). Discontinuous gas flow is an important consideration in air sparging and gas injection (e.g. Roosevelt and Corapcioglu, 1998; Brooks et al., 1999; Geistlinger et al., 2006; Selker et al., 2007), as well as in the potential remediation of NAPL by the injection of gas-supersaturated solutions (Li et al., 2007).

The spatial extent of mobilization depends on the distribution of pore sizes in the porous medium. Media with very narrow pore-size distributions will allow larger-scale mobilization as buoyancy forces capable of producing mobilization at one location are more likely to lead to mobilization at any other subsequent location. Mobilization of this type was observed by Roy and Smith (2007) in their experiments using glass bead packs, where several mobilization events resulted in gas clusters being mobilized to the top of their flow cell. In contrast, macroscopically homogeneous media with wider pore-size distributions, i.e., in the absence of larger-scale preferential pathways, will prevent larger-scale mobilization as local increases in capillary forces associated with narrower pores can trap mobilized clusters, and additional buoyant force is required for re-mobilization.

Vertical gas flow characterized by the repeated trapping and coalescence of mobilized gas clusters was observed in the 1.1 mm-diameter sand used in this experiment, and was reported by Mumford et al. (2008b). Repeated trapping and coalescence is an important consideration for mass transfer from mobilized clusters to the surrounding groundwater. The observed frequency of mobilization events in laboratory experiments (Mumford et al., 2008b) suggests that the time between coalescence-driven mobilization events is sufficiently long to allow significant mass transfer from trapped clusters.

5.3 Laboratory Experiments

5.3.1 Flow cell and porous media

Aqueous-phase 1,1,1-TCA concentrations were measured during an intermediate-scale flow cell experiment. The same experiment was also used to investigate the transient distribution of a discontinuous gas phase above a 1,1,1-TCA pool (Mumford et al., 2008b). The experiment was conducted in a two-dimensional flow cell (Figure 5.1) composed of two 1-cm thick glass plates sealed to a brass frame and an aluminum top plate. The flow cell was packed with 6 mm-diameter glass beads (Propper Manufacturing Co., Inc. 030010) along the influent edge, 0.5 mm-diameter sand (40/50 Accusand, Unimin Corporation) along the top and bottom, and 1.1 mm-diameter sand (12/20 Accusand, Unimin Corportation) in the center 62 x 44 x 1 cm^3 region. Properties of the two sands are reported by Schroth et al. (1996), and selected properties are listed in Table 5.1. Initially saturated conditions were created by placing the sand in water under vacuum prior to packing, and continuously pouring the wet sand into the water-filled flow cell. A reasonably homogeneous pack was created by the continuous pouring and by tapping the glass plates with a rubber mallet following the pour. A porosity of 0.40±0.03 was calculated based on the volume of the flow cell and the mass of sand used in the packing.

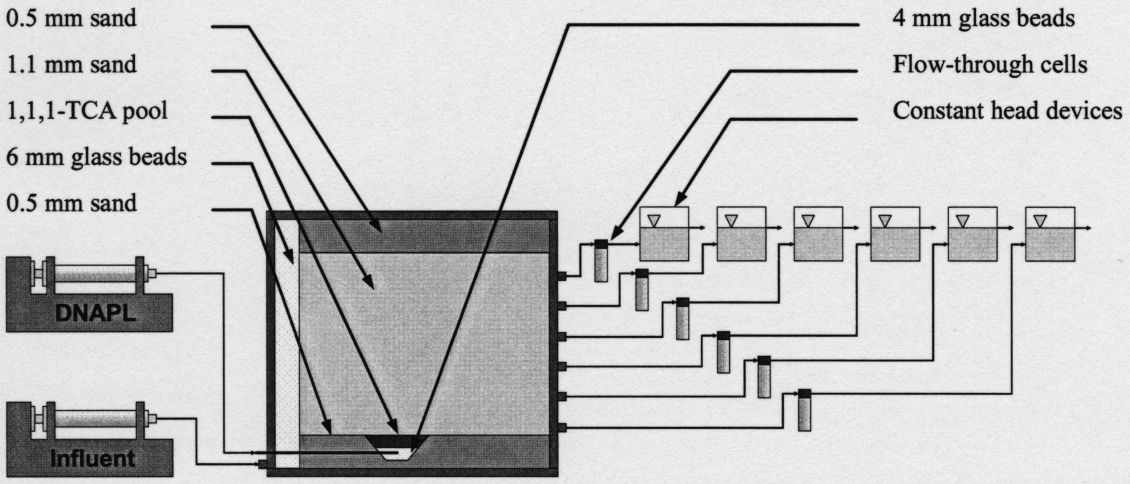

Figure 5.1. Experimental set-up for the intermediate-scale flow cell showing the DNAPL-injection and influent pumps, and the individual constant head devices and sampling cells attached to the effluent ports.

Table 5.1. Selected properties of sand used in flow cell experiment[1]

Property	1.1 mm sand	0.5 mm sand
Size fraction	12/20	30/40
Median grain size (mm)	1.105	0.532
Uniformity coefficient	1.231	1.19
Air-entry pressure (cm of H_2O)	5.42	13.03
Pore-size distribution index	3.94	6.91
Residual water saturation	0.03	0.05
Residual air saturation	0.08	0.11

[1]Schroth et al. (1996)

5.3.2 DNAPL and initial gas emplacement

A pool of 1,1,1-TCA (VWR Canlab, 99.5%), dyed red with 100 mg/L Sudan 4 (Acros Organics) was emplaced near the bottom of the flow cell (Figure 5.1). A 17-cm long pool was created by injecting 16 mL of dyed 1,1,1-TCA at a rate of 2 mL/hr using a syringe pump (Cole-Parmer EW-74901-10) and a 25-mL gastight syringe (Hamilton 82520) through a 16-gauge stainless-steel needle (Hamilton 7748-02) inserted into the side of the flow cell and packed into a layer of 4 mm-diameter glass beads (Propper Manufacturing Co., Inc. 030008) embedded within a depression in the bottom of the 0.5 mm-diameter sand layer.

An initial discontinuous residual gas phase was emplaced using a constant head device by lowering the water table at a rate of 3 cm every 15 min until contact between the air and the surface of the DNAPL pool was observed. The water table was then immediately raised, at the same rate at which it was lowered, to trap air at a residual saturation expected to be similar to the reported residual air saturation for this sand (Table 5.1). This procedure resulted in the formation of multiple discontinuous gas clusters throughout the 1.1 mm-diameter sand pack, including several gas clusters in direct contact with the surface of the DNAPL pool (Mumford et al., 2008b). Refilling the flow cell following contact with the DNAPL pool also resulted in high aqueous-phase 1,1,1-TCA concentrations throughout the flow cell prior to beginning the experiment, which prevented the collection of meaningful aqueous-phase concentration data at early time.

5.3.3 Influent supply, effluent collection, and sample analysis

A 200 mg/L solution of sodium azide (Fisher Scientific, >99%) in Nanopure water (Barnstead D11951) equilibrated with laboratory air at 25°C was supplied to the flow cell throughout the experiment. The sodium azide acted as a biocide (Seagren et al., 1999; Chrysikopoulos et al., 2000; Roy et al., 2004) to prevent the generation of biologically-derived gases, and equilibration with laboratory air was used to supply dissolved atmospheric gases. The influent solution was supplied at a rate of 0.93±0.02 mL/min for 70 days, corresponding to a pore-water velocity of 70 cm/day, using a continuous-cycle syringe pump (Cole-Parmer EW-74901-50) equipped with 60-mL syringes (BD 309653). The influent flow rate was measured by periodically placing the influent reservoir on an analytical balance (Mettler Toledo BD1201). Influent flow was distributed across the height of the 1.1 mm-diameter sand pack, by the 6 mm glass beads packed along the influent edge, to create a reasonably horizontal flow field. The suitability of the flow field was verified by conducting a tracer test prior to DNAPL and initial gas emplacement. A tracer solution of 70 mg/L of NaBr was pumped through the flow cell at 9.6 mL/min after filling the influent glass bead pack with tracer solution. Breakthrough curves were obtained by analyzing effluent samples for Br^- by ion chromatography

(Varian Prostar 230 pump; Varian Prostar 410 autosampler; Dionex CD25 conductivity detector; Dionex IonPac AG12A, AS12A 4 mm column; 1.5 mL/min 2.7 mM Na_2CO_3, 0.3 mM $NaHCO_3$ eluent; Dionex AMMS 111 4-mm suppressor with 25mN H_2SO_4).

Effluent exited the flow cell through six ports installed in the effluent edge of the flow cell frame, at 1.8, 9.3, 16.5, 23.8, 31.2, and 38.4 cm above the pool surface (Figure 5.1). The effluent ports were connected to individual constant head devices, which were independently adjusted at the beginning of the experiment to balance the flow through each port. Flow through each port was measured periodically by weighing effluent on an analytical balance (Mettler Toledo AB204-S). To sample the effluent, flow-through cells were constructed from 1.5 mL vials, capped with PTFE-faced septa, and two stainless steel needles. The flow-through cells were in-line between the effluent port and the constant head devices, and were kept full of aqueous phase at all times. To collect an effluent sample, a vial was disconnected from the tubing by pulling the two stainless steel needles out of the PTFE-faced septa and replacing it with a new, water-filled vial. The sample vial was then sub-sampled for immediate analysis of 1,1,1-TCA by gas chromatography-mass spectroscopy (Agilent 6890 GC, Agilent 5973 MS mass selective detector, Restek Rtx-502.2 60 m, 0.32 mm ID, 1.8 μm film thickness column) equipped with a headspace autosampler (Agilent 7694E) based on EPA method 8260B. Samples expected to have concentrations greater than 2 mg/L were analyzed using total ion current, with a detection limit of 70 μg/L, and samples expected to have concentrations less than 2 mg/L were analyzed using selected ion monitoring, with a detection limit of 1 μg/L. Selected ion monitoring was not implemented until 28.7 days into the 70-day experiment. Therefore, the early data have a detection limit of 70 μg/L. The residence time in each vial (3-160 min) was much shorter than the time between sampling events (2-15 days) to ensure that the sampled aqueous phase was representative of effluent from the flow cell. For confirmation, the water in the replaced vials was dyed with red food dye to provide visual confirmation that the initial water had been flushed from the vial prior to sampling.

5.3.4 Visualization of the discontinuous gas phase

Images of the evolving discontinuous gas phase were collected by backlighting the flow cell with a fluorescent light box (JUST Normlicht, Model No. 12849) and recording the transmitted-light image every hour using a CCD camera (Canon A640). These images provided a visual representation of the depth-averaged gas saturation by light transmission (Tidwell and Glass, 1994; Niemet and Selker, 2001; Oostrom et al., 2007) at a resolution of approximately $(0.2\ mm)^2$/pixel. Details of the image collection process are given by Mumford et al. (2008b). For the purpose of this work, images of the discontinuous gas phase were processed to obtain binary images using a combination of erode and dilate functions in the software ImageJ (http://rsb.info.nih.gov/ij/). Remaining obvious noise in the image was removed by deleting selected pixels manually. Information concerning the relative gas saturation at points within the gas clusters is lost using this type of processing, but the principle macroscopic features are made clearer.

5.4 Model Description

A combination of two established models was used to aid the interpretation of the data from the laboratory experiment by simulating the partitioning of 1,1,1-TCA from a repeatedly mobilized, discontinuous gas phase. This provided further insight into the transient nature of the mass transfer process, which was not clear in the analysis of the laboratory data alone.

The expansion and dissolution of discontinuous gas phases was simulated using the equilibrium, multi-component partitioning model presented by Cirpka and Kitanidis (2001). While this model is capable of simulating small-scale expansion (i.e. expansion that is confined to a single numerical grid block), it is not capable of simulating larger-scale expansion and mobilization (Cirpka and Kitanidis, 2001) that is characteristic of spontaneous expansion above DNAPL pools. Therefore, the expansion to adjacent grid blocks within the model, as well as the fragmentation and mobilization of gas clusters, was simulated using macroscopic invasion percolation (IP) techniques (Kueper and

McWhorter, 1992; Yortsos et al., 1993; Ewing and Gupta, 1993; Ioannidis et al., 1996; Glass et al., 2001; Glass and Yarrington, 2003), with modifications for IP in a gradient (Wilkinson, 1984; Ioannidis et al., 1996) and migration and fragmentation of the invading gas phase (Wagner et al., 1997; Glass and Yarrington, 2003; Tsimpanogiannis and Yortsos, 2004). A macroscopic IP approach was adopted due to the inability of continuum-based numerical models to simulate the processes that control the unstable flow of non-wetting fluids in porous media (Glass et al., 2000; Geistlinger et al., 2006; Selker et al., 2007). An approach using local capillary pressure-saturation relationships at each grid block (Kueper and McWhorter, 1992; Yortsos et al., 1993; Ioannidis et al., 1996), rather than a single characteristic pore radius (Ewing and Gupta, 1993; Glass et al., 2001; Glass and Yarrington, 2003), was used to allow simulation of the pressurization of the gas phase within an invaded block due to multi-component partitioning.

This combination of models made use of the following assumptions:

1. Horizontal solute transport is dominated by aqueous advection, and longitudinal dispersion in the aqueous phase is negligible
2. Vertical solute transport is dominated by the mobilization of discrete gas clusters, and transverse dispersion in the aqueous phase is negligible
3. Local equilibrium between the aqueous and gas phases, and between the DNAPL and gas phases, is achieved instantaneously
4. Aqueous flow is not significantly affected by local changes in gas saturation
5. Gas-phase pressure does not vary with space throughout each connected gas cluster
6. Gas-phase expansion occurs as a quasi-static displacement
7. Gas-phase mobilization occurs much faster than expansion or dissolution, such that mass transfer during mobilization is negligible

5.4.1 Governing equations

Solute transport and mass transfer were simulated using the model of Cirpka and Kitanidis (2001), modified to include the capillary pressure-saturation relationship.

Multi-component mass transfer was simulated using Eqs. (5.1)-(5.6), and solute transport in the aqueous phase was simulated using

$$\theta \frac{\partial C^t{}_i}{\partial t} = -q \frac{\partial C_i}{\partial x} \tag{5.7}$$

where θ is the total porosity of the porous medium, and q is the specific discharge. To allow expansion between grid blocks, and the mobilization of gas clusters, each grid block in the model domain was assigned an entry pressure (P^e), a terminal pressure (P^t), and the capillary pressure-saturation parameters P_d, S_{wr}, and λ. Two thresholds were then defined at each grid block

$$T^e = P^e + P_w \tag{5.8}$$

$$T^t = P^t + P_w \tag{5.9}$$

$$P_w = \rho_w g h + P_w(h_0) \tag{5.10}$$

where T^e is the threshold for drainage, T^t is the threshold for imbibition, P_w is the water pressure, g is the acceleration due to gravity, h is the height of water, and $P_w(h_0)$ is the water pressure at the top of the domain.

During simulation, the solute transport was calculated using Eq. (5.7), and the gas saturation was solved using Eqs. (5.1)-(5.6). The gas saturation in each grid block was treated independently until a critical gas saturation was reached (S_g^*), where S_g^* represents the gas saturation required to span the block and allow connection to gas in other blocks. Once $S_g = S_g^*$, that block was tagged as being available for inclusion in a multi-block gas cluster, and allowed to expand to adjacent cells according to macroscopic IP rules (i.e. expand to block j if $P_g > T^e_j$). Adjacent tagged cells (a co-ordination number

of 4 was used) were treated as a connected cluster, and gas-phase mass was redistributed at the end of each transport step such that the gas-phase mass of each component was the same in connected blocks. Mobilization of a gas cluster was calculated using modified IP rules for fragmentation and mobilization (i.e. relocate gas from block k to block j if $T^t_k > T^e_j$). The aqueous concentrations were calculated from Eq. (5.2) at the end of each expansion and mobilization step.

5.4.2 Implementation

Simulations were conducted on a 44 x 44 cm^2 two-dimensional grid divided into 4 x 4 mm^2 blocks. Uniform values of θ, λ, and S_{wr} were assigned to each grid block (Table 5.2). Local displacement pressures (P_D) were assigned to each block by randomly selecting P_c values from the cumulative distribution function defined by Eq. (5.6) (Glass et al., 2001). Local entry pressures were assigned using Eq. (5.6) for $P_d = P_D$ and $P^e = P_c(S_w = 1 - S_g^*)$. Local terminal pressures were assigned using $P^t = \alpha P^e$ (Ioannidis et al., 1996). A value of $\alpha = 0.57$ was used through the domain based on capillary pressure measurements made during slow air injection experiments conducted in the 1.1 mm-diameter sand used in this experiment (Mumford et al., 2008c). Eq. (5.7) was solved using a finite difference approach with explicit, upstream differentiation, and using a Courant number less than unity ($v\Delta t/\Delta x < 1$) for numerical stability (Table 5.2). The influent was saturated with respect to O_2 and N_2, and contained no 1,1,1-TCA. The gas saturation in a grid block adjacent to the lower boundary and 13.4 cm from the influent boundary, which represents the upgradient edge of the 1,1,1-TCA pool, was initially set to Sg=0.08. The aqueous concentration of 1,1,1-TCA in this grid block, and any grid block in a connected gas cluster that included this grid block, was maintained at the solubility limit for 1,1,1-TCA. All boundaries were treated as impermeable with respect to gas flow.

Table 5.2. Parameter values used in simulations

Fluid properties	
1,1,1-TCA vapour pressure (Pa)[1]	1.66×10^4
1,1,1-TCA aqueous solubility (mg/L)[1]	1310
1,1,1-TCA molecular weight (g/mol)	133.4
Water density (kg/m^3)	1000
Partitioning parameters	
Henry's law coefficients (Pa m^3/mol)	
1,1,1-TCA[1]	1.7×10^3
O_2[2]	8.0×10^4
N_2[2]	1.6×10^5
Temperature (K)	298
Porous media properties	
Total porosity (θ)	0.40
Displacement pressure (P_d) (Pa)[3]	5.31×10^2
Pore-size distribution index (λ)[3]	3.94
Residual water saturation (S_{wr})[3]	0.03
Spanning gas saturation (S_g^*)	0.30
P^t/P^e ratio (α)[4]	0.57
Numerical parameters	
Time step (s)	170
Horizontal grid spacing (mm)	4
Vertical grid spacing (mm)	4
Courant number ($v\Delta t/\Delta x<1$)	0.34
Boundary conditions	
Specific discharge (cm/day)	28
1,1,1-TCA concentration at pool surface (mg/L)	1310
Pool length (cm)	17
Upper boundary water pressure ($P_w(h_0)$) (Pa)	1.01×10^5
Partial pressures at influent boundary	
O_2	$0.21P_w(h)$
N_2	$0.79P_w(h)$
1,1,1-TCA	0

[1]Pankow and Cherry (1996)
[2]Perry et al. (1997)
[3]Schroth et al. (1996)
[4]Mumford et al. (2008c)

5.5 Results and Discussion

5.5.1 Tracer test and effluent flow measurements

Figure 5.2a shows the Br^- breakthrough curves generated from analysis of the samples collected during the tracer test. The time to reach a breakthrough concentration of C/C_0=0.5, where C_0 is the injection concentration, was determined from the breakthrough curves, and is shown in Figure 5.2b. The breakthrough times are reasonably uniform, with an average value of 130 min, and a coefficient of variation of 12%. The increase in breakthrough times with height is attributed to the placement of the injection port near the bottom corner of the influent glass bead pack, which resulted in the slower flow near the top of the 1.1 mm-diameter sand.

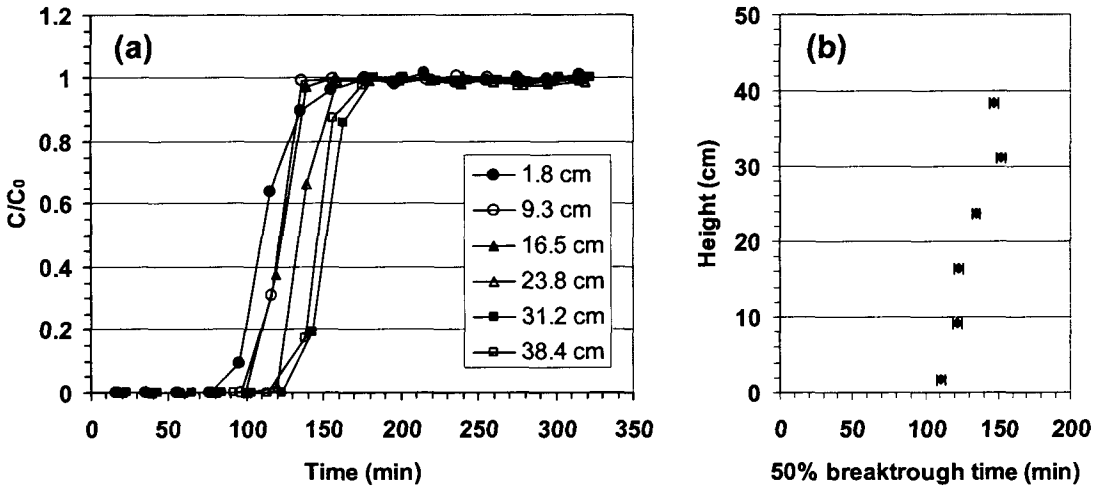

Figure 5.2. (a) Tracer breakthrough curves measured in each of the six effluent ports prior to DNAPL and gas emplacement, and (b) time to reach a breakthrough concentration of C/C_0=0.5 at each of the six effluent port heights.

Variation in effluent flow was observed during the experiment, however the total cell flow rate was constant as set by the syringe pump constant flux injection rate. The effluent flow measured at each port is shown in Figure 5.3 as a contribution to the total flow at each measurement time. Significant variation in flow rate was observed at each of the effluent ports (shown as the height of each colored sub-bar), with flow occasionally stopping in the 1.8-cm and 16.5-cm ports. This variation was at least partially

attributable to the design of the effluent sampling system, in that the effluent tubing could become partially or completely blocked by the local degassing of water. While the additional flow resistance caused by this degassing likely changed the vertical components of the aqueous flow, it was expected that these changes occurred close to the effluent edge of the flow cell. It was also expected that partial or complete blocking of ports changed the depth interval sampled by each port. This change was taken into account in the analysis of the effluent aqueous-phase 1,1,1-TCA concentrations.

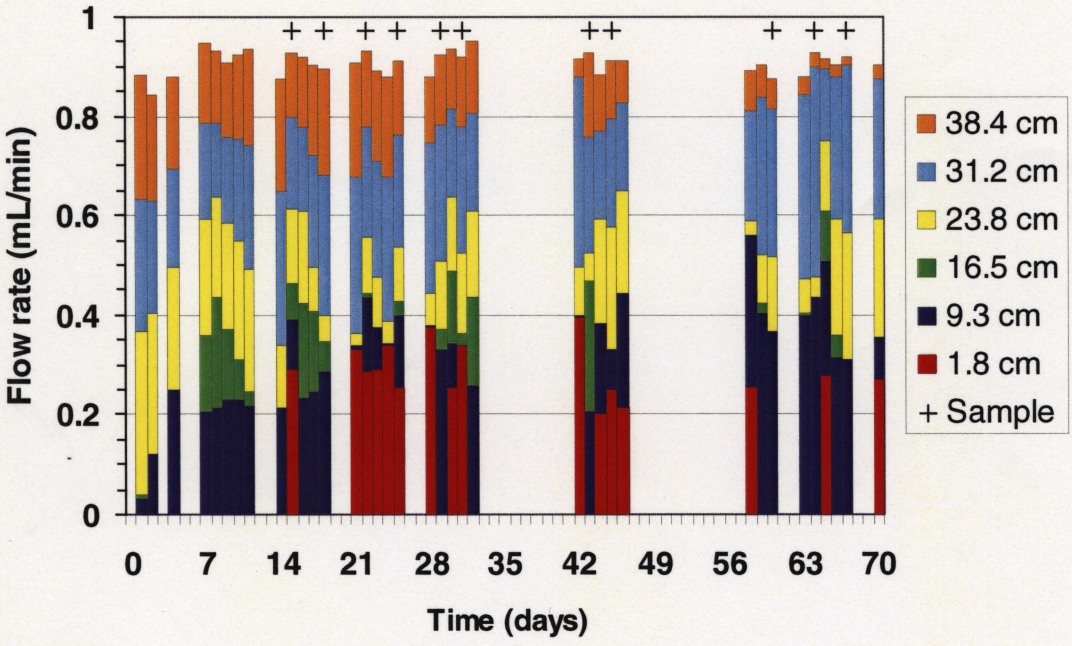

Figure 5.3. Flow rates measured in each effluent port throughout the 70-day experiment shown as a contribution (height of each colored sub-bar) to the total flow at each measurement time (total height of all bars at each time). Flow measurements taken on the same day as an effluent sample was collected are indicated by the symbols (+).

5.5.2 Evolution of the discontinuous gas phase

Visualization data showed that the initial residual gas phase expanded above the 1,1,1-TCA pool, and produced discontinuous gas flow in the form of two macroscopic gas fingers (Figure 5.4). Gas flow proceeded as a series of bursts (Wagner et al., 1997), which were observed at both the upper-most finger tips and in the main bodies of the

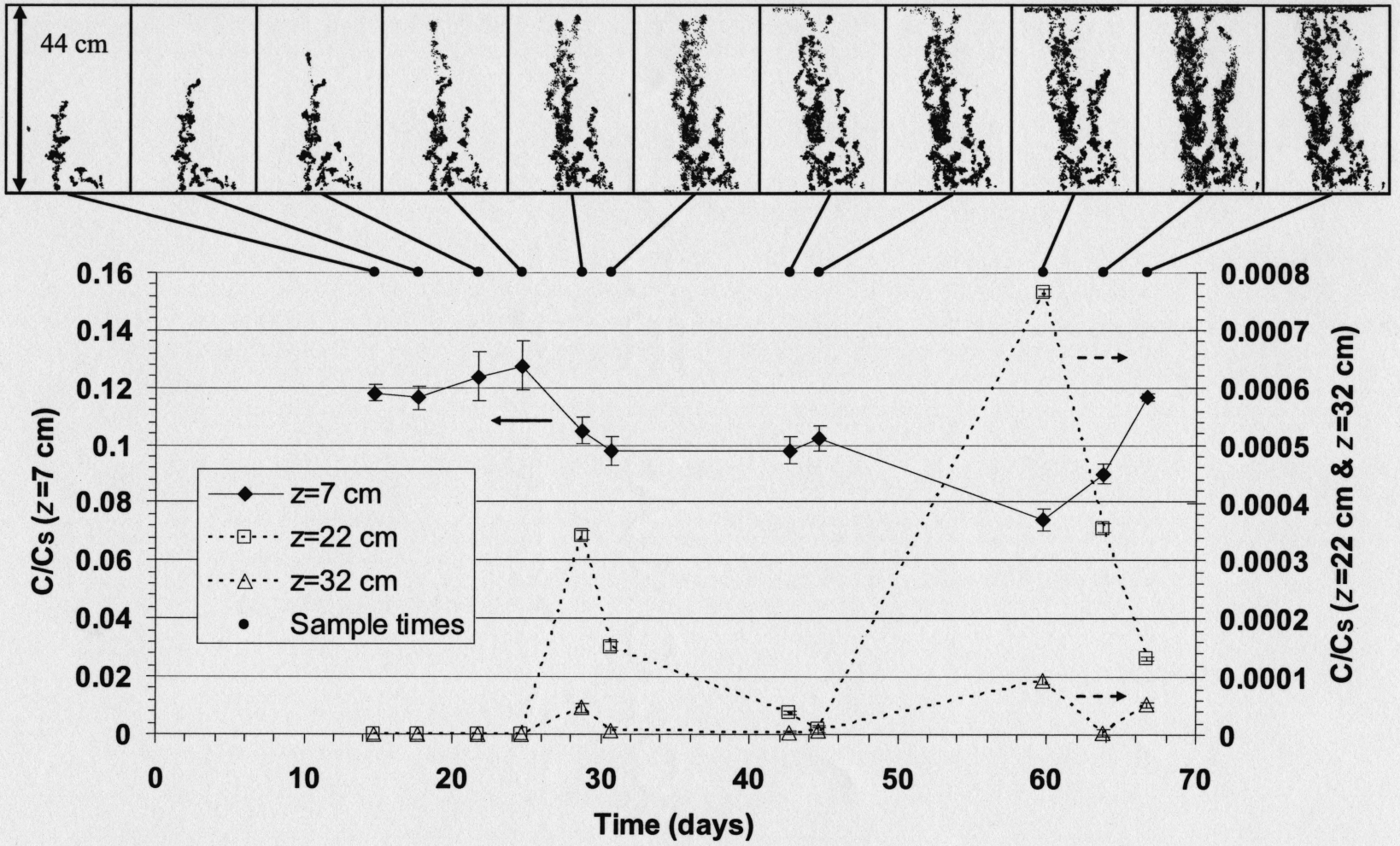

Figure 5.4. Relative effluent aqueous phase 1,1,1-TCA concentrations measured at z=7 cm, z=22 cm, and z=32 cm during the 70-day experiment. The images above the plot show the gas distribution 13 hours before sample collection, which corresponds to the approximate travel time between the gas and the effluent ports.

fingers. These bursts were attributed to the repeated fragmentation and mobilization of disconnected gas clusters throughout the macroscopic finger, and are indicative of discontinuous gas flow (Wagner et al., 1997). Additional details concerning gas-phase growth are given by Mumford et al. (2008b).

5.5.3 Spatial distribution of aqueous-phase 1,1,1-TCA

The aqueous-phase concentrations of 1,1,1-TCA in the sampled effluent are shown in Figure 5.4. Only effluent concentrations from the 1.8-cm, 23.8-cm, and 31.2-cm ports are shown. At sample times when there was no flow in the 1.8-cm port, data from the 9.3-cm port were used. Based on the effluent flow data (Figure 5.3), it was expected that the depth interval sampled by each of these selected effluent ports was reasonably consistent between sample times. Taking the depth fraction sampled by each port to be equal to the fraction of the total flow emitted by each port, the 1.8- or 9.3 cm port sampled an interval 15±3 cm deep, centered 7±1 cm above the pool; the 23.8-cm port sampled an interval 7±4 cm deep, centered 22±2 cm above the pool; and the 31.2-cm port sampled an interval 13±3 cm deep, centered 32±2 cm above the pool. Therefore, the effluent concentration data in Figure 5.4 is referred to the three different elevations: z=7 cm, z=22 cm, and z=32 cm.

The aqueous-phase 1,1,1-TCA concentrations are greater than those predicted for DNAPL-water systems (i.e. no gas phase) under similar flow conditions. Predicted values are used here for comparison to the experimental data because the dissolution of the 1,1,1-TCA pool was not measured in the absence of a discontinuous gas phase. Aqueous-phase concentrations above a DNAPL pool, assuming a sharp pool interface, horizontal flow, and negligible longitudinal dispersion, can be approximated using (Johnson and Pankow, 1992)

$$\frac{C}{C_S} = erfc\left(\frac{z}{2\sqrt{D_z L_p / v}}\right) \tag{5.11}$$

where C_S is the aqueous solubility of the DNAPL, z is the height above the pool surface, D_z is the vertical dispersion coefficient, L_p is the length of the pool in the direction of flow, and v is the pore-water velocity. Taking v=70 cm/day, L_p=17 cm, and D_z=1x10^{-9} m/s predicts a value of C/C_S=0.03 for the interval z=0-15 cm, which is significantly lower than the concentrations of C/C_S=0.07-0.13 observed at z=7 cm (Figure 5.4). The value of D_z=1x10^{-9} m/s is an approximate value based on the value of molecular diffusion (Pankow and Cherry, 1996), and larger values of D_z would result in higher predicted values of C/C_S for the z=0-15 cm interval. However, it is unlikely that transverse vertical dispersion would be substantially greater than molecular diffusion under the experimental conditions used in this study, and would not account for the high observed concentrations. This prediction does not consider the possible existence of a transition zone near the top of the DNAPL pool (Moreno-Barbero and Illangasekare, 2006), which could increase mass transfer rates and produce higher aqueous-phase concentrations than those predicted with a sharp interface model (Glover et al., 2007).

Contact of the discontinuous gas clusters with the pool likely allowed the rapid mass transfer of 1,1,1-TCA to the gas phase, and maintenance of gas-phase 1,1,1-TCA concentrations near saturation throughout the cluster during expansion, due to rapid gas-phase diffusion within the cluster. This expansion of gas clusters connected to the pool surface would increase the effective surface area available for mass transfer to the surrounding groundwater above that of the DNAPL pool alone, resulting in more rapid mass transfer and higher aqueous-phase concentrations. The effect of these connected gas clusters would be limited to a height above the pool surface equal to the critical cluster length, at which an expanding cluster would become disconnected from the pool surface by fragmentation and mobilization. In this sand, the critical cluster length is on the order of 2-4 cm (Mumford et al., 2008c). However, if this mechanism were active in finer media, with larger critical cluster lengths, the increase in mass transfer rate through connected gas clusters could be greater than observed here.

The substantial increase in effluent concentrations above predicted values is consistent with previous observations (Roy and Smith, 2007), which showed a 50% increase in the effluent mass flux of aqueous-phase TCE in the presence of a spontaneous expanding gas phase, due primarily to increases in aqueous-phase concentrations near the pool surface. The experiment conducted by Roy and Smith (2007) was similar to this work in that the expanding gas phase was in direct contact with the surface of the DNAPL pool. This is different from systems where the gas is not in direct contact with the DNAPL pool, where significant increases are expected only for long pools and slow groundwater velocities (Mumford et al., 2008a).

Eq. (5.11) also predicts C/C_S=0 for z>15 cm, which is significantly lower than the peak concentrations of C/C_S=8x10^{-4} and C/C_S=9x10^{-5} observed at z=22 cm and z=32 cm, respectively (Figure 5.4). These greater-than-predicted aqueous-phase concentrations are due to the partitioning of 1,1,1-TCA from discontinuous gas phases that were mobilized following expansion near the surface of the DNAPL pool, and became trapped well above the pool surface during discontinuous gas flow. Aqueous-phase concentrations of this magnitude have not been previously reported at these elevations above a DNAPL pool in the presence of an expanding and mobilized gas phase. They cannot be explained by modifying elements of conventional conceptual models, such as increasing transverse vertical dispersion or changing the pool morphology. These results show that the effects of spontaneous gas expansion are not limited to the local environment of the DNAPL pool surface, and that both the gas saturation (Mumford et al., 2008b) and the downgradient aqueous-phase concentrations can potentially be affected on the scale of at least 10s of cm.

5.5.4 Transient distribution of aqueous-phase 1,1,1-TCA

In addition to showing greater-than-predicted concentrations at all elevations, Figure 5.4 also shows significant, and unexpected, transient behavior in the aqueous-phase 1,1,1-TCA concentrations. The concentrations measured at z=7 cm increased and decreased

throughout the experiment, and the concentrations measured at z=22 cm and z=32 cm showed concentration peaks at 28.7 days and 59.7 days. This type of behavior was not observed in previous small-scale experiments conducted in glass beads (Roy and Smith, 2007), where concentrations within 7 cm of the pool surface increased throughout the 92-day experiment.

The data in Figure 5.4 suggest that the discontinuous gas flow produced episodic effluent concentration events. The aqueous-phase 1,1,1-TCA concentrations near the pool surface likely increased and decreased as gas clusters connected to the pool surface expanded and fragmented, although changes in pool morphology during dissolution also likely contributed to the observed concentration changes. As expanding gas clusters near the pool surface were mobilized and became trapped at higher elevations, the 1,1,1-TCA partitioned from the gas phase to the aqueous phase, and produced significant effluent concentrations at these higher elevations. While this interpretation is consistent with the data, effluent samples were not collected at a sufficient frequency to capture and resolve multiple effluent concentration events associated with the discontinuous gas flow. In addition, the data in Figure 5.4 do not clearly show why effluent concentrations at z=22 cm and z=32 cm were not maintained despite the presence of a gas phase at those elevations both before and after the concentrations peaks observed at 28.7 days and 59.7 days.

To gain further insight, the expansion of a discontinuous gas phase and the resulting discontinuous gas flow was simulated using the combined multi-component mass transfer and macroscopic IP model. This simulation was not intended to accurately match the experimental results, and no attempts were made to calibrate the model results. The simulation was conducted to investigate whether the expansion of a discontinuous gas phase by multi-component partitioning, and the resulting discontinuous gas flow, could produce short-lived increases in aqueous-phase 1,1,1-TCA effluent concentrations under conditions similar to those of the laboratory experiment.

The results of a single simulation are shown in Figure 5.5 for times following the mobilization of a gas cluster from the surface of the DNAPL pool after 23.2 days. The macroscopic gas finger, produced by discontinuous gas flow, is shown in black, and consists of multiple disconnected clusters. These clusters resulted from the mobilization of a gas cluster from the pool surface, coalescence with previously mobilized clusters, and the fragmentation and mobilization of the coalesced clusters. Once mobilization ceased, 1,1,1-TCA began to partition to the aqueous phase from the gas clusters that were not connected to the pool surface. This partitioning proceeded rapidly under the local equilibrium conditions employed in the simulation, and resulted in a short-term pulse of 1,1,1-TCA released to the aqueous phase. However, since the influent was saturated with O_2 and N_2, the gas clusters did not completely dissolve as the 1,1,1-TCA was removed. The fractions of O_2 and N_2 in the gas-phase increased as the fraction of 1,1,1-TCA decreased, and the gas clusters then began to dissolve very slowly due to the small O_2 and N_2 concentration gradients created by capillary pressure. The 1,1,1-TCA pulse, with a width defined by an aqueous concentration of 1 μg/L corresponding to C/C_S=1x10^{-6}, broke through at peak concentration approximately 12 hours after mobilization, and completely exited the domain approximately 18 hours after mobilization. Above the gas cluster connected to the pool surface, the peak concentrations in the pulse ranged from C/C_S=1x10^{-2} to C/C_S=1x10^{-4}, with decreasing concentrations further away from the pool surface. The episodic nature of the increased aqueous-phase 1,1,1-TCA concentrations, the persistence of the gas phase during these events, and the magnitude of the peak concentrations in the simulation are consistent with the experimental results. These simulation results support the explanation that the transient, higher-than-predicted aqueous-phase 1,1,1-TCA concentrations observed in the experiment are due primarily to the spontaneous expansion and mobilization of discontinuous gas clusters from the surface of the DNAPL pool.

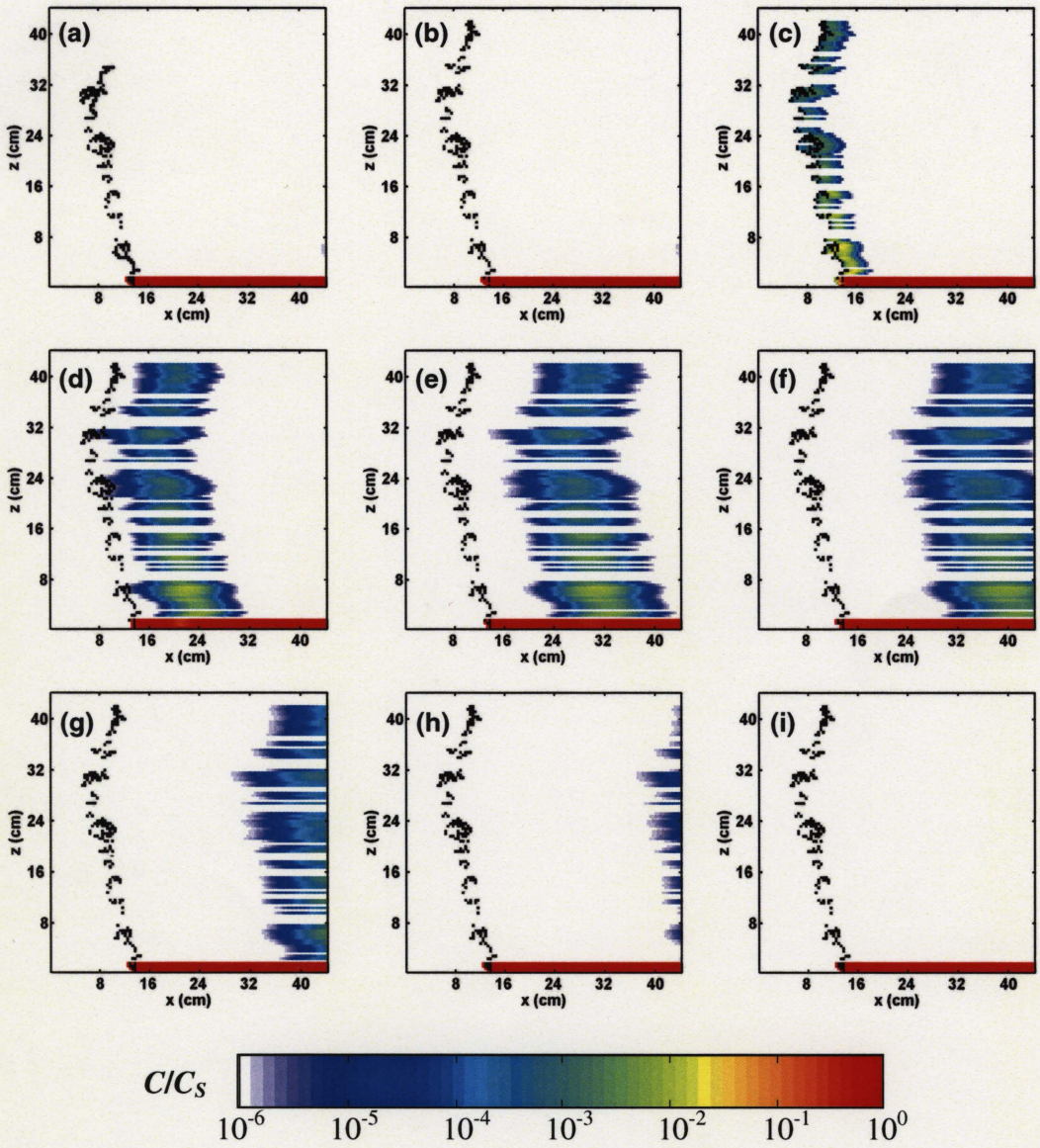

Figure 5.5. Simulated aqueous-phase 1,1,1-TCA concentrations following the mobilization of a gas cluster from the pool surface, and the resulting coalescence and mobilization of gas clusters at higher elevations, immediately (a) before, and (b) after a mobilization event at 23.2 days. Also shown are the aqueous-phase 1,1,1-TCA concentrations (c) 0.5, (d) 3.5, (e) 6.5, (f) 9.5, (g) 12.5, (h) 15.5, and (i) 18.5 hours following mobilization. The gas-occupied blocks are shown in black, and the relative aqueous-phase 1,1,1-TCA concentration is shown on a log scale from white to red.

5.6 Summary and Conclusions

Results of the intermediate-scale, two-dimensional flow cell experiment conducted in this study show that the spontaneous expansion and mobilization of a discontinuous gas phase produced aqueous-phase 1,1,1-TCA concentrations that were greater than expected based on predictions made using a conventional model for DNAPL pool dissolution in the absence of a discontinuous gas phase. Relative aqueous-phase 1,1,1-TCA concentrations of C/C_S=0.07-0.13 were observed 7 cm above the pool surface, and peak relative concentrations of C/C_S=8x10^{-4} and C/C_S=9x10^{-5} were observed at 22 cm and 32 cm above the pool surface, respectively. These were significantly greater than the predicted relative concentrations of C/C_S=0.03 at z=7 cm, and C/C_S=0 at z=22 cm and z=32 cm. These results show that the spontaneous expansion and mobilization of a discontinuous gas phase above a DNAPL pool can produce previously unexpected, higher aqueous-phase concentrations of the DNAPL constituent downgradient of the pool, which result from the vertical transport of DNAPL constituent mass by discontinuous gas flow, and the partitioning of that mass from the gas phase to the aqueous phase well above the pool surface. The experimental results, in combination with the simulation results based on multi-component partitioning and gas movement by macroscopic IP, also show that the discontinuous nature of the gas flow produces transient behavior in these downgradient concentrations. Multi-component partitioning from gas clusters away from the DNAPL pool produced short-term, pulse-like events with elevated aqueous-phase 1,1,1-TCA concentrations, but allowed the discontinuous gas phase to persist with a composition made up of the other dissolved gases.

These results have potential implications for the diagnosis of DNAPL source zones based on the analysis of aqueous-phase concentrations. The current conceptual models commonly applied to DNAPL-contaminated sites do not include mechanisms capable of generating the aqueous-phase concentrations at the elevations above a DNAPL pool surface that were observed in this study, for horizontal flow fields with low vertical transverse dispersivity. Therefore, if this mechanism were active at a contaminated site,

detectable aqueous-phase concentrations produced by the partitioning of DNAPL constituents from a mobilized gas phase would likely be mistakenly attributed to a shallower, upgradient DNAPL source. Transient behavior of these aqueous-phase concentrations, as was observed in this study, could further complicate investigation efforts by generating detectable concentrations that may not be present during all considered sampling periods. It is expected that finer media, which require a longer time to generate the larger gas clusters necessary for mobilization, would produce less frequent events, and make detection even less likely. It is also expected that coarser media, multiple fingers, and greater travel times between the fingers and the sampling point would produce less separation between concentration events, and make detection more likely. The need to understand the potential effects of spontaneous expansion and mobilization under a wider variety of conditions warrants additional experimental investigation as well as the development of comprehensive numerical models to accurately simulate this only recently reported complex process.

Acknowledgements

This research was supported by the Natural Sciences and Engineering Research Council (NSERC) of Canada through its Discovery Grant Program and a Canada Graduate Scholarship to the first author. We gratefully acknowledge the technical assistance of Jennie Kirby and Anna Robertson.

References

Amos, R.T., Mayer, K.U., 2006a. Investigating the role of gas bubble formation and entrapment in contaminated aquifers: Reactive transport modeling. J. Contam. Hydrol. 87, 123-154.

Amos, R.T., Mayer, K.U., 2006b. Investigating ebullition in a sand column using dissolved gas analysis and reactive transport modeling. Environ. Sci. Technol. 40 (17), 5361-5367.

Balcke, G.U, Meenken, S., Hoefer, C., Oswald, S.E., 2007. Kinetic gas-water transfer and gas accumulation in porous media during pulsed oxygen sparging. Environ. Sci.Technol. 41 (12), 4428-4434.

Brooks, M.C., Wise, W.R., Annable, M.D., 1999. Fundamental changes in in situ air sparging flow patterns. Ground Water Monit. R. 19(2), 105-113.

Chrysikopoulos, C.V., Lee, K.Y., Harmon, T.C., 2000. Dissolution of a well-defined trichloroethylene pool in saturated porous media: Experimental design and aquifer characterization. Water Resour. Res. 36 (7), 1687-1696.

Cirpka, O.A., Kitanidis, P.K., 2001. Transport of volatile compounds in porous media in the presence of a trapped gas phase. J. Contam. Hydrol. 49, 263-285.

Ewing, R.P., Gupta, S.C., 1993. Modeling percolation properties of random media using a domain network. Water Resour. Res. 29 (9), 3169-3178.

Geistlinger, H., Beckmann, A., Lazik D., 2005. Mass transfer between a multicomponent trapped gas phase and a mobile water phase: experiment and theory. Water Resour. Res. 41, doi:10.1029/2004WR003885.

Geistlinger, H., Krauss, G., Lazik, D., Luckner, L., 2006. Direct gas injection into saturated glass beads: Transition from incoherent to coherent gas flow pattern. Water Resour. Res. 42, doi:10.1029/2005WR004451.

Glass, R.J., Yarrington, L., 2003. Mechanistic modeling of fingering, nonmonotonicity, fragmentation, and pulsation within gravity/buoyant destabilized two-phase/unsaturated flow. Water Resour. Res. 39 (3), doi:10.1029/2002WR001542.

Glass, R.J., Conrad, S.H., Peplinski, W., 2000. Gravity-destabilized nonwetting phase invasion in macroheterogeneous porous media: Experimental observations of invasion dynamics and scale analysis. Water Resour. Res. 36 (11), 3121-3137.

Glass, R.J., Conrad, S.H., Yarrington, L., 2001. Gravity-destabilized nonwetting phase invasion in macroheterogeneous porous media: Near-pore-scale macro modified invasion percolation simulation of experiments. Water Resour. Res. 37 (5), 1197-1207.

Glover, K.C., Munakata-Marr, J., Illangasekare, T.H., 2007. Biologically enhanced mass transfer of tetrachloroethene from DNAPL in source zones: experimental evaluation and influence of pool morphology. Environ. Sci. Technol. 41 (4), 1384-1389.

Holocher, J., Peeters, F., Aeschbach-Hertig, W., Kinzelbach, W., Kipfer, R., 2003. Kinetic model of gas bubble dissolution in groundwater and its implications for the dissolved gas composition. Environ. Sci. Tecnol. 37 (7), 1337-1343.

Ioannidis, M.A., Chatzis, I., Dullien, F.A.L., 1996. Macroscopic percolation model of immiscible displacement: effects of buoyancy and spatial structure. Water Resour. Res. 32 (11), 3297-3310.

Johnson, R.L., Pankow, J.F., 1992. Dissolution of dense chlorinated solvents into groundwater. 2. source functions for pools of solvent. Environ. Sci. Technol. 26 (5), 896-901.

Kueper, B.H., McWhorter, D.B., 1992. The use of macroscopic percolation theory to construct large-scale capillary pressure curves. Water Resour. Res. 28 (9), 2425-2436.

Li, T.M.W., Ioannidis, M., Chatzis, I., 2007. Recovery of non-aqueous phase liquids from ground sources. United States patent no. US 7300227 B2, November 27, 2007.

Moreno-Barbero, E., Illangasekare, T.H., 2006. Influence of dense nonaqueous phase liquid pool morphology on the performance of partitioning tracer tests: evaluation of the equilibrium assumption. Water Resour. Res. 42, doi:10.1029/2005WR004074.

Mumford, K.G., Smith, J.E., Dickson, S.E., 2008a. Mass flux from a non-aqueous phase liquid pool considering spontaneous expansion of a discontinuous gas phase. J. Contam. Hydrol. 98, 85-96.

Mumford, K.G., Smith, J.E., Dickson, S.E., 2008b. New observations of gas-phase expansion above a dense non-aqueous phase liquid pool. Vadose Zone J. In press.

Mumford, K.G., Dickson, S.E., Smith, J.E., 2008c. Slow gas expansion in saturated natural porous media by gas injection and partitioning with non-aqueous phase liquids. Submitted to Adv. Water Resour.

Niemet, M.R., Selker, J.S., 2001. A new method for quantification of liquid saturation in 2D translucent porous media systems using light transmission. Adv. Water Resour. 24, 651-666.

Oostrom, M., Dane, J.H., Wietsma, T.W., 2007. A review of multidimensional, multifluid, intermediate-scale experiments: Flow behavior, saturation imaging, and tracer detection and quantification. Vadose Zone J. 6 (3), 610-637.

Pankow, J.F., Cherry, J.A., 1996. Dense Chlorinated Solvents and other DNAPLs in Groundwater. Waterloo Press, Portland, Oregon.

Perry, R.H., Green, D.W., Maloney, J.O. (Eds.), 1997. Perry's Chemical Engineers' Handbook, 7th ed. McGraw-Hill, New York.

Roosevelt, S.E., Corapcioglu, M.Y., 1998. Air bubble migration in a granular porous medium: experimental studies. Water Resour. Res. 34 (5), 1131-1142.

Roy, J.W., Smith, J.E., 2007. Multiphase flow and transport caused by spontaneous gas phase growth in the presence of dense non-aqueous phase liquid. J. Contam. Hydrol. 89, 251-269.

Roy, J.W., Smith, J.E., Gillham, R.W., 2004. Laboratory evidence of natural remobilization of multicomponent DNAPL pools due to dissolution. J. Contam. Hydrol. 74, 145-161.

Schroth, M.H., Ahearn, S.J., Selker, J.S., Istok, J.D., 1996. Characterization of miller-similar silica sands for laboratory hydrologic studies. Soil Sci. Soc. Am. J. 60 (5), 1331-1339.

Seagren, E.A., Rittman, B.E., Valocchi, A.J., 1999. An experimental investigation of NAPL pool dissolution enhancement by flushing. J. Contam. Hydrol. 37, 111-137.

Selker, J.S., Niemet, M., Mcduffie, N.G., Gorelick, S.M., Parlange, J.-Y., 2007. The local geometry of gas injection into saturated homogeneous porous media. Transport Porous Med. 68 (1), 107-127.

Stöhr, M., Khalili, A., 2006. Dynamic regimes of buoyancy-affected two-phase flow in unconsolidated porous media. Phys. Rev. E. 73, 036301.

Tidwell, V.C., Glass, R.J., 1994. X-ray and visible-light transmission for laboratory measurement of 2-dimensional saturation fields in thin-slab systems. Water Resour. Res. 30 (11), 2873-2882.

Tsimpanogiannis, I.N., Yortsos, Y.C., 2004. The critical gas saturation in a porous medium in the presence of gravity. J. Colloid Interface Sci. 270, 388-395.

Wagner, G., Meakin, P., Feder, J., Jossang, T., 1997. Buoyancy-driven invasion percolation with migration and fragmentation. Physica A. 245, 217-230.

Wilkinson, D., 1984. Percolation model of immiscible displacement in the presence of buoyancy forces. Phys. Rev. A. 30 (1), 520-531.

Williams, R.L., Mayer, K.U, Amos, R.T., Blowes, D.W., Ptacek, C.J., Bain J.G., 2007. Using dissolved gas analysis to investigate the performance of an organic carbon permeable reactive barrier for the treatment of mine drainage. Appl. Geochem. 22 (1), 90-108.

Yortsos, Y.C., Satik, C., Bacri, J.-C., Salin, D., 1993. Large-scale percolation theory of drainage. Transport Porous Med. 10 (2), 171-195.

Chapter 6

Conclusions and Recommendations

6.1 Overall Conclusions

The goal of this research was to develop a quantitative understanding of discontinuous gas phase expansion and mobilization above a DNAPL pool. The following conclusions can be made based on the results of this research:

1. A discontinuous gas phase in the vicinity of a DNAPL pool will expand if the sum of the partial pressures in equilibrium with the surrounding bulk aqueous phase is greater than the sum of the hydrostatic pressure and local capillary entry pressure. This condition is more likely to occur, and will be faster, in shallower systems (i.e lower hydrostatic pressures) containing coarser media (i.e. lower capillary pressures), more volatile DNAPL, and higher concentrations of other dissolved gases (i.e. higher partial pressures).

2. The expansion of a discontinuous gas phase in the vicinity of a DNAPL pool is due to multi-component partitioning. Therefore, the presence of volatile DNAPL alone is not sufficient to produce expansion; the concentration of all dissolved, volatile species must be considered when assessing the potential for spontaneous expansion, and the resulting expansion rate.

3. Spontaneous expansion of a discontinuous gas phase will significantly affect the mass transfer rate from a DNAPL pool only under a limited set of conditions. If the gas phase is not in contact with the DNAPL pool, the mass transfer will be significant only for high gas coverage close to the surface of long pools, under slow groundwater flow conditions. The mass transfer rate can be significantly greater if the gas is in contact with the DNAPL pool, as rapid mass transfer occurs by gas-phase diffusion through the gas cluster connected to the pool surface. However, the effect of clusters connected to the pool surface would be limited to a height above the pool surface equal to the critical cluster height, at which fragmentation and mobilization of the gas cluster would occur.

4. Spontaneous expansion above a DNAPL pool will result in expansion rates that produce discontinuous gas flow in fine to coarse sand. This discontinuous gas flow is characterized by repeated trapping and coalescence of gas clusters, where rapid, large-scale vertical transport of the gas phase is made possible by the coalescence of clusters from near the pool surface with those trapped higher above (i.e. pipeline behaviour). This pipeline behaviour is an important consideration for mass transfer from DNAPL pools due to spontaneous expansion and mobilization, as large-scale vertical transport will only be possible under conditions where the dissolution of trapped clusters above the pool is slower than the expansion of those near the pool surface.

5. The combination of image analysis and pressure measurements can provide meaningful insight into transient discontinuous gas flow, including measurements of entry and terminal pressure values, and critical cluster lengths.

6. In relatively homogeneous sands, discontinuous gas flow produced by spontaneous expansion results in the formation of macroscopic gas fingers composed of multiple discrete gas clusters, which can reach substantial heights above the DNAPL pool

surface. The fingers evolve at higher-to-lower rates along the flow direction, as other dissolved gases in the upgradient aqueous phase are removed due to the growth of upgradient fingers. This preferential upgradient growth suggests that the larger-scale effects of this mechanism will be limited to the leading edge of DNAPL pools, in the absence of an additional mechanism that produces dissolved gases further downgradient.

7. Spontaneous expansion and mobilization of discontinuous gas from the surface of a DNAPL pool can produce aqueous-phase DNAPL constituent concentrations that are greater than expected based on theoretical calculations for strictly DNAPL-water systems, even at elevations where the concentrations are expected to be zero. The increased concentrations well above the pool surface appear as short-duration events in the presence of a sustained gas phase, due to the partitioning of DNAPL constituents from the gas to the aqueous phase during multi-component mass transfer.

These conclusions provide the necessary basis to begin incorporating this fundamental mechanism into the conceptual and mathematical models used for DNAPL-related research, the investigation of DNAPL-contaminated sites, and the design and application of DNAPL remediation technologies. They also provide the broader hydrogeologic engineering and science community with additional knowledge pertaining to multi-phase, transient systems in porous media, which are of interest to those studying topics such as biologically produced gases, air injection, and carbon dioxide storage.

6.2 Contributions

This research established a detailed conceptual model for the spontaneous expansion and mobilization of a discontinuous gas phase above a DNAPL pool. In this conceptual model, multi-component partitioning produces discontinuous gas flow, in the form of macroscopic gas fingers at the pool's leading edge, which results in transient changes to

the aqueous-phase DNAPL constituent concentrations well above the pool surface. During this research, the following specific contributions were made to science and engineering:

1. The small-scale vial experiments (Chapter 2) provided the first clear evidence of discontinuous gas phase expansion driven by the partitioning of DNAPL constituent to the gas phase. This supported previously published results, and helped to established spontaneous expansion as a fundamentally important mechanism.

2. The screening-level relative flux model (Chapter 2) provided the first information concerning the conditions under which mass transfer due to spontaneous expansion could be significant at DNAPL-contaminated sites. This established the potential importance of spontaneous gas expansion with respect to mass transfer from DNAPL pools, and showed that further research into this mechanism would be valuable.

3. The small-scale vial experiments (Chapter 2) and the small-scale DNAPL flow cell experiments (Chapter 4) provided the first measurements of spontaneous expansion rate in the presence of a DNAPL pool, and the first evidence of faster expansion for more volatile DNAPL. This established the gas flow conditions, and corresponding mass transfer conditions, relevant to this mechanism.

4. The small-scale air injection experiments (Chapter 4) presented a technique to measure the critical cluster length in a porous media model thicker than one grain diameter, and provided the first measurements of critical cluster length in natural porous media. This provided a tool for the detailed study of discontinuous gas flow in natural porous media.

5. The intermediate-scale flow-cell experiment (Chapter 3) provided the first evidence of macroscopic gas mobilization due to spontaneous expansion above a DNAPL

pool, and preferential expansion at the leading edge of the pool due to the availability of other dissolved gases. This established a clear conceptual basis to begin the incorporation of this mechanism into our conceptual models for DNAPL-contaminated sites.

6. The intermediate-scale flow-cell experiment (Chapter 5) also showed the first evidence of transient aqueous-phase DNAPL constituent concentrations in the form of short-term, pulse-like events. These events resulted from the partitioning of DNAPL constituent from a mobilized gas phase, and produced significant peak concentrations at elevations not explained by a conventional DNAPL-water pool dissolution model. This provided an important addition to the conceptual model by identifying a previously unrecognized transient behaviour.

7. The numerical model (Chapter 5) combined multi-component mass transfer to a discontinuous gas phase with a macroscopic invasion percolation approach for the expansion and mobilization of gas. This provided a useful tool for understanding the transient, macroscopic nature of DNAPL mass transfer in the presence of a discontinuous gas phase, and represents a valuable first step in the development of multi-component, near-pore scale models of mass transfer in variably saturated systems.

6.3 Recommendations for Future Work

Several recommendations for future work have been identified based on the results presented here. Future experimental and numerical studies should be conducted to:

1. Extend the conceptual model from relatively homogeneous systems to more heterogeneous systems. Relevant systems may include horizontal layers that prevent vertical gas transport and create pools of gas which act as large-scale source zones, horizontal layers that control the critical cluster length and produce large-scale

mobilization events in overlying coarse material, and sloping layers that create preferential gas flow pathways.

2. Investigate the potential increase in mass transfer rates above DNAPL pools in finer media, where larger critical cluster lengths could produce extensive connected gas pathways that allow rapid transport of DNAPL constituents away from the surface of the pool over larger distances.

3. Develop new numerical models that incorporate processes relevant to multi-component mass transfer to discontinuous gas phases, including fragmentation and mobilization, relative permeability effects, changes in interfacial properties, and rate-limited mass transfer, to facilitate the detailed prediction of DNAPL behaviour in the presence of discontinuous gas phases.

4. Establish a conceptual basis for spontaneous expansion above three-dimensional pool sources, and in residual source zones, for both DNAPL and LNAPL. Three-dimensional pools could show behaviour similar to a leading-edge effect at all boundaries, and have the potential for significant bypassing of the bulk aqueous phase. Residual source zones could show significant effects of NAPL displacement due to an expanding gas phase.

5. Determine the conditions that control branching during discontinuous gas flow under very slow flow conditions, which can have a significant effect on the distribution of any slow growing, unstable gas phase.

6. Develop numerical tools to simulate this mechanism at the larger scales representative of contaminated sites, while preserving the essential physics of fragmentation, mobilization, coalescence, and trapping that control discontinuous gas flow.

Appendix A

Evidence of DNAPL mobilization during the expansion of a discontinuous gas phase above a DNAPL pool

Digital images taken during experiment #2, and presented in chapter 4, showed the spontaneous expansion and mobilization of discontinuous gas above a trans-1,2-dichloroethene DNAPL pool (Figure 4.3). The digital images also showed the upward mobilization of DNAPL from the pool into the 1.1 mm-diameter sand, which was not discussed in chapter 4. DNAPL mobilization was observed by Roy and Smith (2007), which resulted from the expansion of discontinuous gas into DNAPL-occupied pore spaces, and the subsequent displacement of DNAPL into adjacent pores. Roy and Smith (2007) also observed the upward mobilization of DNAPL that was dragged behind vertically mobilized gas, or that filled pores vacated by mobilized gas. Similar mobilization was observed in experiment #2, with upward mobilization occurring by dragging (Figure A1), and by pore-filling behind mobilized gas (Figure A2). In addition, substantial spreading of DNAPL over the gas-liquid interface during gas expansion was also observed (Figure A2). The combination of these mechanisms has the potential to significantly change the morphology of the pool surface, and lead to greater mass transfer rates.

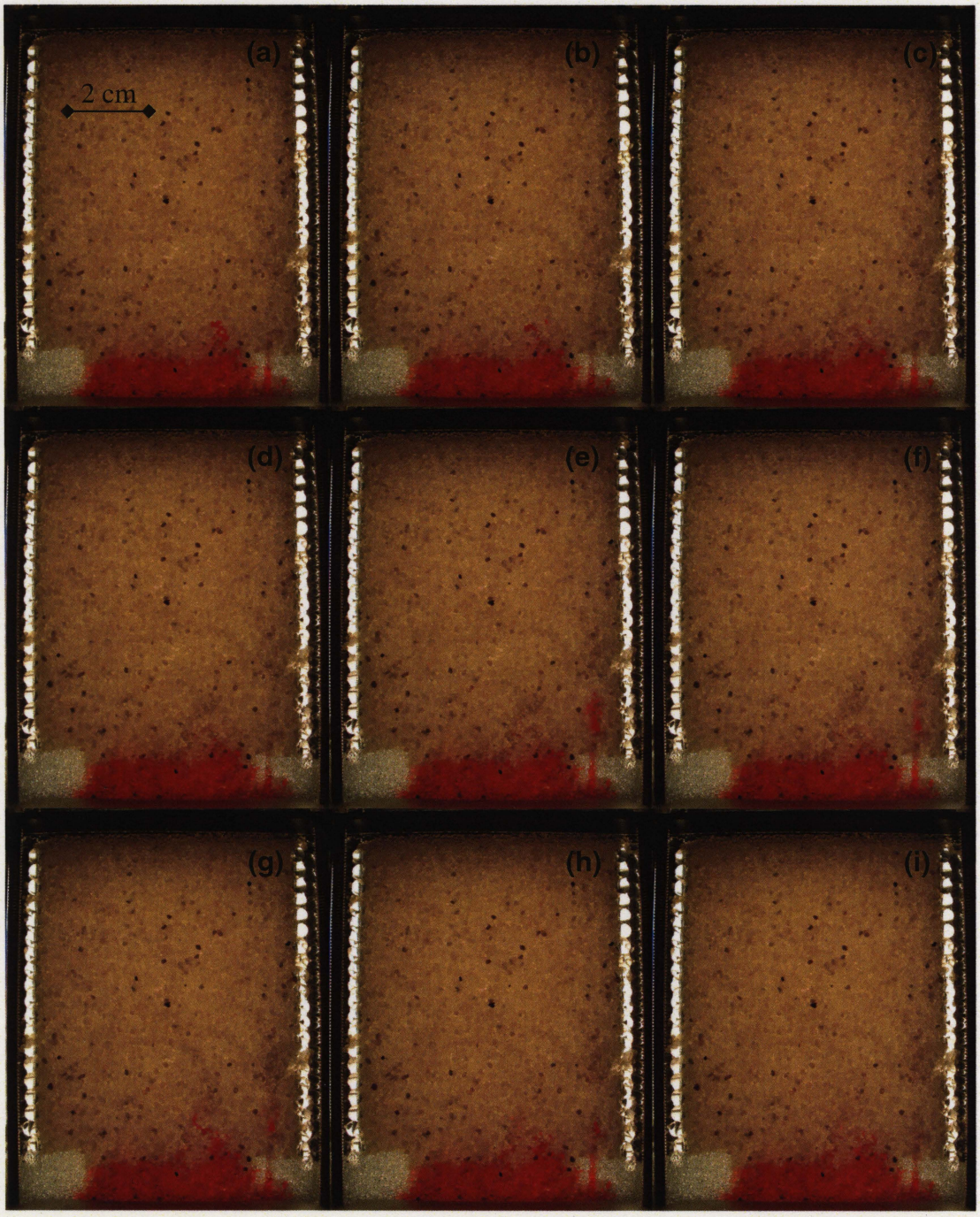

Figure A1. Digital images of the flow cell during experiment #2 after (a) 5.7, (b) 6.7, (c) 7.7, (d) 8.7, (e) 9.7, (f) 10.7, (g) 11.7, (h) 12.7, and (i) 13.7 hours, showing the sudden upward mobilization (e) of the DNAPL, through the pathway in the fine glass bead layer created by the needle during DNAPL emplacement, due to the expansion and mobilization of gas at the base of the pathway.

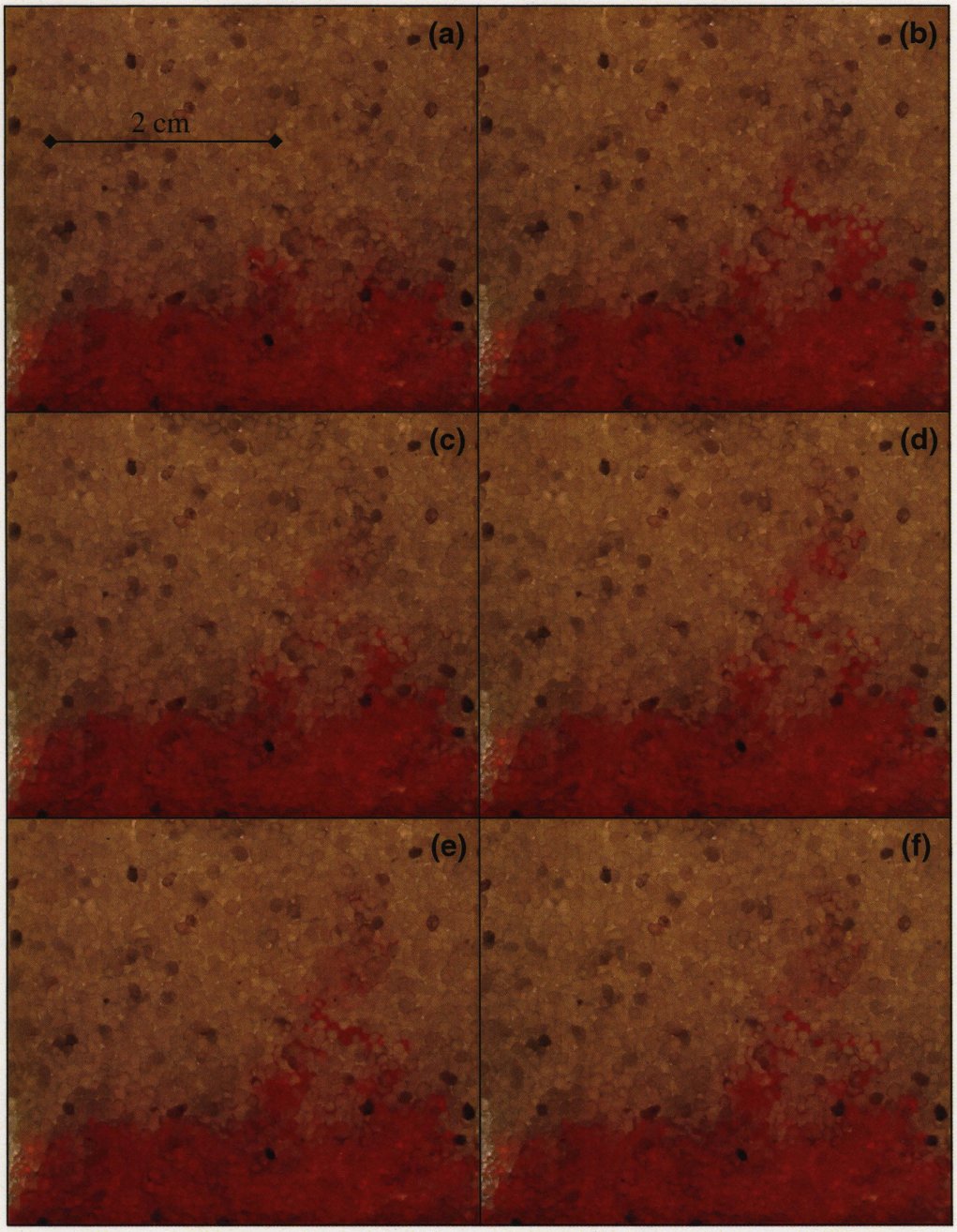

Figure A2. Digital images of the flow cell during experiment #2 after (a) 11.9, (b) 12.9, (c) 13.9, (d) 14.9, (e) 15.9, and (f) 16.9 hours, showing upward mobilization of the DNAPL by the combination of pore-filling behind mobilized gas, and spreading over the gas-liquid interface.

Appendix B

Capillary pressure data from gas injection experiments

Results from 15 gas-injection experiments were presented in chapter 4 for the injection of air at 1 μL/min and 10 μL/min into 1.1 mm, 0.7 mm, and 0.5 mm sand. The following figures (B1-B15) present the capillary pressure at the injection point for each of the 15 experiments, of which only data from the representative experiments #8, #12, and #16 were presented in chapter 4. These data were used to calculate the minimum (P_t) and maximum (P_e) capillary pressures during the fluctuation phases, and were used in combination with image results to determine the critical cluster lengths (Table 4.3). Also presented here are the capillary pressure data used to verify the effect of the volume of the injection syringe and pressure sensor tubing on transient capillary pressure at the beginning of each fluctuation cycle in the gas injection experiments (Figure B16), as discussed in section 4.4.3.

The results of a gas injection experiment that was not discussed in chapter 4 are also shown. This experiment involved the injection of air into the experimental set-up without any porous media in the flow cell. The results provided a measure of the capillary pressure response due to the injection tube (Figure B17), and were used to verify that sudden changes in the capillary pressure coincided with observed snap-off of the gas phase at the end of the injection tube (Figure B18).

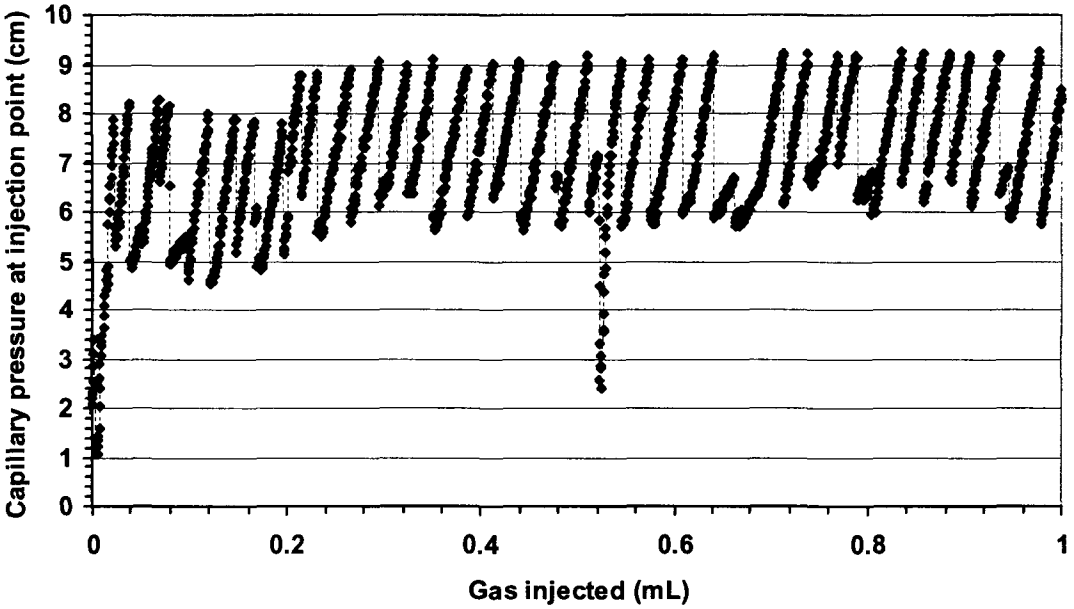

Figure B1. Capillary pressure measured at the gas injection point during experiment #3 (porous medium: 1.1 mm sand, air injection rate: 1 μL/min).

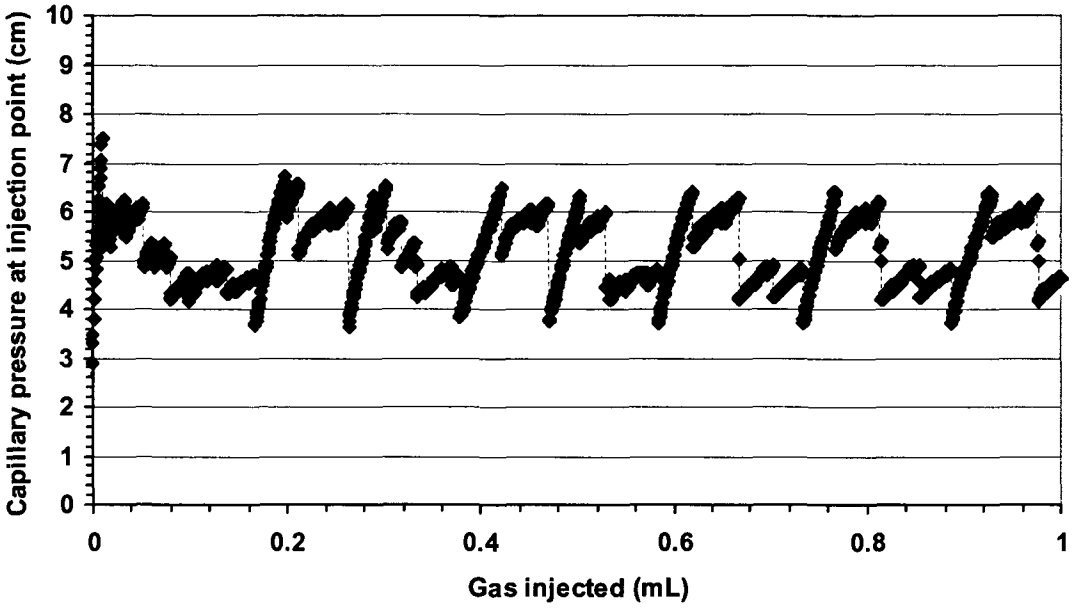

Figure B2. Capillary pressure measured at the gas injection point during experiment #4 (porous medium: 1.1 mm sand, air injection rate: 1 μL/min).

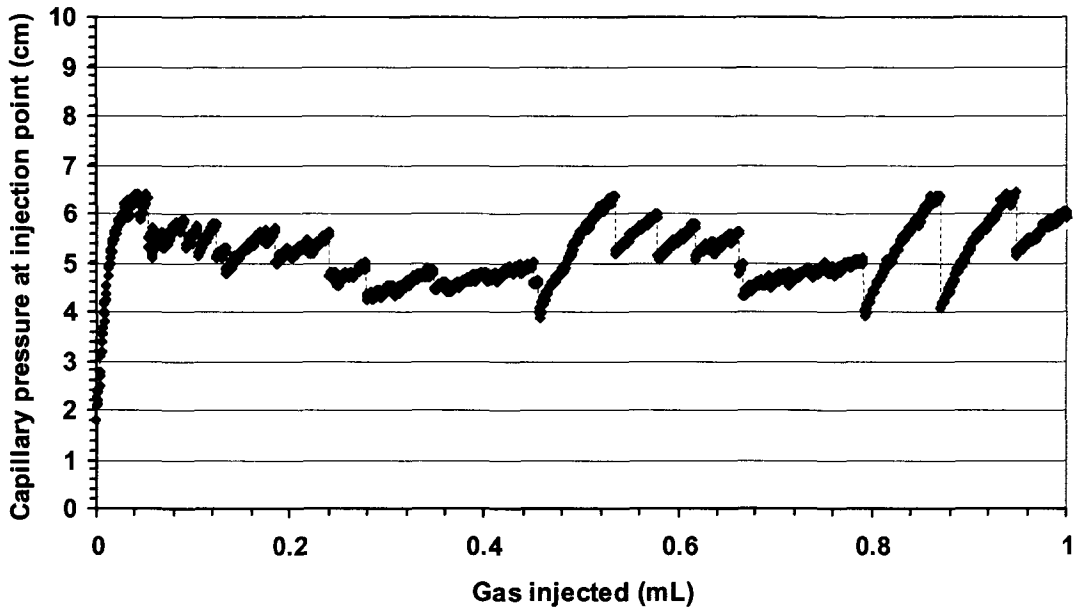

Figure B3. Capillary pressure measured at the gas injection point during experiment #5 (porous medium: 1.1 mm sand, air injection rate: 1 μL/min).

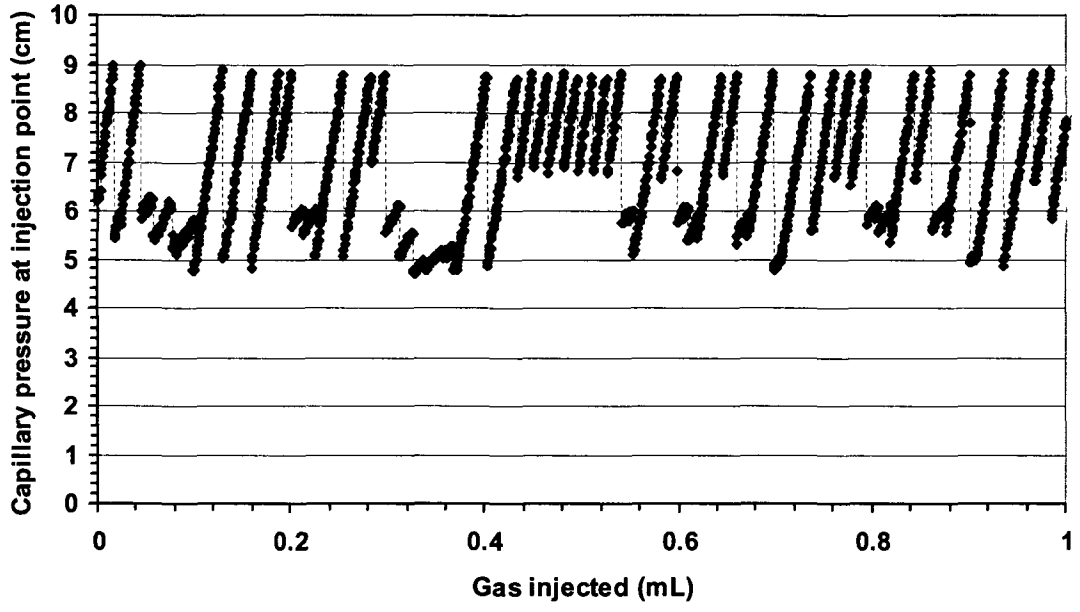

Figure B4. Capillary pressure measured at the gas injection point during experiment #6 (porous medium: 1.1 mm sand, air injection rate: 10 μL/min).

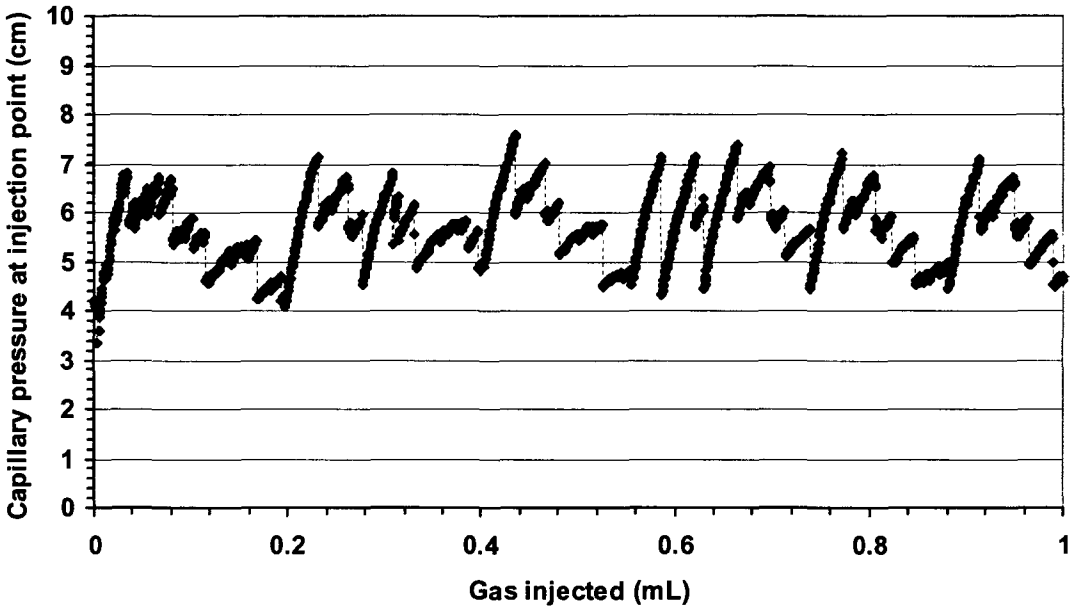

Figure B5. Capillary pressure measured at the gas injection point during experiment #7 (porous medium: 1.1 mm sand, air injection rate: 10 μL/min).

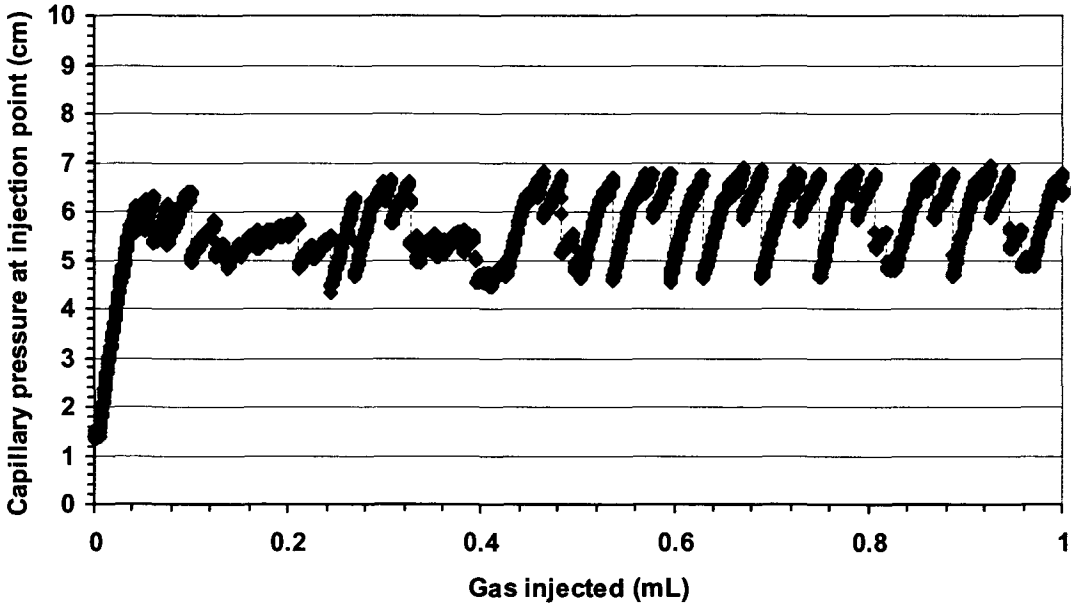

Figure B6. Capillary pressure measured at the gas injection point during experiment #8 (porous medium: 1.1 mm sand, air injection rate: 10 μL/min).

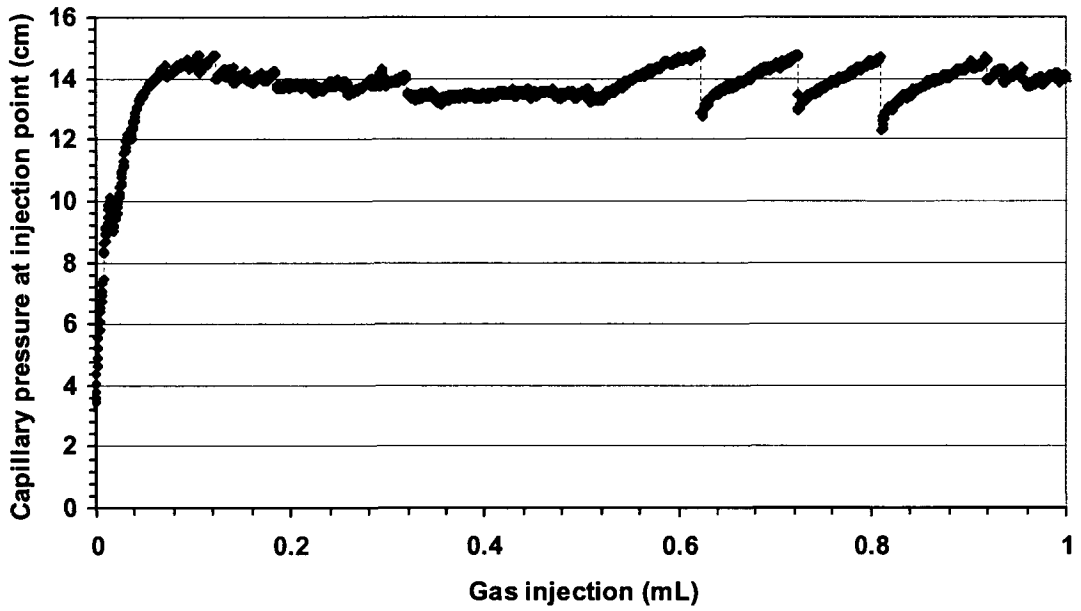

Figure B7. Capillary pressure measured at the gas injection point during experiment #9 (porous medium: 0.7 mm sand, air injection rate: 1 μL/min).

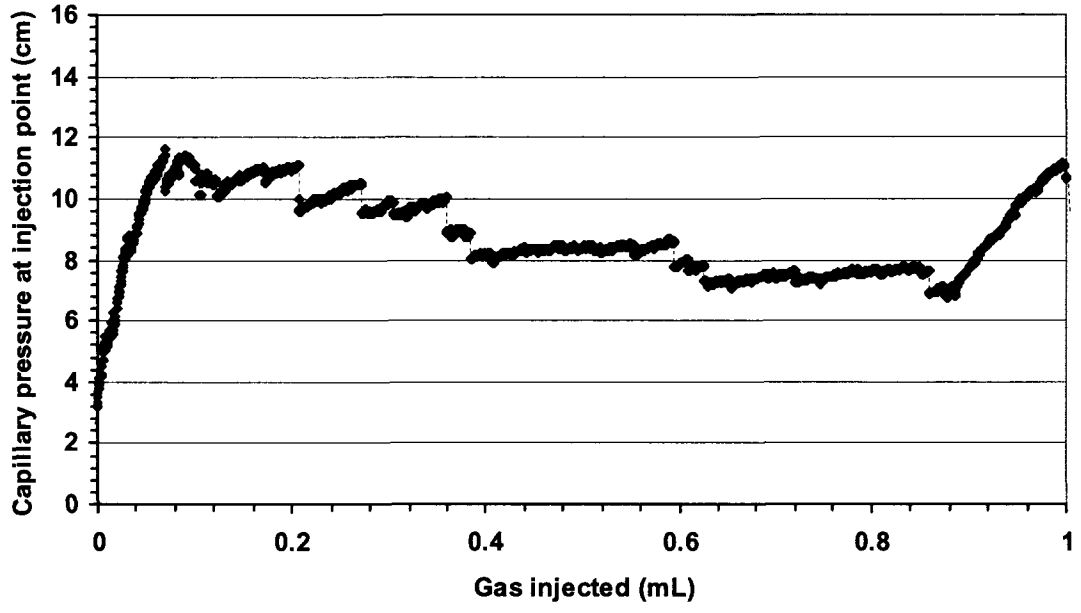

Figure B8. Capillary pressure measured at the gas injection point during experiment #10 (porous medium: 0.7 mm sand, air injection rate: 1 μL/min).

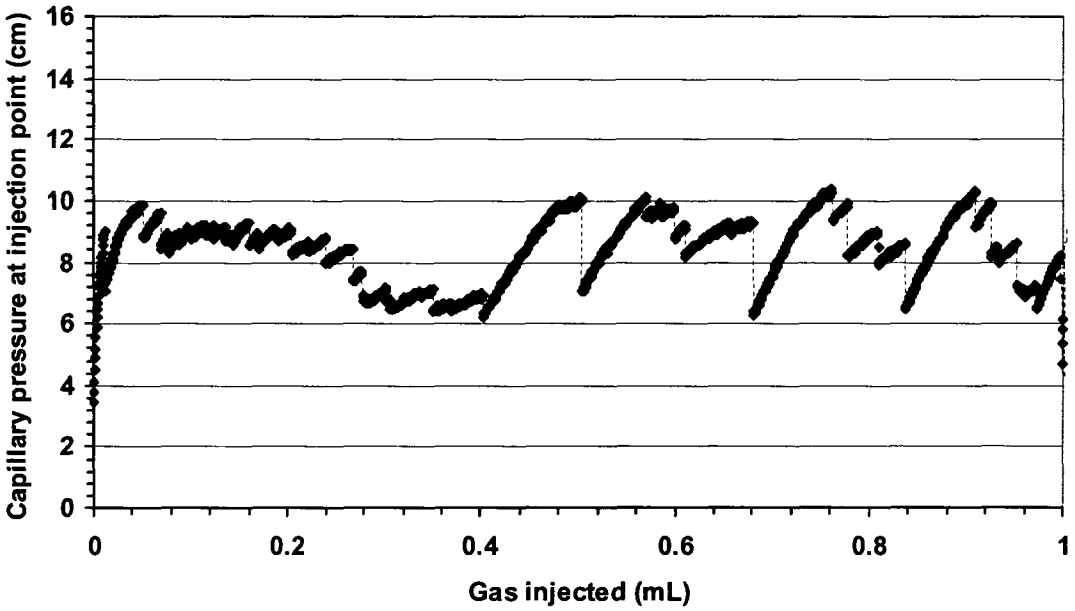

Figure B9. Capillary pressure measured at the gas injection point during experiment #11 (porous medium: 0.7 mm sand, air injection rate: 1 μL/min).

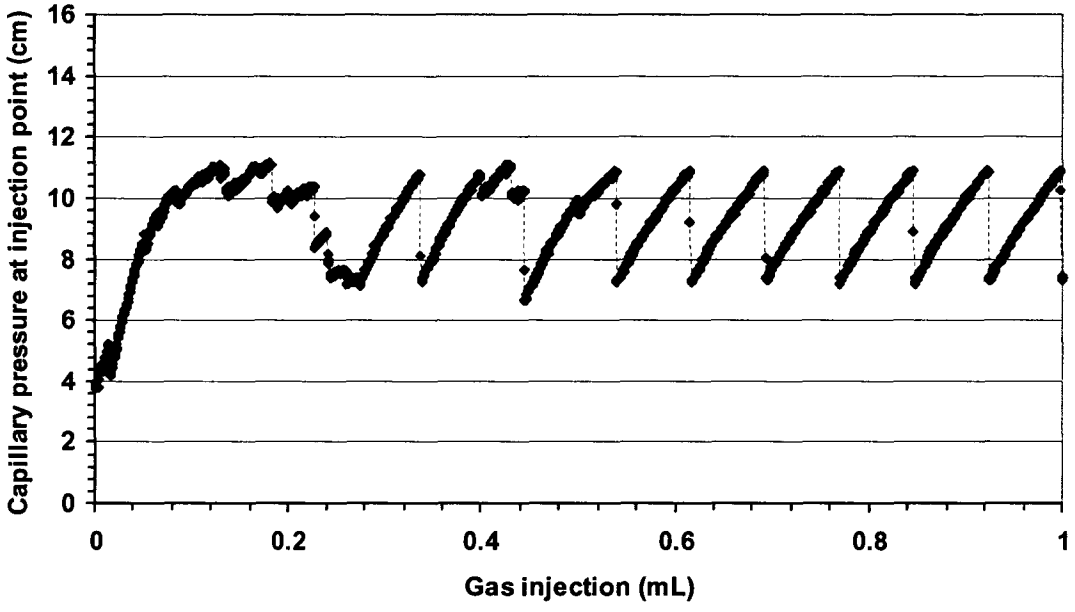

Figure B10. Capillary pressure measured at the gas injection point during experiment #12 (porous medium: 0.7 mm sand, air injection rate: 10 μL/min).

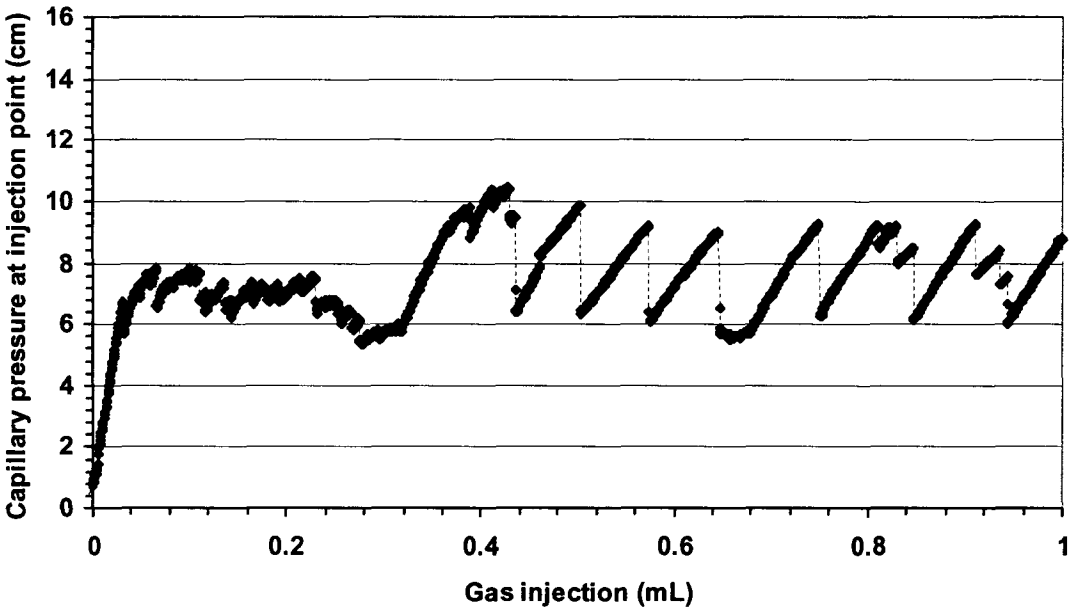

Figure B11. Capillary pressure measured at the gas injection point during experiment #13 (porous medium: 0.7 mm sand, air injection rate: 10 μL/min).

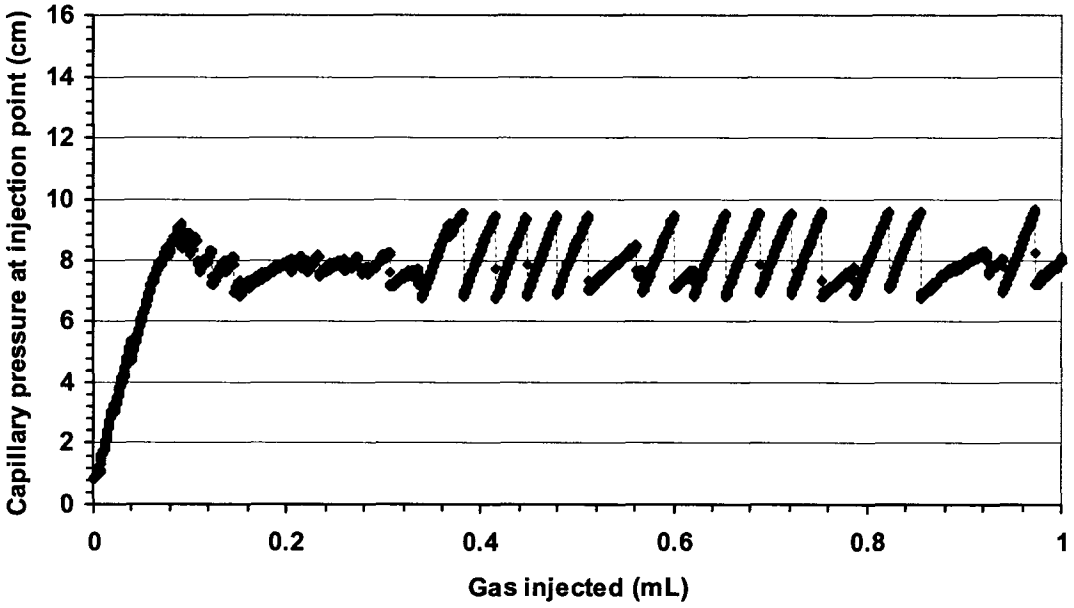

Figure B12. Capillary pressure measured at the gas injection point during experiment #14 (porous medium: 0.7 mm sand, air injection rate: 10 μL/min).

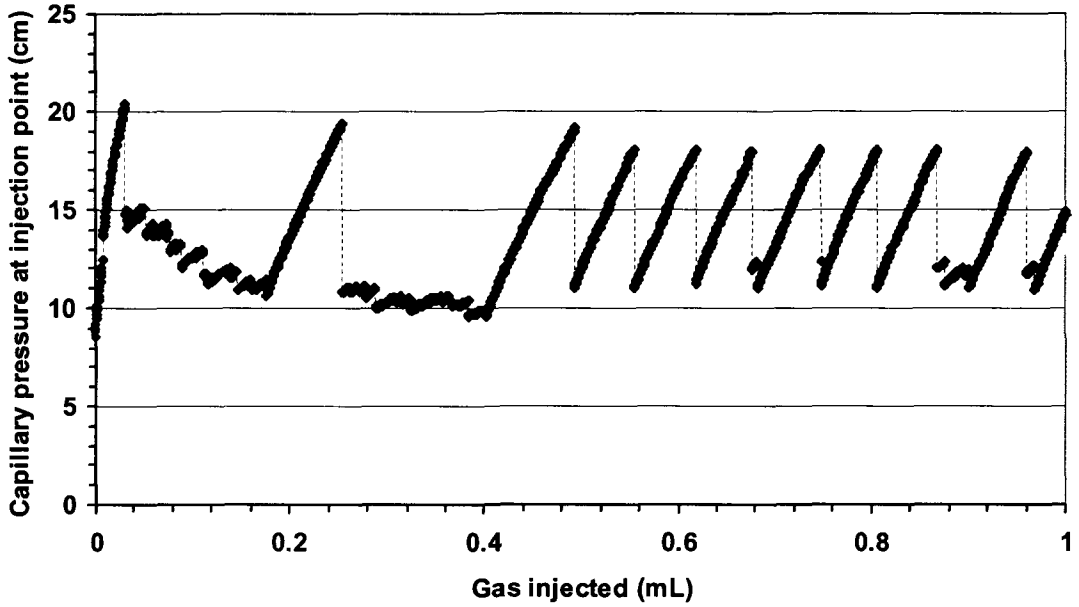

Figure B13. Capillary pressure measured at the gas injection point during experiment #15 (porous medium: 0.5 mm sand, air injection rate: 1 μL/min).

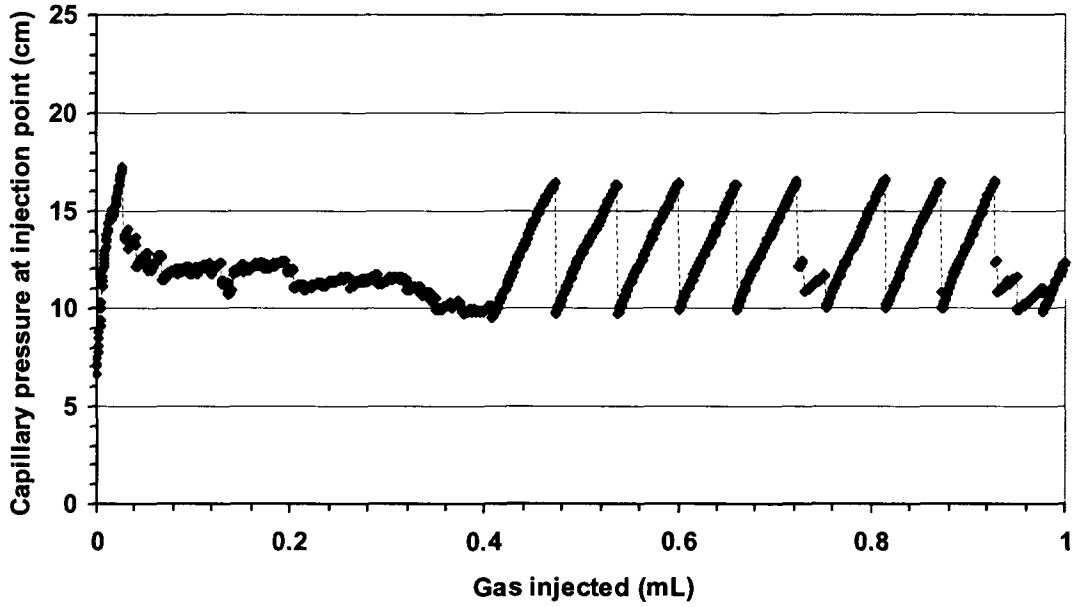

Figure B14. Capillary pressure measured at the gas injection point during experiment #16 (porous medium: 0.5 mm sand, air injection rate: 1 μL/min).

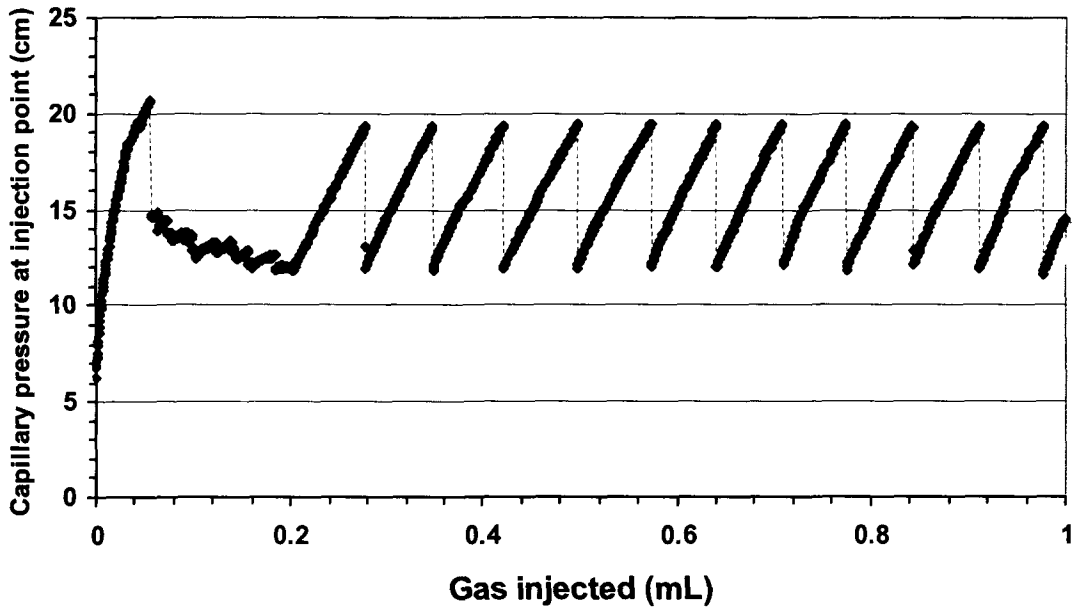

Figure B15. Capillary pressure measured at the gas injection point during experiment #17 (porous medium: 0.5 mm sand, air injection rate: 1 μL/min).

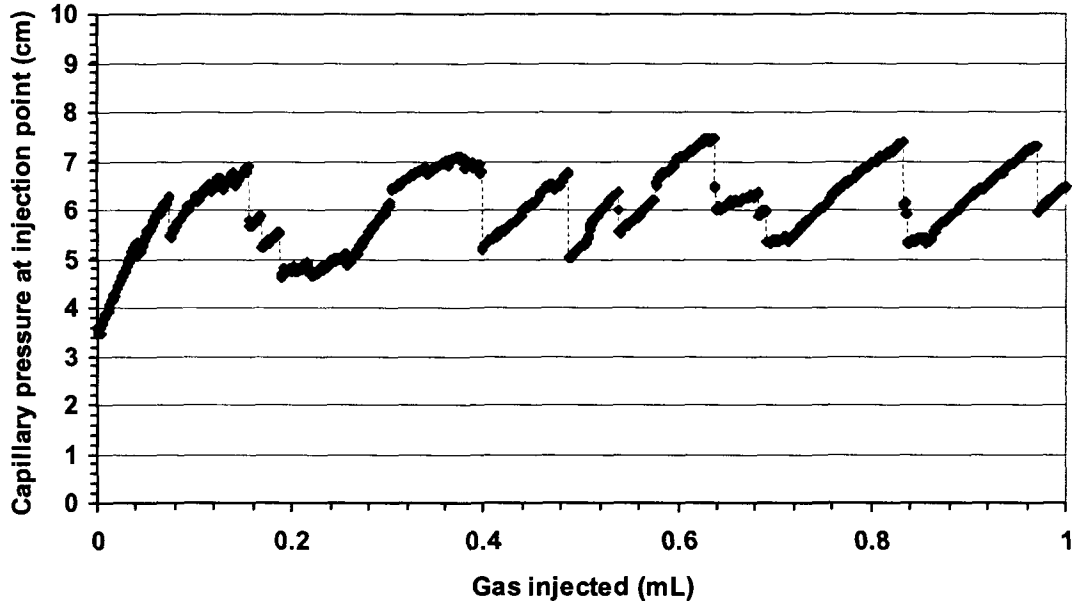

Figure B16. Capillary pressure measured at the gas injection point during injection into 1.1 mm sand at 10 μL/min, where the volume of the injection system was increased from 9 mL to 35 mL.

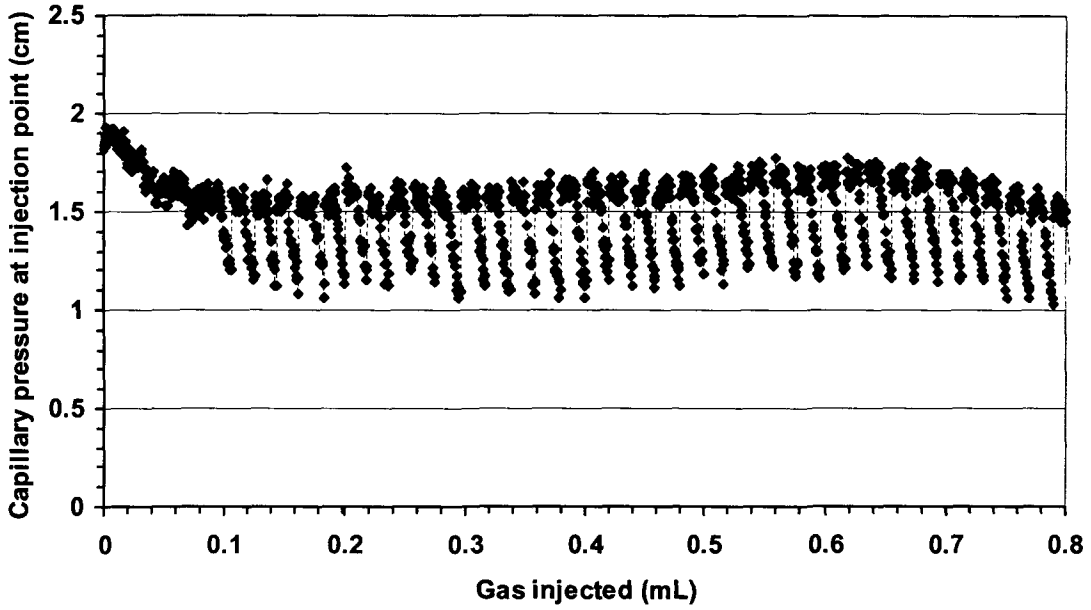

Figure B17. Capillary pressure measured at the gas injection point during injection into water (i.e. no porous media) at 10 μL/min using the same experimental set-up used for the injection experiments in porous media.

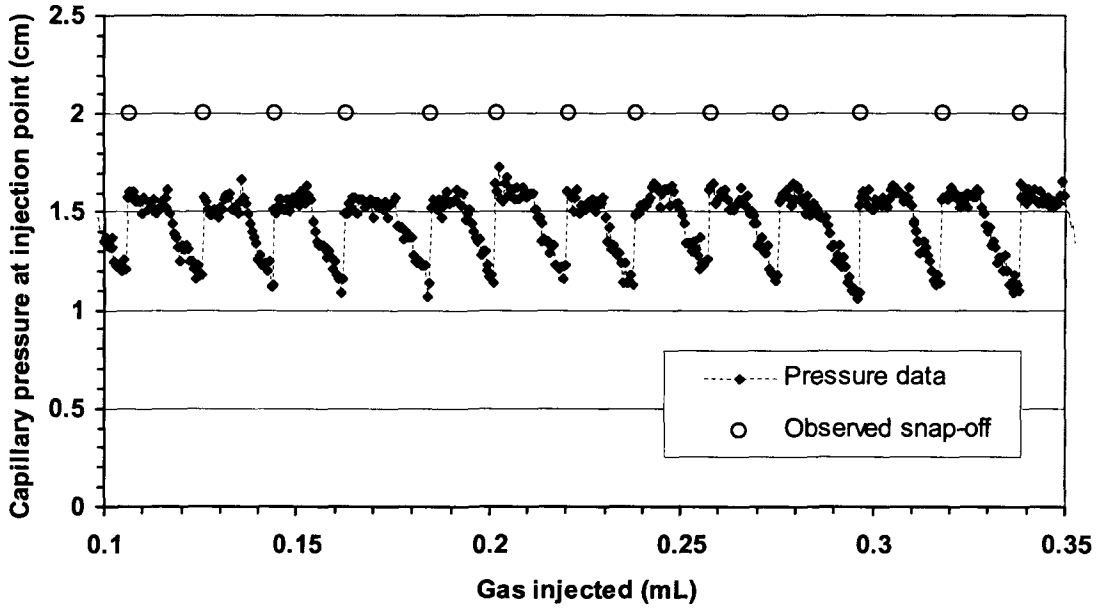

Figure B18. Capillary pressure measured at the gas injection point during injection into water (i.e. no porous media) at 10 μL/min using the same experimental set-up used for the injection experiments in porous media, indicating when snap-off of the bubble at the tube tip was observed, between the injection of 0.1 mL and 0.35 mL of gas.